WestVirginiaUniversity
THE RESEARCH REPOSITORY @ WVU

Graduate Theses, Dissertations, and Problem Reports

2021

From inner segment to outer segment: Palmitoylation of photoreceptor Na+, K+-ATPase and the importance of PRCD in photoreceptor outer segment morphogenesis

Emily R. Sechrest
West Virginia University, ersechrest@mix.wvu.edu

Follow this and additional works at: https://researchrepository.wvu.edu/etd

Part of the Biochemistry Commons, Cell Biology Commons, Eye Diseases Commons, Molecular Biology Commons, and the Pharmacy and Pharmaceutical Sciences Commons

Recommended Citation

Sechrest, Emily R., "From inner segment to outer segment: Palmitoylation of photoreceptor Na+, K+-ATPase and the importance of PRCD in photoreceptor outer segment morphogenesis" (2021). *Graduate Theses, Dissertations, and Problem Reports*. 8099.
https://researchrepository.wvu.edu/etd/8099

This Dissertation is protected by copyright and/or related rights. It has been brought to you by the The Research Repository @ WVU with permission from the rights-holder(s). You are free to use this Dissertation in any way that is permitted by the copyright and related rights legislation that applies to your use. For other uses you must obtain permission from the rights-holder(s) directly, unless additional rights are indicated by a Creative Commons license in the record and/ or on the work itself. This Dissertation has been accepted for inclusion in WVU Graduate Theses, Dissertations, and Problem Reports collection by an authorized administrator of The Research Repository @ WVU. For more information, please contact researchrepository@mail.wvu.edu.

From inner segment to outer segment: Palmitoylation of photoreceptor Na^+, K^+-ATPase and the importance of PRCD in photoreceptor outer segment morphogenesis

Emily R. Sechrest

Dissertation submitted to the School of Pharmacy
at West Virginia University

in partial fulfillment of the requirements for the degree of

Doctor of Philosophy in
Pharmaceutical and Pharmacological Sciences

Saravanan Kolandaivelu, Ph.D., Chair
Visvanathan Ramamurthy, Ph.D.
Peter Mathers, Ph.D.
Maxim Sokolov, Ph.D.
Werner Geldenhuys, Ph.D.
Vazhaikkurichi Rajendran, Ph.D.

Department of Pharmaceutical Sciences

Morgantown, West Virginia
2021

Keywords: PRCD, Na^+,K^+-ATPase, retinal degeneration, retinitis pigmentosa, palmitoylation

Copyright 2021 Emily R. Sechrest

Abstract

From inner segment to outer segment: Palmitoylation of photoreceptor Na^+, K^+-ATPase and the importance of PRCD in photoreceptor outer segment morphogenesis

Emily R. Sechrest

Photoreceptors are specialized neuroepithelial cells which are optimized for efficient capture of light and initiation of visual transduction. These cells have several compartments which are very important for proper visual function and segregation of cellular processes, including the outer segment (OS), inner segment (IS), nucleus, and synapse. The IS houses all of the cellular organelles and biosynthetic molecular machinery the cell requires and is the site of protein synthesis. The light-sensing OS is a highly modified, primary cilium, which contains many stacks of double membranous discs which house proteins required for formation and maintenance of OS structure, as well as phototransduction. These structural and phototransduction proteins are synthesized in the IS and subsequently trafficked to the OS through the narrow connecting cilium. Many of these proteins undergo post-translation lipid modifications for proper subcellular localization and association with the OS disc membranes. While the proteins involved in the phototransduction cascade are crucial for generating signals of vision, regulation of the photocurrent is needed for proper depolarization and hyperpolarization of the photoreceptor neuron, a process which is required for the cell to transduce electrical impulses to downstream neurons. Many ion channels, exchangers, and pumps, including the CNG channels and the NCKX in the OS, as well as the Na^+, K^+-ATPase and the HCN channel in the IS, are involved in this process of maintaining the photocurrent in both dark and light. One small OS disc-specific protein whose function has not yet been elucidated is progressive rod-cone degeneration, or PRCD. Previous studies in our lab have identified that PRCD is post-translationally lipid modified by S-palmitoylation on its sole cysteine, which is required for its stability and localization to the OS. Though PRCD has been shown to be important in OS disc morphogenesis and maintenance, its specific role in this process remains unclear. In this dissertation, I utilize a *Prcd*-KO animal our lab generated using CRISPR/Cas9 genome editing in order to investigate photoreceptor function, OS ultrastructure, and rhodopsin packaging into disc membranes in the absence of PRCD. Furthermore, I utilize acyl resin-assisted capture and mass spectrometry in order to identify novel proteins in the retina which undergo S-palmitoylation and validate palmitoylation profiles of several proteins using additional well-established techniques in the field. In Chapter 1 of this dissertation, I review the functional and structural needs of photoreceptor neurons, as well as the roles of both PRCD and the β2-subunit of the retinal Na^+, K^+-ATPase (ATP1B2) in these requirements. In Chapter 2, I characterize the functional and structural consequences of loss of PRCD in our lab-generated *Prcd*-KO mouse model, demonstrating through atomic force microscopy (AFM) analysis the role PRCD plays in regulation of rhodopsin incorporation into OS disc membranes. In Chapter 3, I use various techniques to reveal and validate that the ATP1B2 is palmitoylated on its N-terminal cysteine at the 10th amino acid (Cys^{10}). Finally, in Chapter 4, I discuss the results and conclusions of my dissertation work and propose experiments to further

investigate the specific role of PRCD in photoreceptors and the importance of palmitoylation of ATP1B2 in the retina. Elucidation of the specific role PRCD plays in disc morphogenesis and investigation of its interaction with rhodopsin will help to further the field and provide a deeper look into how discs are formed and maintained. Further investigation of the role palmitoylation plays in ATP1B2 function will help to establish the unique requirement of expression of ATP1B2 in the retina and identify new roles for ATP1B2 in cells where it is expressed.

Dedication

To my MaMa and Pap for preaching the importance of education and for encouraging me to reach for the stars.

To my Aunt Kim, for showing me how colorful and fun life can be.

I miss you so much and think of you daily.

Acknowledgements

First and foremost, I would like to thank my mentor, Dr. Saravanan Kolandaivelu, for his continuous support, encouragement, and patience the past 5½ years. Thank you for accepting me into your lab as your 1st graduate student at a time when I questioned my ability to be a scientist. You have been a wonderful mentor, teacher, and friend throughout my time in your lab. Thank you for teaching me to look for a positive in every negative, for pushing me, for helping me to believe in my own abilities, and for always being kind.

To my committee members, thank you for all of the invaluable advice and helpful discussion through the years, it has really helped me to become the scientist I am today.

I would next like to thank my labmates. Joe, thank you for teaching me so much when I first started and for being so patient. David, even though I started in the lab as a 3rd year grad student and you started as a senior in high school, I feel that in many ways, we grew up together in lab. Thank you for always lending a listening ear, a helping hand, and for challenging me to think more critically. Gabi, from our first trip to Starbucks during your interview until now (and all the flat whites and everything bagels in between), you have been a wonderful friend! Thank you for always listening to me vent and for helping me with countless experiments. I appreciate you! To my other labmates – Connor, Travis, Karthik, Boyden, and Sree – thank you for all of your help and feedback through the years. I've enjoyed our game nights and pot lucks! To the Ramamurthy, Sokolov, and Du labs – thank you for making the WVU Eye Institute such a warm and supportive environment. I am grateful for the discussions and celebrations we had with one another!

To the people I have met at WVU who started as friends but have become family – thank you for being by my side at my best and my worst, I'm so glad we've been able to EMBARK on this journey together. To my other closest friends from various stages of my life – Joshua, Emily, Gibb, Frank, Megan, and Chelsea – thank you for your constant love and support. During my time in Morgantown, I was also able to get involved with and serve on the Board of Directors of a local cat rescue called Homeward Bound WV, so I'd also like to thank my fellow board members – especially Jenny and Sandy – for their friendships and support.

Lastly, I want to thank my incredibly supportive family. Thank you to my little sister, Genny, for being the very best sounding board and best friend for 27 years. To you and our older sisters – Carly, Gretchen, and Shannon – your intelligence, tenacity, and strength inspire me. To my grandma, thank you for all of the birthday and Christmas cards, love, and encouragement through the years. It also wouldn't be me if I didn't acknowledge how much I love and appreciate my cat Rufus, who makes me happy after stressful days at work. Most importantly, I want to thank my parents, Gene and Kathy. Words cannot describe how thankful I am to have you both. Thank you for always believing in me and for years of patience. Your unconditional love and never-ending support have helped me to conquer so many more obstacles than I ever thought was possible. I am so grateful and honored to share all of my accomplishments with you, as I would not have been able to achieve them without you. I love you so much!

Table of Contents

Abstract ii

Dedication iv

Acknowledgements v

Table of Contents vi

Chapter 1 – Review of the Literature 1

1.1 The Vertebrate Retina 1

1.2 Photoreceptors 3
1.2.1 Photoreceptor structure 4
1.2.1.1 OS formation, maintenance, and disc morphogenesis 5
1.2.1.1a OS disc morphogenesis 6
1.2.1.1b OS renewal 9
1.2.1.1c Proteins required for disc formation 9
1.2.2 Photoreceptor function 11
1.2.2.1 Initiation of phototransduction 12
1.2.2.2 The retinoid cycle 14
1.2.2.3 Termination of phototransduction 15
1.2.2.4 Major regulators of the photocurrent 16
1.2.3 Photoreceptor health and disease 19

1.3 Progressive rod-cone degeneration (PRCD) 21
1.3.1 Progressive rod-cone degeneration in canines 24
1.3.1.1 Miniature poodles 24
1.3.1.2 English cocker spaniels 25
1.3.1.3 Biochemical studies in PRCD-affected canines 26
1.3.2 Palmitoylation of PRCD 27

1.4 Na^+, K^+-ATPase 28
1.4.1 Alternative roles for the Na^+, K^+-ATPase 31
1.4.2 The retinal Na^+, K^+-ATPase 32
1.4.3 The β2-subunit of the Na^+, K^+-ATPase 32
1.4.4 The Na^+, K^+-ATPase is a membrane anchor for retinoschisin-1 34
1.4.5 Disease associated with α3-subunit of the Na^+, K^+-ATPase 35

1.5 References **36**

Chapter 2 – Loss of PRCD alters number and packaging density of rhodopsin in rod photoreceptor disc membranes **57**

2.1 Abstract **58**

2.2 Introduction **59**

2.3 Results **61**
2.3.1 Generation of *Prcd*-KO mice using CRISPR/Cas9 genome editing 61
2.3.2 Loss of PRCD leads to progressive loss of visual function and slow photoreceptor degeneration 62
2.3.3 *Prcd*-KO retina exhibit reduced levels of rhodopsin and increased structural disorganization of rod OS as disease progresses 63
2.3.4 Disc membranes in *Prcd*-KO rod photoreceptors contain reduced packaging density and number of rhodopsin molecules 65

2.4 Discussion **66**

2.5 Methods **72**
2.5.1 Generation of *Prcd* knockout model 72
2.5.2 Electroretinography 73
2.5.3 Immunoblotting 73
2.5.4 Immunohistochemistry 74
2.5.5 Immunofluorescent staining 75
2.5.6 Transmission electron microscopy 75
2.5.7 Rod outer segment and disc membrane isolation 76
2.5.8 Atomic force microscopy 76
2.5.9 Rhodopsin measurement 77
2.5.10 Statistical analysis 77

2.6 References **78**

2.7 Figures and Figure Legends **83**
Figure 2.1 Generation and validation of *Prcd*-KO animal model. 83
Figure 2.2 Reduced rod photoreceptor function and slow retinal degeneration in animals lacking *Prcd*. 84

Figure 2.3 Reduced rhodopsin concentration and aberrant ultrastructure of photoreceptor OS during disease progression in *Prcd*-KO mice. 86
Figure 2.4 Representative AFM images of ROS disc membranes isolated from WT and *Prcd*-KO retina. 87
Figure 2.5 Quantification of ROS disc membrane properties of WT and *Prcd-KO* mice. 88

2.8 Tables **89**
Table 2.1 List of primary antibodies used in this study 89
Table 2.2 Relative population of regular and irregular discs observed in WT and *Prcd*-KO mice across ages (P30 and P120). 89
Table 2.3 ROS disc properties of 129/SV-E wild-type (WT) and *Prcd*-KO mice across ages (P30 and P120). 90

2.9 Supplementary information **91**

Chapter 3 – The β2-subunit of the retinal Na^+, K^+-ATPase is post-translationally lipid modified by palmitoylation **100**

3.1 Abstract **101**

3.2 Introduction **102**

3.3 Results **104**
3.3.1 Identification of palmitoylated proteins in the retina using acyl-RAC followed by mass spectrometry 104
3.3.2 The β2 subunit of the Na^+, K^+-ATPase (ATP1B2) is palmitoylated in the retina 106
3.3.3 ATP1B2 is palmitoylated on Cys^{10} 107
3.3.4 A C10A mutation in ATP1B2 results in loss of palmitoylation *in vivo* 108

3.4 Discussion **109**

3.5 Methods **114**
3.5.1 Animals 114
3.5.2 Cloning 114
3.5.3 Acyl-RAC Isolation of Palmitoylated Proteins 114
3.5.4 Proteomic analysis 115
3.5.5 Western blotting 115

3.5.6 Carbamidomethylation of acyl-RAC retinal samples 116
3.5.7 Acyl-PEG exchange 117
3.5.8 Subretinal injection 118

3.6 References 120

3.7 Figures and Figure Legends 125
Figure 3.1 Identification of palmitoylated proteins in the murine retina 125
Figure 3.2 The retinal Na^+,K^+-ATPase β2-subunit is palmitoylated in the retina. 126
Figure 3.3 Acyl-PEG exchange confirms palmitoylation of ATP1B2 in the retina. 127
Figure 3.4 MS/MS spectra of carbamidomethyl modified cysteine in ATP1B2 peptides. 128
Figure 3.5 A C10A mutation in ATP1B2 results in loss of palmitoylation 129

3.8 Tables 130
Table 3.1 List of primers used for cloning of WT and C10A ATP1B2 constructs 130
Table 3.2 List of primary antibodies used in this study 130

Chapter 4 – The β2-subunit of the retinal Na+, K+-ATPase is post-translationally lipid modified by palmitoylation 131

4.1 Conclusions and Future Directions – Chapter 2 131

4.2 Conclusions and Future Directions – Chapter 3 137

4.3 References 143

Chapter 1 – Review of the Literature

1.1 The Vertebrate Retina

Visual perception is initiated in the retina, a 200 μm-thick tissue located at the very back of the eye[1]. Light enters the eye through the pupil, which dilates or constricts in order to control the amount of light which enters the eye[2]. Once light reaches the retina, a series of electrochemical events are triggered, resulting in conversion of light into electrical impulses[3]. These impulses are subsequently transduced from the retina to the optic nerve, and then to the brain for visual processing within the visual cortex[1].

The vertebrate retina is a highly laminated structure, with the cell bodies and processes of each retinal cell type segregated into alternate layers[1,3-6]. The outermost cells in the retina (those closest to the back of the eye) are the photoreceptor neurons, which are specialized neuroepithelial cells[7]. Photoreceptors are responsible for capturing photons of light and converting those stimuli into electrical impulses which are sent to downstream neurons[1,3-5]. The nuclei of photoreceptors are located in an anatomical region termed the outer nuclear layer (ONL). The cell bodies of inner retinal neurons (bipolar, amacrine, and horizontal cells) collectively form the inner nuclear layer (INL). Finally, the ganglion cell layer (GCL) occupies the innermost part of the retina. The synapses of photoreceptors contact bipolar and horizontal cell dendrites in the outer plexiform layer (OPL). Meanwhile, the inner plexiform layer (IPL) connects bipolar, amacrine, and ganglion cells (Fig. 1.1)[1,5,6].

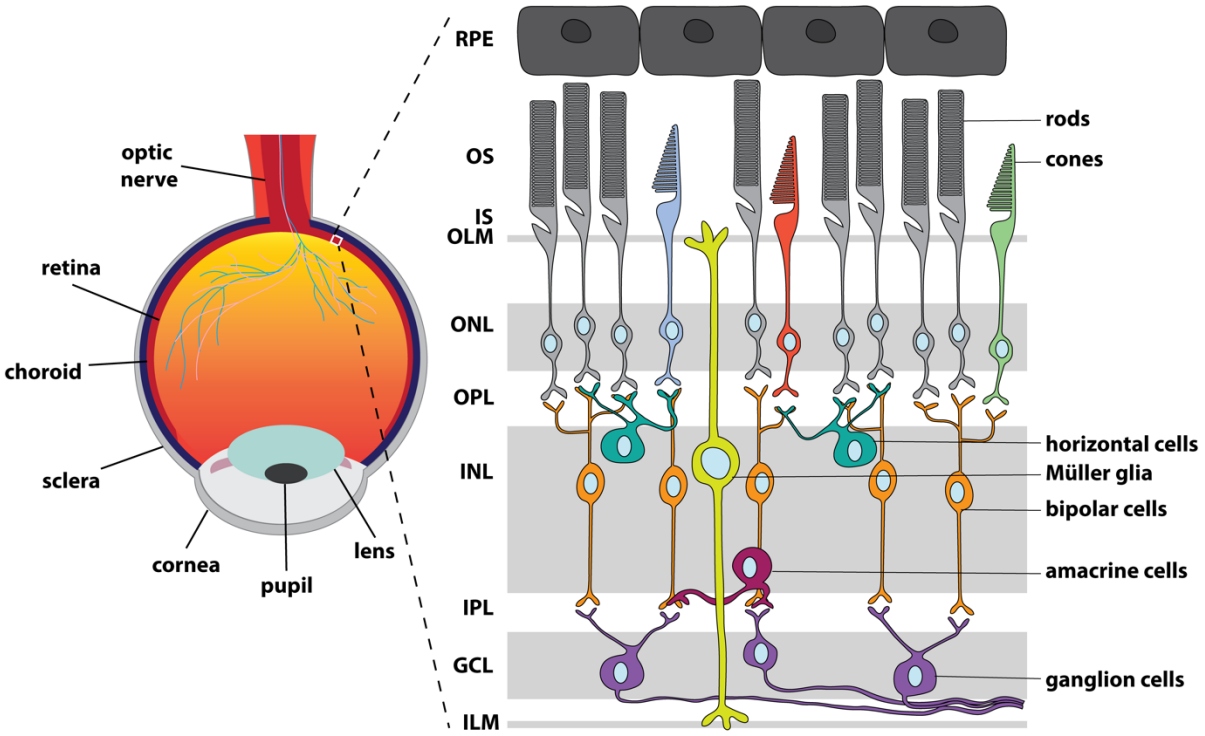

Figure 1.1. The vertebrate retina. A cross-section of the eye (left) shows the anatomical locations of several important visual structures. A white square is enlarged to depict the laminar structure of the retina (right), with the RPE at the outermost portion of the retina and the ganglion cell layer at the innermost region of the retina.

In addition to the aforementioned cell types, Müller glia are also present in the vertebrate retina and have been shown to be important modulators of retinal homeostasis[8]. Müller glia, whose cell bodies reside within the INL, have processes which span the entire thickness of the retina[9]. This feature enables Müller glia to support the structural integrity of the retina[8]. Additionally, Müller glia help to form the outer limiting membrane (OLM) and inner limiting membrane (ILM)[10]. Adherens junctions between Müller glia and photoreceptor inner segment (IS) comprise the OLM, which is a functional barrier that separates the subretinal space and the neural retina[8,11]. An additional barrier is formed by the ILM to separate the vitreous from the inner retina and it is formed by Müller glia endfeet and astrocytes[8]. Behind the neural retina exists a pigmented layer of cells known

as the retinal pigmented epithelium (RPE), which are responsible for several different processes that are crucial to vision, but also help to absorb any scattered light which is not absorbed by the photoreceptor neurons[4].

1.2 Photoreceptors

The vertebrate retina contains two general types of photoreceptors, rods and cones, which assume different functional roles in vision. In most vertebrate species (including humans and primates), rods comprise ~95% of photoreceptors and cones make up the remaining ~5%[12]. Notably, rods are extremely sensitive to light and can be stimulated by single photons of light, allowing them to function in predominantly dim light conditions. Cones, on the other hand, are much less sensitive to light and therefore are actively utilized in bright or daylight conditions[3].

The molecular machinery which gives photoreceptors their light-sensing ability is comprised of the apoprotein opsin and its bound chromophore, 11-*cis*-retinal[13]. In rods, there is only one version of this light-sensing machinery, termed rhodopsin. Rhodopsin protein plays a crucial role in both the functional abilities and structural integrity of the rod photoreceptor[14]. In contrast to rods, cones possess multiple opsins, though the exact number depends on the species[15]. In humans, there are three types of cone opsin, allowing for color differentiation. These different cone opsins are sensitive to either short (S), medium (M), or long (L) wavelengths of light and are therefore dictated as S-, M-, or L-cones[16,17].

1.2.1 Photoreceptor Structure

Photoreceptor neurons contain four distinct compartments, including an outer segment (OS), inner segment (IS), nucleus, and synapse[4,14,18,19]. The OS is a highly modified primary cilium and serves as the photon-sensing compartment of the photoreceptor[4]. The OS contains hundreds of tightly-stacked double membranous discs which contain both structural proteins required for proper OS structure, as well as most of the phototransduction proteins required for photoreceptor light sensing, including rhodopsin[14].

Although phototransduction takes place in the OS, all phototransduction proteins are synthesized in the IS, which houses all of the organelles and machinery required for protein biosynthesis [4]. The IS can be broken down into two sub-compartments: the myoid and the ellipsoid regions[4]. The myoid region contains the Golgi apparatus and endoplasmic reticulum, while the ellipsoid region contains the machinery to support the metabolic needs of the photoreceptor, including the mitochondria[19]. After synthesis in the IS, OS proteins are subsequently trafficked through a narrow bridge known as the connecting cilium (CC), which is hypothesized to have certain gate-keeping or otherwise regulatory abilities[18].

Transduction of electrical impulses from photoreceptors to bipolar cells occurs at the photoreceptor synapse, located in the OPL. Rod synapses are known as rod spherules, while cone synapses are referred to as cone pedicles. When Ca^{2+} levels are elevated in photoreceptors in the dark, vesicles containing glutamate are released into the presynaptic cleft. After light exposure and activation of phototransduction, Ca^{2+} is

depleted and glutamate is no longer released[19]. In contrast to many other neurons which utilize action potentials, photoreceptors are highly active and therefore utilize a specialized type of chemical synapse known as a ribbon synapse[20]. The ribbon synapse is a large plate-like structure which extends from the presynaptic terminal to the active zone and is responsible for mediation of presynaptic communication through regulation of vesicle exocytosis[21-23]. After presynaptic glutamate release, receptors on bipolar cell postsynaptic terminals are stimulated or inhibited depending on whether the bipolar cell is an ON -center or OFF-center bipolar cell.[24] Although all photoreceptors utilize ribbon synapses to communicate with downstream neurons, there are structural variations in the ribbon synapse which differ between rods and cones[20,25].

1.2.1.1 OS formation, maintenance, and disc morphogenesis

Photoreceptor neurons possess a highly modified primary cilium which is specialized to be an efficient light sensor. Cilia are cellular organelles which are comprised of microtubules[26]. Primary cilia, also known as sensory cilia, are non-motile cilia which protrude from the apical surface of most postmitotic mammalian cells[27]. Primary cilia are thought to be cellular 'antennae' which detect diverse stimuli from the extracellular environment[28]. Ciliogenesis—the formation of such primary cilia—depends heavily on the maturation and migration of the centrosome, a cellular organelle with well-documented roles in cell division.[29,30] The centrosome is comprised of two barrel-shaped structures called the mother and daughter centrioles and each centriole is made up of nine triplet microtubules[31]. In quiescent cells, the centrosome migrates to the plasma membrane where the mother centriole docks and matures to form the basal body[32,33]. The basal body

serves as both the anchor of the developing cilia, as well as the template for microtubule nucleation of the core of the ciliary cytoskeleton, known as the axoneme[28,33].

The initial steps of photoreceptor cilia formation follow the same stages of general ciliogenesis[4,34-38]. First, a Golgi-derived vesicle (termed the primary ciliary vesicle) will appear, attach to, and enclose the distal end of the mother centriole[35]. While traversing the cell, the primary ciliary vesicle will fuse with additional post-Golgi vesicles to expand in size, and invaginate to form the ciliary sheath[4,38]. This sheath will encapsulate the growing ciliary bud[26]. Once reaching the plasma membrane, the ciliary vesicle fuses with the plasma membrane of the IS, exposing the newly forming cilium to the extracellular, apical side of the IS. Initiation of ciliogenesis has been shown to vary between photoreceptors, with these first few stages of cilia formation generally occurring by postnatal day 3 (P3) in murine retina[37]. However, short, protruding cilia are evident in some murine photoreceptors beginning at P0[37,39]. Next, the proximal portion of the cilium will become the connecting cilium, or transition zone between the basal body and axoneme, while the distal cilium will form the OS[40]. Finally, the axoneme will continue to nucleate and extend from the basal body into the newly developed OS[34,37].

1.2.1.1a OS disc morphogenesis

Hundreds of double membranous discs are stacked and discretely present in each photoreceptor OS[40]. Mature rod OS disc membranes are completely enclosed within the plasma membrane[14]. Alternatively, a large portion of cone discs are continuous with the plasma membrane and the side of the disc opposite the cilia remains open to the

interphotoreceptor space[41]. The central portion of each mature disc, known as the lamellae, is encompassed fully (in rods) or partially (in cones) by a disc rim[14]. While the mechanism of photoreceptor OS disc formation has been debated for years, two hypotheses have emerged to explain this process, termed the 1) evagination and 2) vesicular fusion models[4,14].

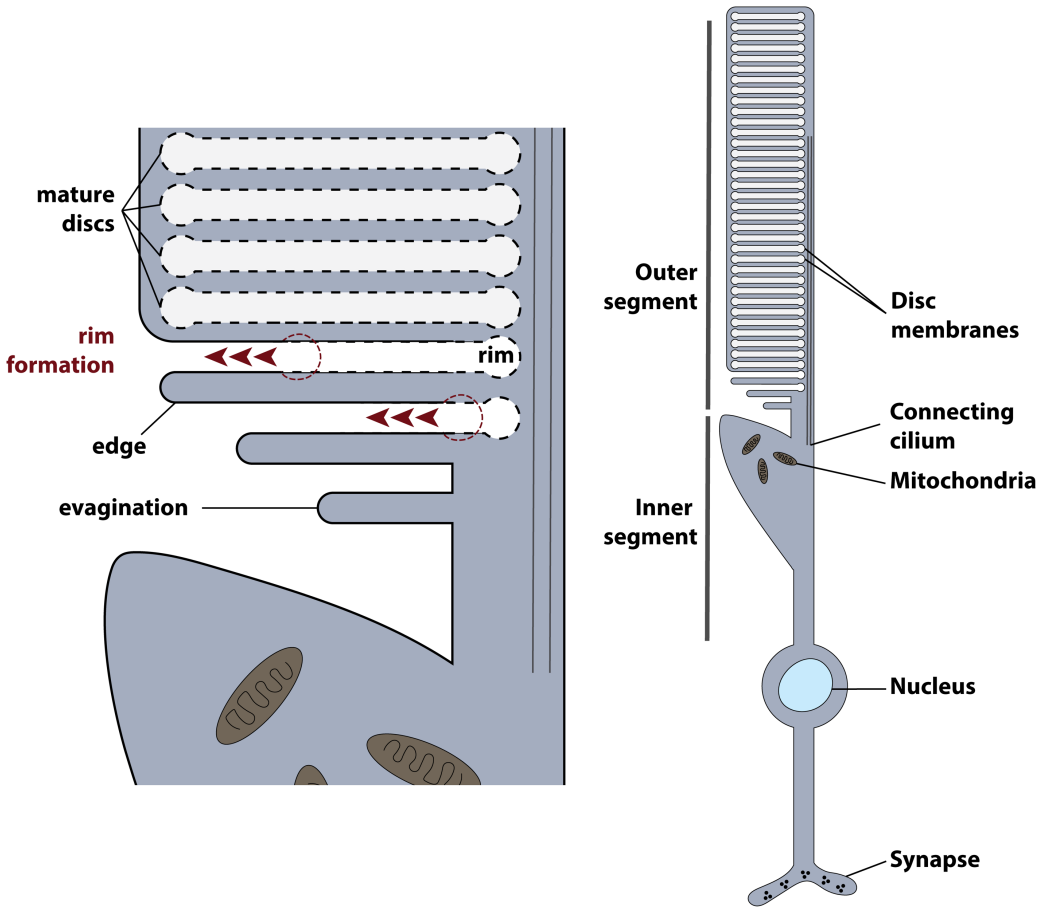

Figure 1.2. Evagination model of photoreceptor OS disc morphogenesis. The photoreceptor neuron (right), depicted as a rod, has several distinct compartments and structural features. The Steinberg *et al* two step model for OS disc morphogenesis shows growing evaginations from the base of the OS and formation of the rim region (arrows) in maturing discs. Mature discs, which are fully encapsulated within the plasma membrane, are depicted by dotted lines. Adapted from Goldberg *et al*[14].

The evagination model describes the first step in disc morphogenesis as growth of membrane protrusions, or evaginations, from the ciliary membrane away from the axoneme (Fig. 1.2)[42-48]. These evaginations, which are contiguous with the plasma membrane and have been shown to be fully open to the extracellular environment, will later become the interdiscal space[47-50]. The space between evaginations will actually become the discs. Several evaginations must form before older discs can undergo disc rim formation, which is the second step of the evagination model of disc morphogenesis[47]. In this step, the disc rim begins to form and encompass the disc membrane[51]. In rods, the disc rim will enclose the entire disc membrane. In cones, although the majority of each disc is circumscribed by a disc rim, the disc rim does not fully form. The evagination closest to the base of the OS is very short in diameter. As each nascent disc forms in rods, the older discs will grow in diameter until the evaginations fuse with the plasma membrane. Mature rod discs are uniform in diameter and in thickness. The diameter of cone discs varies, as the diameter will increase but then taper towards the distal portion of the cone OS.

The vesicular fusion model for disc formation was first observed in the developing kitten retina[52]. Irregular, vesicular structures were shown to accumulate within the ciliary plasma membrane during ciliogenesis before any mature discs were formed. This model postulates that these endocytic vesicles will eventually fuse to form mature, flattened discs. Although the evagination model seems to be more heavily supported, other groups have also shown evidence which upholds the hypothesis that OS morphogenesis occurs due to endocytic membrane fusion[1,39,53,54].

1.2.1.1b OS renewal

The length of the photoreceptor OS must remain constant in order for each photoreceptor neuron to have the proper number of disc membranes available to participate in efficient phototransduction. In order for each photoreceptor to accommodate the nascent discs growing at the base of the OS, discs residing in the apical portion of the photoreceptor must be degraded. It is believed that shedding of the discs at the top of each OS occurs in order to eliminate any damaged molecular components which have been compromised due to continual exposure to photons of light[4,34].

Behind the photoreceptor layer in the retina exist the RPE, which grow long processes known as microvilli. These microvilli contact and sheath approximately 25% of each photoreceptor tip[14]. Classical studies demonstrate that once injected radioactive amino acids are incorporated into newly synthesized proteins in the IS of rod photoreceptors, radioactively-labeled proteins are evident in newly forming discs at the base of the OS[55]. Each day, these radioactively labeled amino acids travel up the OS toward the apical end of the photoreceptor until they are eradicated. After removal from ROS, radioactive molecules are evident within the cytoplasm of the RPE, demonstrating that RPE participate in phagocytosis of shed discs[56]. Although the speed of disc renewal differs between species, approximately 10% of the OS is renewed daily in mouse rods[43,55,57]. The process of disc shedding, RPE phagocytosis, and OS renewal has also been shown to be similar in cone photoreceptors[42,58].

1.2.1.1c Proteins required for disc formation

Mass spectrometry experiments have identified 11 proteins which are localized to OS disc membranes[59]. Two of these proteins, peripherin-2 (PRPH2/RDS) and rhodopsin, are required for OS disc formation. PRPH2 is confined to the disc rim region, while rhodopsin is localized to the lamellae.

PRPH2 is a tetraspanin glycoprotein which has been shown to be crucial in photoreceptor disc morphogenesis[60-66]. Long before the disease-causing mutation was linked to PRPH2, the spontaneously-occurring *rd2* or *rds* mouse was characterized[67]. In this mutant mouse model, OS do not form and it was later found that the phenotype is linked to a mutation in *Prph2* which results in no translated PRPH2 protein[60,62,68-72]. PRPH2 is localized specifically within the disc rim region, where it forms homo-tetramers with itself and hetero-tetramers with its homologue rod outer segment membrane protein-1 (ROM-1)[14,73]. In nascent discs at the base of the OS, PRPH2 is only found to localize to the hairpin-closure on the axonemal side of the immature disc[49,51]. Therefore, it is thought that PRPH2 is initially concentrated in this location, and subsequently spreads throughout the entire disc rim during rim formation. Notably, disc formation still proceeds in the absence of ROM-1, though it is thought that ROM-1 plays an important modulatory role in disc morphogenesis, as discs appear much larger in size when ROM-1 is not present[74].

In addition to rhodopsin's central role in the phototransduction cascade (discussed below), proper expression of rhodopsin is also crucial for OS disc morphogenesis[75,76]. Strikingly, rhodopsin comprises approximately 90% of protein in the OS[77]. Not only is the density of rhodopsin kept extremely high at around 20,000 molecules/μm^2, but has also been

observed to form ordered nanodomains in the disc membrane[78-80]. Rods lacking rhodopsin, or rods containing rhodopsin mutants which exhibit trafficking defects, do not form OS[75,76]. Studies have also been done to determine whether OS development is affected by the bioavailability of rhodopsin protein through characterization of a rhodopsin over-expressing and under-expressing animal model[81-83]. In animals over-expressing rhodopsin, where mouse retina also expresses bovine rhodopsin, OS are larger in diameter[81]. In the under-expressing rhodopsin model (Rho+/-), where rhodopsin expression is about half of wild-type (WT), OS are smaller in diameter and shorter[83]. Alternatively, Interestingly, in these animals, rhodopsin density is kept constant in the OS disc membranes though the diameter of discs and the length of the OS is altered[84].

1.2.2 Photoreceptor Function

The main role of the photoreceptor is to initiate phototransduction in order to generate signals of vision which can be transduced to downstream neurons and sent to the brain for visual processing. These functions are detailed in rod photoreceptors below, although phototransduction occurs similarly in cones, just with different protein isoforms. There are five main steps which are required for initiation of phototransduction in rods, including 1) activation of rhodopsin, 2) activation of the G-protein transducin, 3) activation of phosphodiesterase 6 (PDE6), 4) hydrolysis of the secondary messenger of phototransduction (cGMP), and 5) closure of cyclic nucleotide-gated (CNG) channels in the OS plasma membrane (Fig. 1.3)[85-87]. Equally as important are the steps involved in inactivation of the phototransduction cascade. While these steps of initiation and termination of phototransduction are required for generating signals of vision, regulation

of the photoreceptor membrane potential (photocurrent) is also crucial for proper depolarization and hyperpolarization of the photoreceptor, a process which is required for the cell to transduce these generated signals to downstream neurons. Many ion channels, exchangers, and pumps in both the IS and OS are involved in this process of photocurrent modulation[88,89].

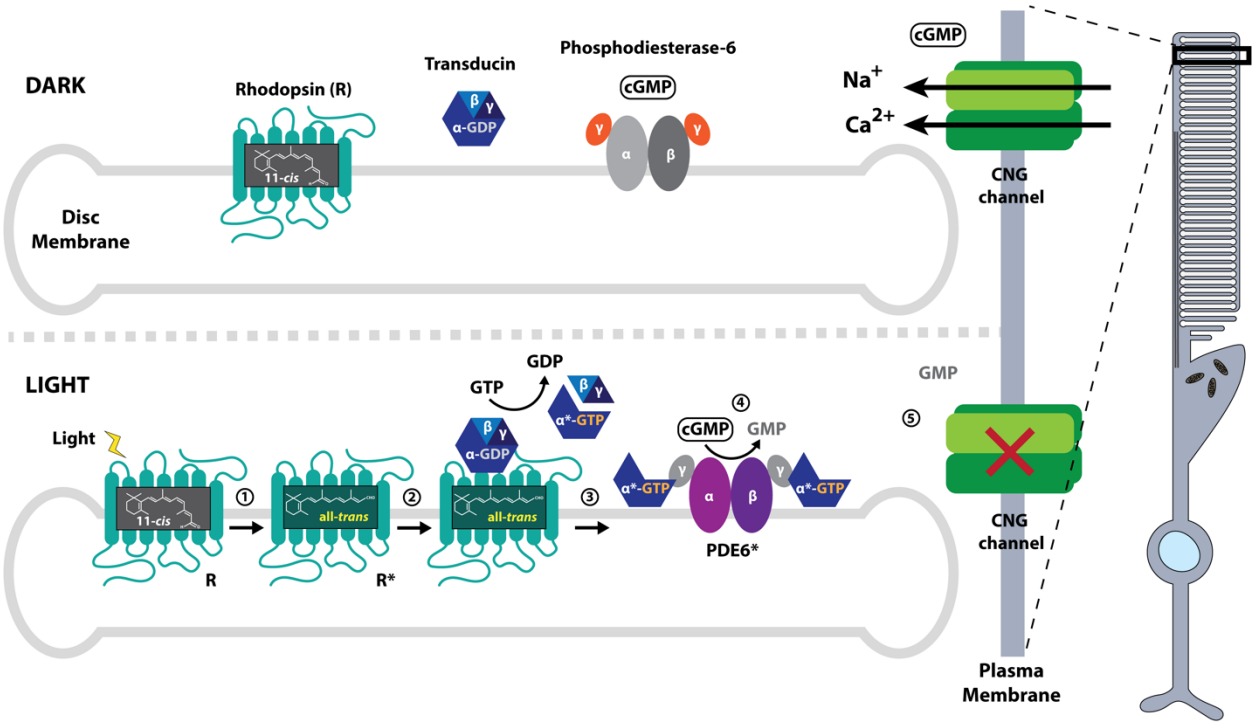

Figure 1.3. Initiation of the phototransduction cascade. Scheme representing the activation of several key proteins in phototransduction within the rod OS disc membranes. In the dark (top), proteins involved in the phototransduction cascade are inactive. However, the high concentration of cGMP allows for opening of CNG channels, resulting in the influx of Na^+ and Ca^{2+}. After light exposure (bottom), initiation of phototransduction occurs in 5 steps. (1) activation of rhodopsin (R*), (2) activation of the G-protein transducin, (3) activation of phosphodiesterase 6 (PDE6*), (4) hydrolysis of cGMP by PDE6*, and (5) closure of CNG channels in the OS plasma membrane.

1.2.2.1 Initiation of phototransduction

Once light enters the eye and reaches the OS, rhodopsin becomes activated. As mentioned previously, rhodopsin is comprised of an apoprotein called opsin and retinal,

a chromophore[13]. In the dark, retinal exists as the isomer 11-*cis*-retinal, and in this state rhodopsin is inactive. Photons reaching the OS are absorbed by 11-*cis*-retinal and induce its isomerization to all-*trans*-retinal. This conformational change in rhodopsin results in its activation; in this state it is often denoted as R* (Fig. 1.3, step 1)[90-92].

Once rhodopsin is activated (R*), its partner G-protein, transducin is able to bind[93]. Inactive transducin is a heterotrimeric protein comprised of one alpha, one beta, and one gamma subunit ($G\alpha_t\beta\gamma$)[94]. While inactive, $G\alpha_t$ is bound to GDP. Once rhodopsin is activated, transducin transiently binds and $G\alpha_t$ exchanges GDP for GTP. This GTP switch results in activated $G\alpha_t$ (Fig. 1.3, step 2)[85-87]. Activated $G\alpha_t$ is then able to activate phosphodiesterase 6 (PDE6) by binding to its regulatory gamma subunits (PDE6γ). In rods, PDE6 is comprised of its catalytic subunits, PDE6α and PDE6β, as well as its two inhibitory gamma subunits. Once activated $G\alpha_t$ binds both PDE6γ subunits, PDE6 is fully active (PDE6*) (Fig. 1.3, step 3) and begins to hydrolyze cGMP (Fig. 1.3, step 4)[85-87].

In the dark, cGMP levels are kept fairly high and constant, maintaining a balance between hydrolysis of cGMP and synthesis of cGMP by guanylate cyclase 1 and 2 (GC-1 and GC-2) which are exclusively present in the disc membranes[86]. Under these conditions, relatively abundant cGMP molecules bind to CNG channels in the OS plasma membrane and keep them open. When open, these channels allow for influx of both Ca^{2+} and Na^{+} into the cell, which collectively support the dark current, rendering the photoreceptor depolarized[88]. Once the phototransduction cascade becomes activated and PDE6* begins hydrolyzing cGMP, cGMP is no longer available to bind to CNG channels, resulting

in their subsequent closure and a decreased number of cations entering the cell[85-87]. This overall decrease in circulating cations results in a more negative membrane potential and the photoreceptor hyperpolarizes[88]. This hyperpolarization results in closure of Ca^{2+} channels at the synapse and clearance of glutamate from the post-synaptic cleft[88].

1.2.2.2 The retinoid cycle

Once 11-*cis*-retinal isomerizes to all-*trans*-retinal in response to light, it is no longer active and must be regenerated. Vertebrates utilize an enzymatic process known as the retinoid cycle, commonly referred to as the visual cycle, in order to replenish visual pigment in rods and cones[90,95,96]. While several pathways are hypothesized to supply enough 11-*cis*-retinal to photoreceptors, the predominant pathway which has been characterized is the classical visual cycle pathway[97]. Interestingly, it has been shown that much of this pathway occurs in the RPE, as photoreceptors do not contain the proper machinery to do so.

The classical visual cycle is largely mediated by retinol dehydrogenases (RDHs)[98]. As a first step, all-*trans*-retinal is released by opsin and reduced to all-*trans*-retinol by NADPH-dependent all-*trans*-RDH within the photoreceptor OS[98,99]. Next, all-*trans*-retinol is translocated to the RPE, a process mediated by ATP-binding cassette transporter 4 (ABCA4)[100]. Once in the RPE, all-*trans*-retinol is esterified by an enzyme called lecithin:retinol acyltransferase (LRAT)[101]. Retinoid isomerase (RPE65) then binds and isomerizes all-*trans*-retinyl esters in order to synthesize new 11-*cis*-retinol[102]. Lastly, this

11-*cis*-retinol is oxidized to 11-*cis*-retinal by other RDHs or generic dehydrogenases and diffuses back to the photoreceptors, where it binds with opsin[97,98].

1.2.2.3 Termination of phototransduction

Once visual transduction has taken place, a series of steps is required to terminate phototransduction, preventing perpetual stimulation and allowing the photoreceptor to respond to new stimuli. First, R* is hyperphosphorylated by rhodopsin kinase, or GRK1[86]. Although multiple phosphorylation sites are available on the C-terminus of rhodopsin, studies have shown that it must be phosphorylated three times in order to bind an inhibitory protein called arrestin-1[86,103,104]. Next, $G\alpha_t$ must be inactivated in order to inactivate PDE6*[86]. The GTPase activating-protein (GAP) complex, comprised of regulator of G-protein signaling 9 (RGS9), G protein β5 subunit ($G\beta5$), and RGS9 anchor protein (R9AP), is responsible for hydrolysis of the GTP attached to $G\alpha_t$ and its subsequent deactivation[105-107]. Although RGS9 is the only protein which has known GAP activity, all proteins in this complex are crucial for inactivation of transducin.[86,105-107]

Lastly, cGMP levels must be restored to allow the photoreceptor to depolarize. As mentioned above, GC-1 and GC-2 are responsible for synthesis of cGMP. Very little cGMP is synthesized in the dark because the proteins which activate GC-1 and GC-2, known as guanylate cyclase activating proteins (GCAPs), are bound to Ca^{2+} when intracellular Ca^{2+} levels are high in the dark[86]. After light-induced hyperpolarization of the photoreceptor, Ca^{2+} levels drop and GCAPs dissociate to bind and activate GC, resulting in restoration of cGMP levels[86]. Once cGMP levels reach a certain threshold, CNG

channels open to increase the amount of cations within the cell, causing cell depolarization[86]. Once this occurs, the photoreceptor is ready to sense new stimuli.

1.2.2.4 Major regulators of the photocurrent

Although the CNG channels in the OS plasma membrane play a crucial role in mediating the photoreceptor's response to light, several other ion channels, exchangers, and pumps also contribute to generation and shaping of the light response (Fig. 1.4)[108]. When the photoreceptor is depolarized in the dark, the membrane potential of the cell is less negative at -40 mV, and when it is hyperpolarized in the light, it becomes more negative at -75 mV[88]. Many cations contribute to the dark current, but it has been shown that 80% of the positive ions contributing originates from the influx of Na^+ ions, 15% from influx of Ca^{2+}, and 5% from influx of other ions, mainly Mg^+ ions[109].

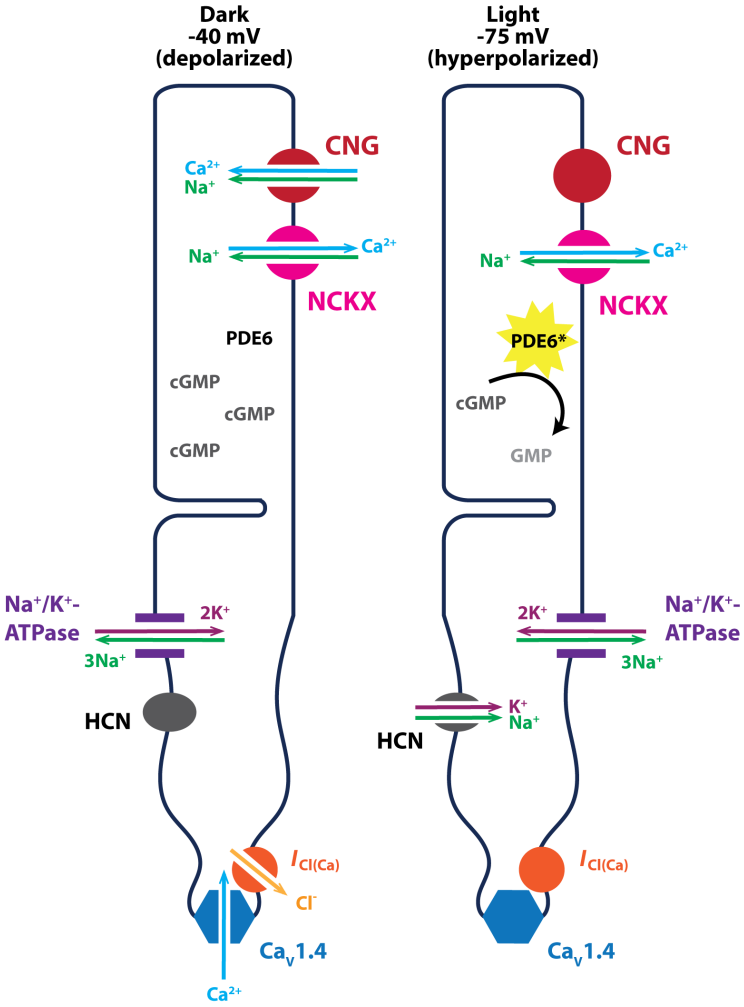

Figure 1.4. Maintenance of the photocurrent. Several ion channels, pumps, and exchangers are involved in maintenance of the photocurrent, including the dark current (left) when the photoreceptor is depolarized and in the light when the photoreceptor is hyperpolarized (right).

Apart from CNG channels, the other ion transporter localized to the OS plasma membrane is the NCKX exchanger, which works to rid the cell of excess Ca^{2+} ions[88]. Interestingly, CNG channels actually form a complex with NCKX dimers in the OS[110]. For every Ca^{2+} ion that is effluxed by the NCKX exchanger, one K^+ ion is also effluxed, and four Na^+ ions are brought into the cell[111]. Due to the importance of the negative feedback between Ca^{2+} and synthesis of cGMP by GC-1/GC-2, clearance of Ca^{2+} is very important to maintain appropriate levels of cGMP.

In the IS plasma membrane, the main ion pump that helps to modulate the concentration of intracellular Na^+ is the Na^+/K^+-ATPase. This enzyme, which will be discussed in more detail in later sections, has been shown to use approximately 50% of ATP in the retina[112]. For every ATP that is hydrolyzed, the Na^+/K^+-ATPase removes three Na^+ ions from the cell and brings two K^+ into the cell. In the dark, the Na^+/K^+-ATPase uses a high amount of available ATP in order to help remove accumulating Na^+ entering the OS[88]. In the light, the Na^+/K^+-ATPase is still active, but utilizes less energy as the OS is more metabolically active at that time[88].

A total of four voltage-dependent currents have been shown to exist in the photoreceptor IS or synapse, including the hyperpolarization-activated current (I_h), a dihydropyridine-sensitive L-type calcium current (I_{Ca}), as well as two voltage-sensitive K^+ channels, I_{kx} and a TEA-sensitive delayed-rectifier type current [$I_{K(V)}$]. Additionally, there are two Ca^{2+}-dependent currents, a Ca^{2+}-activated Cl^- current [$I_{Cl(Ca)}$] and a Ca^{2+}-activated K^+ current [$I_{K(Ca)}$][89,113,114]. These currents are mediated by a number of ion channels and exchangers.

Hyperpolarization-activated cyclic nucleotide-gated (HCN) ion channels in the IS membrane of rods and cones, which are similar to the CNG channels in the OS, have been shown to modulate the inward I_h current[115]. HCN channels open after light stimulation in response to hyperpolarization of the photoreceptor, which counteracts the loss of positive ions entering the cell in the OS, helping the cell to return to resting membrane potential[116]. When these HCN channels are pharmacologically inactive, photoreceptor light responses are heightened and last much longer, suggesting an important role in recovery after light stimulation[115,117]. The I_{kx} current works in tandem with the I_h current in order to filter rod light response, ridding the cell of accumulating K^+ when HCN channels are open following hyperpolarization, whereas the $I_{k(v)}$ current helps to remove K^+ in the dark current[88]. Although the exact K^+ channels responsible for mediating these currents are not quite understood, several have been identified, including Kv1.2, Kv2.1, Kv4.2, Kv7, Kv11.1, Kv8.2, and Ether-à-go-go (EAG)[118-122].

In the synapse of photoreceptors are L-type voltage-gated calcium channels (VGCC) which help to mediate the I_{Ca} current and synaptic transmission[88,123]. Although four isoforms of VGCCs have been identified (Ca_v1.1-1.4), Ca_v1.4 has been shown to be the isoform expressed in the photoreceptor synapse and is localized to the synaptic ribbon[88,123]. Ca_v1.4 channels are open in the dark when the photoreceptor is depolarized, allowing for influx of Ca2+ into the photoreceptor[76]. Influx of Ca^{2+} signals for neurotransmitter-carrying synaptic vesicles to fuse with the plasma membrane and release glutamate into the synaptic cleft[76]. In order to limit the amount of glutamate released in the dark, there is an internal mechanism in place which involves intracellular

Cl^- and the $I_{Cl(Ca)}$ current[76]. High intracellular Ca^{2+} signals for efflux of Cl^- through channels in the synapse; in rods these are channels which belong to the anoctamin or TEMEM16 family[124,125]. However, once intracellular Cl^- decreases, $Ca_v1.4$ channels are inhibited to reduce influx of Ca^{2+}[124,125]. Once photoreceptors hyperpolarize in the light, these $Ca_v1.4$ channels will close, resulting in inhibition of glutamate release[76].

1.2.3 Photoreceptor health & disease

All of the aforementioned structural and functional features of photoreceptors depend heavily on the proper expression and function of a diverse set of visual and non-visual proteins. Accordingly, mutations in hundreds of genes have been shown to cause inherited blinding disorders with varying degrees of severity and etiologies. Additionally, many other factors contribute to general retinal health, including age, diet, tobacco use, and UV exposure[126]. A few blinding disorders which are particularly relevant to photoreceptor health and function are retinitis pigmentosa (RP), Leber congenital amaurosis (LCA), and macular degeneration.

The most common form of inherited blinding disorder affecting the retina is RP, which affects 1 in every 3,000 to 5,000 people in the world[127]. Hundreds of mutations in over 50 different genes have been linked to RP (https://sph.uth.edu/retnet/home.htm)[128], which makes RP extremely heterogeneous in disease manifestation[129]. Many of these genes code for proteins crucial to rod photoreceptor function and structure. The majority of RP cases are autosomal recessive, while some are also X-linked recessive or autosomal dominant. Patients diagnosed with non-syndromic RP present exclusively with visual

defects, while mutations which cause syndromic RP also affect other sensory systems or tissues[130]. RP is generally characterized by slow, progressive degeneration of rod photoreceptors, with patients first experiencing night blindness. However, depending on which specific RP-causing mutations are present, disease severity will vary. Patients with mutations causing more severe forms of RP will experience complete loss of vision, while others with mild RP may only lose a portion of their visual field[129,130].

Although more rare, LCA is the most severe form of inherited retinal blindness and is the main cause of childhood blindness, occurring in 1 in 30,000 to 81,000 people[131]. LCA is generally characterized by severe vision loss or complete blindness from birth, with a reduced or absent electroretinogram (ERG) by 6 months of age[131,132]. Two other clinical features of LCA are amaurotic pupils and involuntary eye movement (sensory nystagmus)[131,132]. A total of 14 genes have now been linked to LCA, most of which play crucial roles in retinal function, including photoreceptor development and structure, the retinoid cycle, transport across the connecting cilium, and phototransduction[128,131].

Patients diagnosed with macular degeneration, commonly known as age-related macular degeneration (AMD), experience central vision loss due to degeneration of the macula, but often still retain peripheral vision[133]. The macula is a region in the center of the human retina with a high concentration of cone photoreceptors; the very center of the macula contains only cones and is called the fovea[134]. AMD can present as neovascular (“wet”) or non-neovascular (“dry”), depending on the presence of abnormal retinal vascularization which leaks blood or fluids into the macula[133]. In addition to degeneration of

photoreceptors in the macula, AMD is also characterized by atrophy of RPE cells. A hallmark of AMD is the presence of lipid deposits, known as drusen, on the basal and apical side of RPE cells[133,135]. Many RPE- and photoreceptor-specific genes—including BEST1, PROM1, PRPH2, ABCA4, and CTNNA1—have been linked to macular degeneration, although other factors such as smoking and age are demonstrated risk factors[126,128].

Unfortunately, due to the number of disease-causing mutations which cause inherited blinding disorders and the heterogeneity of disease, treatment is difficult and no comprehensive cures exist. One of the most promising treatments of inherited diseases of the retina is gene therapy, which describes the use of viral vectors to deliver normal copies of the affected genes into diseased retina[136,137]. The hope is that delivery of healthy versions of affected genes will result in expression of normal, functional proteins, to slow degeneration and delay blindness[137]. Adeno-associated viruses (AAVs) are a promising gene delivery vehicle, although there are limitations; gene therapy is not useful in patients who have already experienced severe retinal degeneration[137]. Several other techniques are being studied to help alleviate the burden of inherited blinding diseases, including immunomodulatory therapy, stem cell therapy and regenerative medicine, as well as artificial intelligence[136].

1.3 Progressive rod-cone degeneration (PRCD)

Progressive rod-cone degeneration, or PRCD, is a photoreceptor-specific protein which is localized to OS disc membranes[59,138]. Mutations in PRCD are linked to retinitis

pigmentosa (RP) in dogs and humans. Although the specific role of PRCD has not yet been ascertained, it seems to play an important role in high-fidelity disc morphogenesis[139]. PRCD is a 54-amino acid protein (53 amino acids in mice), predicted to contain several structural domains despite its structure being unsolved (Fig. 1.5). The sole cysteine residue of PRCD is located on the N-terminus at the second amino acid and is post-translationally lipid modified[140,141].The next 13 amino acids comprise the hydrophobic region of the protein, thought to be a transmembrane domain[140]. Immediately following these amino acids lies a polybasic region, comprised of three arginine residues[140]. Interestingly, polybasic regions are known to be important for strengthening a protein's interaction with the plasma membrane through electrostatic interactions between the positively charged amino acids and the negatively charged phospholipid head groups[142-144]. Several amino acids after the polybasic region, PRCD also contains a VxPx motif, which is a motif implicated in ciliary targeting of proteins[145]. However, trafficking of PRCD to the OS has not been well described and it is unclear whether the photoreceptor utilizes this VxPx motif to target PRCD to the cilium, though association with rhodopsin does seem to be crucial for trafficking[141]. Finally, although its significance is still not well understood, a portion of

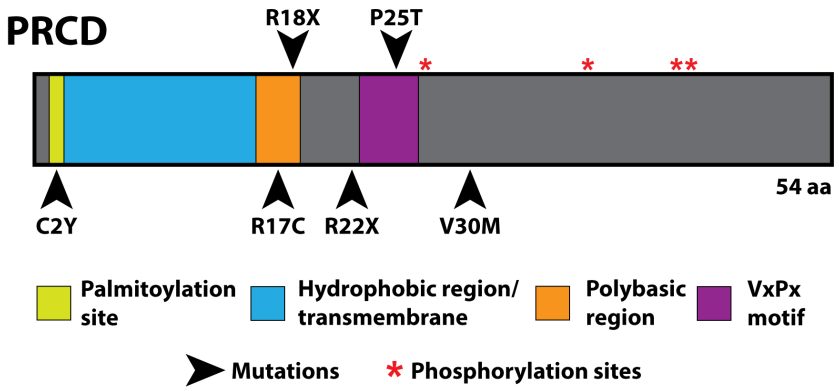

Figure 1.5. Structural domains and post-translational modifications of PRCD. PRCD is a 54 amino acid protein (53 aa in mice), with several predicted structural domains, RP-causing mutations, and phosphorylation sites.

PRCD is phosphorylated[141]. Multiple phosphorylated residues have been identified in this small protein, including serines 27, 38, and 44, as well as threonine 45[146].

Interestingly, several mutations have been identified in this small protein which are linked with RP (Fig. 1.5). The first and most prevalent mutation in PRCD is a cysteine to tyrosine mutation at the second amino acid (PRCD-C2Y). Moreover, this PRCD-C2Y mutation was first documented in and has been most studied in canines, as this mutation results in the most common form of inherited blinding disease in dogs. However, this homozygous mutation was also linked to a human patient with RP from Bangladesh[147]. Another RP-linked PRCD mutation, found in one proband of Indian origin, is a heterozygous arginine to cysteine mutation at the 17th amino acid (R17C), within the polybasic region[147]. Interestingly, this heterozygous mutation has also been documented in people of Indian or Pakistani origin who do not present with an RP phenotype[147]. Another mutation which lies within the polybasic region is a homozygous R18X mutation, which results in an early stop codon and has been documented in three siblings of Turkish origin with RP[148]. A more prevalent homozygous R22X mutation has been reported in 18 different RP patients between nine families from a Muslim Arab village in northern Israel[149]. Notably, a patient from Germany with RP was found to have inherited a different heterozygous mutation from each of her parents[150]. In addition to inheriting a heterozygous mutation for R18X from one parent, the patient was also found to carry a mutation in the 25th amino acid, with a substitution of tyrosine for proline (P25T)[150]. Lastly, a heterozygous valine to methionine (V30M) mutation is also linked to RP[147].

1.3.1 Progressive rod-cone degeneration in canines

In the 1970s and 80s, a recessive hereditary disorder termed progressive rod-cone degeneration (PRCD), which later became the namesake of the affected protein, was first extensively characterized in miniature poodles. PRCD-affected canines have retina which develop normally with normal differentiation of photoreceptors, but later show signs of improper disc stacking, disorganization and damage to the photoreceptor OS[151-154]. To date, PRCD is the most common inherited blinding disease in canines, affecting over 30 dog breeds[147,155,156].

1.3.1.1 Miniature poodles

The first study, which focused on visual response in the retina of miniature poodles through analysis of electroretinography (ERG), showed that affected dogs presented with reduced ERGs as early as 9.5 weeks[154]. Additionally, autoradiography using ^{3}H-leucine demonstrated that the process of OS renewal is slower in PRCD-affected animals, although RPE appear normal[151]. This reduced rate of OS renewal was also later confirmed using 3H-fucose[152]. In contrast to the first study analyzing ERGs where visual defects were visible at 9.5 weeks, a second study from the same research group demonstrated that defects in ERG response of tested canines were not evident until 28 weeks, a discrepancy which was attributed to increased genetic heterogeneity from continued breeding of the colony of miniature poodles and potentially anesthesia[151,154].

Although no morphological defects were apparent in PRCD-affected retina at 14.5 weeks by light microscopy, electron microscopy revealed early PRCD disease onset, with

vesicular profiles near the OS and within RPE microvilli, as well as rods with disorganized OS and disoriented disc membranes[151]. At 30 weeks, abnormalities in morphology were evident by light microscope, mainly affecting rods with ROS appearing both irregular and indented. By 10 months of age, rod IS appeared shorter and OS were disorganized with disoriented disc membranes, with areas of the outer nuclear layer (ONL) lacking rods altogether. At 60 months, only cone photoreceptors remained and were localized strictly to the posterior pole of the retina. Interestingly, a hallmark of PRCD-associated disease in the miniature poodle is the presence of vesicular profiles near the OS membrane[154].

1.3.1.2 English cocker spaniels

Recessively inherited retinal degenerative disorders which are similar to PRCD have been identified in other dog breeds, such as the English cocker spaniel (ECS)[153]. A hereditary blinding disease affecting ECS was found to generally mirror PRCD-associated disease in miniature poodles, with very progressive retinal degeneration and loss of vision. In contrast, the time of disease onset is much later and disease progression is much slower, with elderly dogs still having some remanence of vision. Although disease presented differently in ECS, through a series of cross-breeding experiments it was found that this inherited blinding disease was in fact PRCD. In the majority of ECS with PRCD-associated disease, defects in visual response (measured by ERG) were not evident until animals were over 12 months old, with rods affected much sooner than cones. In comparison to miniature poodles, visual function also deteriorated much slower in affected ECS. As in miniature poodles, OS became disorganized and disc membranes

were disoriented. However, disease onset and progression occurred in a very different manner, with spatial and temporal differences compared to the miniature poodle.

Vesicular profiles, which are one of the most prominent phenotypes in PRCD-affected miniature poodles, are absent or sparsely distributed in affected ECS retina. Even in a 6.8 year-old ECS with PRCD, small areas of the retina contain rods and cones, although there is evidence of OS disorganization and disc disorientation. Overall, researchers found that PRCD-associated disease varies in location and time of disease onset and progression, likely due to the genetic heterogeneity in each dog breed background. Moreover, it was determined that although phenotypes of PRCD-associated disease manifest differently between dog breeds, disease is a result of a single or multiple mutations in a single genetic locus, as opposed to mutations at multiple genetic loci[153].

1.3.1.3 Biochemical studies in PRCD affected canines

As disc orientation and stacking were highly affected in canines with PRCD, researchers were interested in determining whether changes in opsin levels could lead to the defects seen in rods, as opsin comprises the majority of protein in discs. Several other photoreceptor-specific proteins were also analyzed. It was found that while opsin mRNA levels became undetectable well into degeneration and started to decrease during early degeneration, they were completely normal early in disease[157]. Although there was differential expression of several photoreceptor-specific proteins, it seems that these changes were not uniform and varied on a protein-by-protein basis[158]. While some proteins were dramatically reduced in this time, including S-antigen, others were only

slightly reduced, such as cone PDE6[157,158]. Interestingly, both β-transducin and phosducin expression seemed to increase in the ROS early in disease, but varied later[158]. Researchers also studied the role of the interphotoreceptor matrix in disease and degeneration through staining for wheat germ agglutinin (WGA) and peanut agglutinin (PNA), however all changes observed were concluded to be adaptive structural responses following degeneration and subsequent cell death[159].

1.3.2 Palmitoylation of PRCD

PRCD is one of 11 known proteins localized to photoreceptor OS discs[59]. Although no transmembrane domain has been confirmed, PRCD does contain an N-terminal stretch of hydrophobic amino acids thought to be crucial for membrane association[140]. PRCD also contains a single cysteine residue, located at the second amino acid, which is palmitoylated in retina and in cell culture[140,141].

Palmitoylation is a unique post-translational lipid modification which involves the reversible attachment of the 16-carbon fatty acid palmitate to cysteine residues on a protein[160]. Lipidation of proteins generally increases their hydrophobicity and assists with membrane association; however, palmitoylation also facilitates a variety of other biological processes, including protein-protein interactions, maturation, signaling, activity, and targeting to specific membrane microdomains[144,161-163]. Unlike many other post-translational lipid modifications, palmitoylation is reversible, which grants it a dynamic role in these processes. Protein palmitoylation is mediated by a class of enzymes known as DHHC motif-containing palmitoyl acyltransferases (DHHC-PATs), of which 23 human

isoforms exist with distinct tissue and subcellular distributions[164-166]. Depalmitoylation of proteins is accomplished by enzymes known as palmitoyl-protein thioesterases (PPTs)[167,168].

Acyl resin-assisted capture (acyl-RAC), hydroxylamine treatment, and click chemistry have been used to confirm palmitoylation of wild-type PRCD (PRCD-WT) both *in vivo* and in cell culture[140,141]. PRCD is likely palmitoylated in the Golgi by zDHHC3, as co-transfection of zDHHC3 enhances PRCD-WT palmitoylation[123]. Importantly, the RP-linked PRCD-C2Y mutation discussed above results in loss of palmitoylation. Since PRCD-C2Y protein levels are destabilized by more than 90% compared to PRCD-WT in cell culture, palmitoylation appears to have a major role in PRCD protein level stability[140]. In addition to destabilization of mutant PRCD-C2Y protein, loss of PRCD palmitoylation also leads to its mislocalization[140,141]. Strikingly, PRCD-C2Y is not trafficked to the OS like PRCD-WT, but instead accumulates within the IS, likely within subcellular compartments[140,141].

1.4 Na^+, K^+-ATPase

The Na^+, K^+-ATPase is a P-type ATPase which plays a major role in maintenance of ion homeostasis in all cell types[169]. The pump hydrolyzes one molecule of ATP in order to extrude Na^+ from the cell and bring K^+ into the cell in a 3 Na^+:2 K^+ ratio. The Na^+, K^+-ATPase is an integral membrane protein and a heterodimer, made up of one alpha (α-) and one beta (β-) subunit (Fig. 1.6). The α-subunit is the catalytic subunit of the pump, containing the sites for ATP binding and hydrolysis and ion binding[169]. The α-subunit has

ten transmembrane α-helices and is located mainly on intracellular side of the membrane. On the other hand, the β-subunit is implicated in maturation and trafficking of the entire enzyme to the plasma membrane[170]. The β-subunit has only one transmembrane α-helix, a very short intracellular domain, and a very large extracellular domain with an immunoglobulin-like motif[169]. Studies have shown that the α- and β- subunits must associate with one another at an 1:1 ratio within the endoplasmic reticulum (ER) in order for the complex to exit and traffic to the Golgi[171,172]. If these two subunits do not associate, they are retained in the ER and subsequently degraded[171,172].

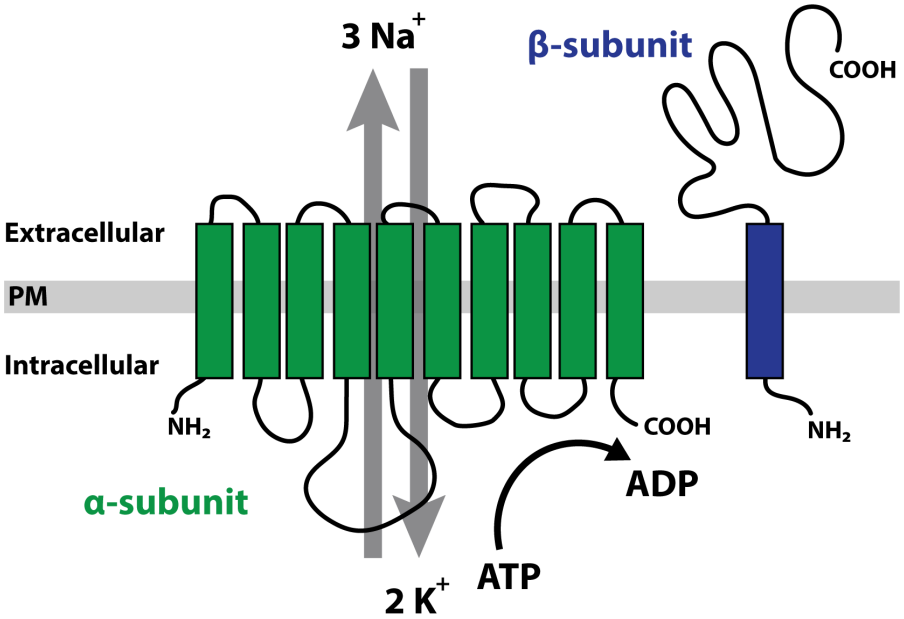

Figure 1.6. Structure of the Na^+, K^+-ATPase. Cartoon representation of the α- and β- subunits of the Na^+, K^+-ATPase.

There are four known isoforms of the α-subunit, including ATP1A1, ATP1A2, ATP1A3, and ATP1A4[169]. Furthermore, three isoforms of the β-subunit have been described, including ATP1B1, ATP1B2, and ATP1B3 (Fig. 1.7)[169]. Although cell culture studies have shown that any α-subunit can associate with any β-subunit, certain α–β preferences do exist, and importantly, subunit isoforms are expressed in a cell-specific manner[169,173]. The isoforms of the α-subunit of the Na^+, K^+-ATPase share a relatively high sequence homology at ~87%, with the lowest between α1 and α4, with 78% similarity. However,

the β-subunits are vastly different. The β2-subunit of the Na^+, K^+-ATPase only shares 58% similarity with β1 and 61% with β3, while β1 and β3 share 68% homology[174]. Even though the different β-subunit isoforms are quite different from one another, they do contain several conserved domains, including three disulfide bonds and an immunoglobulin-like domain within the large extracellular region of the protein[174].

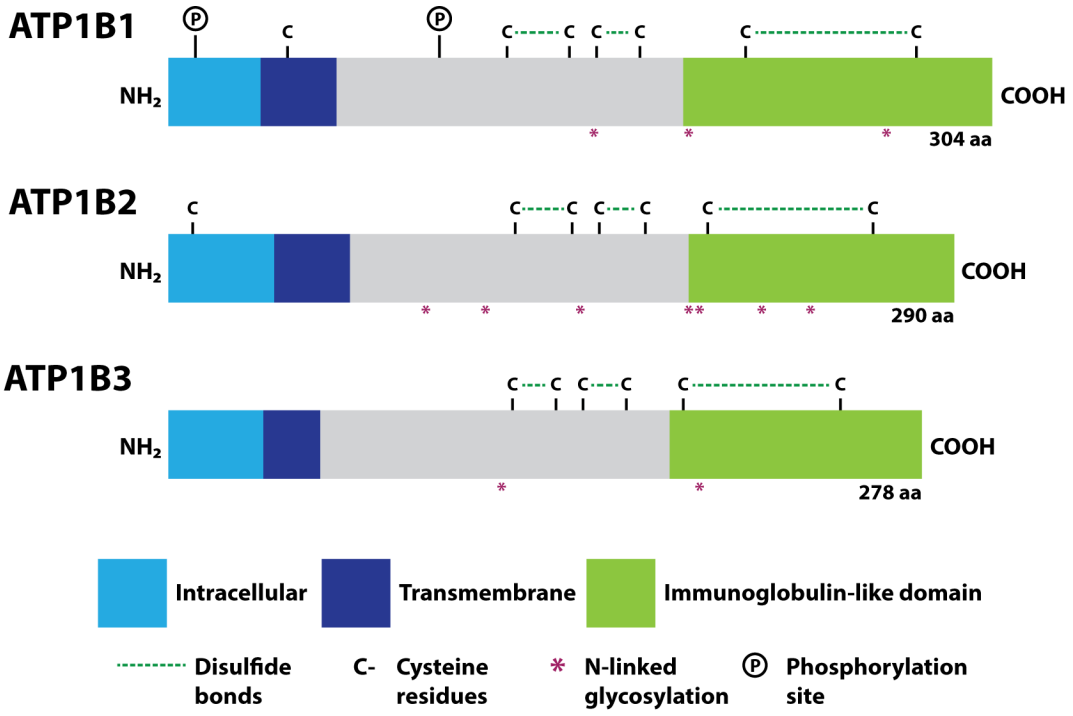

Figure 1.7. Structural domains and post-translational modifications of the β-subunit isoforms of the Na^+, K^+-ATPase.

One additional factor which contributes to the differences between the β-subunit isoforms is the number of N-linked glycosylation sites, which have been implicated in protein folding, maturation, and cell adhesion properties of the Na^+, K^+-ATPase (Fig. 1.6). The β1-subunit contains three N-linked glycosylation sites, while β3 contains only two. Glycosylation of β1 is crucial for proper interactions between β1 subunits of neighboring

cells through localization to the lateral membrane[175]. The β2-subunit has eight different glycosylation sites, which play a role in proper folding and maturation, as interactions with calnexin (an ER lectin chaperone) are lost when ATP1B2 is not properly glycosylated[176].

Although the α- and β- subunits are the only subunits required to form a functional Na^+,K^+-ATPase heterodimer, many tissues also express a regulatory γ-subunit of the Na^+,K^+-ATPase. The γ-subunit is a potent regulator of Na^+,K^+-ATPase activity, with seven known isoforms (FXYD1-7) expressed in a tissue-specific manner[177]. Each γ-subunit isoform of the Na^+,K^+-ATPase has been shown to modulate channel activity differently, either through upregulation or downregulation of pump activity[178].

1.4.1 Alternative roles for the Na^+, K^+-ATPase

In addition to its role in ion transport, there is evidence that the Na^+, K^+-ATPase is also involved in cellular adhesion and signal transduction. Cardiac glycosides such as ouabain and digoxin have been extensively utilized in studying the Na^+, K^+-ATPase, as high levels of ouabain inhibit Na^+, K^+-ATPase ion transport, but lower concentrations have been shown to activate different signal transduction pathways[179]. Using ouabain, it has been shown that the Na^+, K^+-ATPase is involved in mitogen-activated protein kinase (MAPK) signaling, Ca^{2+} signaling, and phosphatidylinositol 3-kinase (PI3K)/Akt signaling[179,180]. Apart from ion transport and signaling, the β1- and β2- subunits of the Na^+, K^+-ATPase have been shown to serve as cell adhesion molecules in order to help mediate cell-cell adhesion[181,182].

1.4.2 The retinal Na^+, K^+-ATPase

The predominant Na^+, K^+-ATPase subunits expressed in the mammalian retina are ATP1A3 (α3) and ATP1B2 (β2); collectively, these subunits are commonly referred to as the retinal Na^+, K^+-ATPase[183-185]. In relatively early investigations of the retinal Na^+, K^+-ATPase, it was found that Na^+, K^+-ATPase expression is enriched within the IS of photoreceptors as well as the inner and outer plexiform layers[186]. Soon after this discovery, it was found that the predominant mRNAs of the Na^+, K^+-ATPase in retina were those of α3 and β2, contributing 85% and 79% of total α-subunit and β-subunit mRNA, respectively[183]. Immunoblotting confirmed these results and immunocytochemistry demonstrated co-localization of α3 and β2 in the photoreceptor IS[183,184]. Photoreceptors also express the β3 subunit late in their differentiation, although α3 and β2 are expressed in undifferentiated photoreceptors at birth[185]. Despite the strong expression of α3 and β2 in the retina and exclusive expression of α3, β2, and β3 in photoreceptors, each of the other subunit isoforms of the Na^+, K^+-ATPase have been identified in at least one retinal cell type, except for α4[185].

1.4.3 The β2-subunit of the Na^+, K^+-ATPase

Originally discovered as adhesion molecule on glia (AMOG), ATP1B2 was later discovered to have sequence homology to the β-subunit of the Na^+, K^+-ATPase[187,188]. At first, ATP1B2 was only found to be expressed in the brain, but has since been detected in many other tissues[189,190]. Apart from its involvement in maturation and trafficking of the ion pump to the plasma membrane, ATP1B2 has been shown to have other roles in the cell. As its original name suggests, ATP1B2 was first discovered to be expressed by

astroglia and was found to be important for mediating interactions between astroglia and neurons[187,191]. Since then, it has also been implicated in neuronal migration, neurite outgrowth, and cell-cell adhesion[187,192].

To examine how ATP1B2 influences development and long-term integrity of neuronal tissue, a mouse global knockout of *Atp1b2* (AMOG$^{-/-}$) was created[193]. Unfortunately, neurological defects begin to affect AMOG$^{-/-}$ mice beginning at P15, resulting in death between P17 and P18. Interestingly, retina from AMOG$^{-/-}$ mice present with 50% reduction in thickness of the outer nuclear layer (ONL) at P17. Furthermore, both IS and OS appear shorter in length compared to control mice (AMOG$^{+/+}$). Although morphological defects were observed in both retina and brain tissue, it was unclear whether the defects were linked to the role of ATP1B2 in ion channel activity or the implications of ATP1B2 in cellular recognition and adhesion[193].

To better address whether neurological defects in AMOG$^{-/-}$ mice were a direct cause of ion channel insufficiencies or non-pump functions of ATP1B2, a β1/β2 knock-in animal was created[194]. This knock-in model expresses *Atp1b1* cDNA in place of *Atp1b2*. Notably, while substitution of ATP1B1 for ATP1B2 in the brain circumvented the neural pathologies of AMOG$^{-/-}$ mice, retina of β1/β2 knock-in mice still degenerated. In β1/β2 knock-in retina, *Atp1b1* mRNA expression only appeared to be ~15% of the *Atp1b2* mRNA expression of wild-type animals. Although photoreceptor neurons still degenerated, degeneration took much longer compared to retina from AMOG$^{-/-}$ mice. While 50% of photoreceptors degenerated in AMOG$^{-/-}$ mice by P17, an equivalent loss of photoreceptors in β1/β2

knock-in animals was not observed until 4 months of age[194]. Slowed photoreceptor degeneration suggests that substitution of ATP1B2 with its homologue ATP1B1 does help to restore normal Na^+, K^+-ATPase function in regard to ion channel activity. However, much remains unknown regarding the specific need for ATP1B2 in the retina, especially in terms of its role as a cell adhesion molecule.

1.4.4 The Na^+, K^+-ATPase is a membrane anchor for retinoschisin-1

An additional role for the retinal Na^+, K^+-ATPase is serving as a membrane anchor for retinoschisin-1 (RS1)[195,196]. Mutations in RS1 are associated with X-linked retinoschisis (XLRS), which results in early macular degeneration, and is characterized by splitting (or "schisis") of the inner layers of the retina[197-201]. RS1 is a secreted protein which is expressed in both photoreceptor neurons and bipolar cells[202]. Once secreted, RS1 uses the retinal Na^+, K^+-ATPase as a membrane anchor to help to maintain the synaptic connections between photoreceptors and bipolar cells and preserve the structural integrity of the retina[195,196,202,203]. Although it was originally thought that the entire retinal Na^+, K^+-ATPase (ATP1A3 and ATP1B2) was required for membrane anchorage of RS1, it was later found that RS1 binding only required expression of ATP1B2 and the α-subunit was interchangeable[180,204]. In the absence of ATP1B2 from the retina, both ATP1A3 and RS1 protein levels are severely reduced, suggesting that no Na^+, K^+-ATPase is present in photoreceptors or bipolar cells when ATP1B2 is not expressed[195].

1.4.5 Disease associated with α3-subunit of the Na^+, K^+-ATPase

Although no disease-causing mutations in *ATP1B2* have been reported, mutations in *ATP1A3* have been linked to various neurological disorders, including alternating hemiplegia of childhood (AHC), rapid-onset dystonia parkinsonism (RDP), human optic atrophy, and CAPOS (cerebellar ataxia, areflexia, pes cavus, optic atrophy, and sensorineural hearing loss) syndrome[205-208]. Interestingly, while disease-causing mutations for two of these disorders lead to atrophy of the optic nerve, no mutations in *ATP1A3* have been linked to retinal degeneration or visual defects despite the prevalence of ATP1A3 in the retina[205,208]. Very recently, a family with cone-rod dystrophy (CORD) presented with a novel mutation in *ATP1A3* which results in residue 591 being mutated from aspartate to valine[209]. Overexpression of mutant ATP1A3-D591V in HeLa cells demonstrated defects in mitochondria resulting in decreased oxygen consumption rate (OCR)[209]. Furthermore, in an animal model expressing mutant ATP1A3-D591V, scotopic and photopic ERG responses were reduced[209]. While no mutations in *ATP1B2* have yet been identified, these disease-causing mutations in *ATP1A3* highlight the crucial role of the Na^+, K^+-ATPase in retinal health, and potential contributions of *ATP1B2* remain understudied.

1.5 References

1 Sung, C.-H. & Chuang, J.-Z. The cell biology of vision. *The Journal of Cell Biology* **190**, 953, doi:10.1083/jcb.201006020 (2010).

2 Mathôt, S. & Van der Stigchel, S. New Light on the Mind's Eye: The Pupillary Light Response as Active Vision. *Curr Dir Psychol Sci* **24**, 374-378, doi:10.1177/0963721415593725 (2015).

3 Molday, R. S. & Moritz, O. L. Photoreceptors at a glance. *Journal of Cell Science* **128**, 4039, doi:10.1242/jcs.175687 (2015).

4 Pearring, J. N., Salinas, R. Y., Baker, S. A. & Arshavsky, V. Y. Protein sorting, targeting and trafficking in photoreceptor cells. *Prog Retin Eye Res* **36**, 24-51, doi:10.1016/j.preteyeres.2013.03.002 (2013).

5 Baccus, S. A. Timing and computation in inner retinal circuitry. *Annu Rev Physiol* **69**, 271-290, doi:10.1146/annurev.physiol.69.120205.124451 (2007).

6 Stenkamp, D. L. Development of the Vertebrate Eye and Retina. *Prog Mol Biol Transl Sci* **134**, 397-414, doi:10.1016/bs.pmbts.2015.06.006 (2015).

7 Brzezinski, J. A. & Reh, T. A. Photoreceptor cell fate specification in vertebrates. *Development (Cambridge, England)* **142**, 3263-3273, doi:10.1242/dev.127043 (2015).

8 Goldman, D. Müller glial cell reprogramming and retina regeneration. *Nat Rev Neurosci* **15**, 431-442, doi:10.1038/nrn3723 (2014).

9 Jadhav, A. P., Roesch, K. & Cepko, C. L. Development and neurogenic potential of Müller glial cells in the vertebrate retina. *Progress in retinal and eye research* **28**, 249-262, doi:10.1016/j.preteyeres.2009.05.002 (2009).

10 Wang, J. *et al.* Anatomy and spatial organization of Müller glia in mouse retina. *The Journal of comparative neurology* **525**, 1759-1777, doi:10.1002/cne.24153 (2017).

11 Pearson, R. A. *et al.* Targeted Disruption of Outer Limiting Membrane Junctional Proteins (Crb1 and ZO-1) Increases Integration of Transplanted Photoreceptor Precursors into the Adult Wild-Type and Degenerating Retina. *Cell Transplantation* **19**, 487-503, doi:10.3727/096368909X486057 (2010).

12 Wang, J. S. & Kefalov, V. J. The cone-specific visual cycle. *Prog Retin Eye Res* **30**, 115-128, doi:10.1016/j.preteyeres.2010.11.001 (2011).

13 Park, P. S. Constitutively active rhodopsin and retinal disease. *Adv Pharmacol* **70**, 1-36, doi:10.1016/b978-0-12-417197-8.00001-8 (2014).

14 Goldberg, A. F. X., Moritz, O. L. & Williams, D. S. Molecular basis for photoreceptor outer segment architecture. *Progress in retinal and eye research* **55**, 52-81, doi:10.1016/j.preteyeres.2016.05.003 (2016).

15 Shichida, Y. & Matsuyama, T. Evolution of opsins and phototransduction. *Philos Trans R Soc Lond B Biol Sci* **364**, 2881-2895, doi:10.1098/rstb.2009.0051 (2009).

16 Roorda, A. & Williams, D. R. The arrangement of the three cone classes in the living human eye. *Nature* **397**, 520-522, doi:10.1038/17383 (1999).

17 Nathans, J., Thomas, D. & Hogness, D. S. Molecular genetics of human color vision: the genes encoding blue, green, and red pigments. *Science* **232**, 193-202, doi:10.1126/science.2937147 (1986).

18 Insinna, C. & Besharse, J. C. Intraflagellar transport and the sensory outer segment of vertebrate photoreceptors. *Dev Dyn* **237**, 1982-1992, doi:10.1002/dvdy.21554 (2008).

19 Kennedy, B. & Malicki, J. What drives cell morphogenesis: a look inside the vertebrate photoreceptor. *Dev Dyn* **238**, 2115-2138, doi:10.1002/dvdy.22010 (2009).

20 tom Dieck, S. & Brandstätter, J. H. Ribbon synapses of the retina. *Cell Tissue Res* **326**, 339-346, doi:10.1007/s00441-006-0234-0 (2006).

21 Lenzi, D. & von Gersdorff, H. Structure suggests function: the case for synaptic ribbons as exocytotic nanomachines. *Bioessays* **23**, 831-840, doi:10.1002/bies.1118 (2001).

22 Heidelberger, R., Thoreson, W. B. & Witkovsky, P. Synaptic transmission at retinal ribbon synapses. *Progress in Retinal and Eye Research* **24**, 682-720, doi:https://doi.org/10.1016/j.preteyeres.2005.04.002 (2005).

23 Matthews, G. & Fuchs, P. The diverse roles of ribbon synapses in sensory neurotransmission. *Nature Reviews Neuroscience* **11**, 812-822, doi:10.1038/nrn2924 (2010).

24 Euler, T., Haverkamp, S., Schubert, T. & Baden, T. Retinal bipolar cells: elementary building blocks of vision. *Nature Reviews Neuroscience* **15**, 507-519, doi:10.1038/nrn3783 (2014).

25 Sterling, P. & Matthews, G. Structure and function of ribbon synapses. *Trends Neurosci* **28**, 20-29, doi:10.1016/j.tins.2004.11.009 (2005).

26 Garcia-Gonzalo, F. R. & Reiter, J. F. Scoring a backstage pass: mechanisms of ciliogenesis and ciliary access. *J Cell Biol* **197**, 697-709, doi:10.1083/jcb.201111146 (2012).

27 Satir, P. & Christensen, S. T. Structure and function of mammalian cilia. *Histochem Cell Biol* **129**, 687-693, doi:10.1007/s00418-008-0416-9 (2008).

28 Malicki, J. J. & Johnson, C. A. The Cilium: Cellular Antenna and Central Processing Unit. *Trends Cell Biol* **27**, 126-140, doi:10.1016/j.tcb.2016.08.002 (2017).

29 Lüders, J. & Stearns, T. Microtubule-organizing centres: a re-evaluation. *Nature Reviews Molecular Cell Biology* **8**, 161-167, doi:10.1038/nrm2100 (2007).

30 Nigg, E. A. & Stearns, T. The centrosome cycle: Centriole biogenesis, duplication and inherent asymmetries. *Nature Cell Biology* **13**, 1154-1160, doi:10.1038/ncb2345 (2011).

31 Doxsey, S. Re-evaluating centrosome function. *Nature Reviews Molecular Cell Biology* **2**, 688-698, doi:10.1038/35089575 (2001).

32 Wang, L. & Dynlacht, B. D. The regulation of cilium assembly and disassembly in development and disease. *Development* **145**, dev151407, doi:10.1242/dev.151407 (2018).

33 Satir, P. & Christensen, S. T. Overview of structure and function of mammalian cilia. *Annu Rev Physiol* **69**, 377-400, doi:10.1146/annurev.physiol.69.040705.141236 (2007).

34 May-Simera, H., Nagel-Wolfrum, K. & Wolfrum, U. Cilia - The sensory antennae in the eye. *Prog Retin Eye Res* **60**, 144-180, doi:10.1016/j.preteyeres.2017.05.001 (2017).

35 Sorokin, S. Centrioles and the formation of rudimentary cilia by fibroblasts and smooth muscle cells. *The Journal of cell biology* **15**, 363-377, doi:10.1083/jcb.15.2.363 (1962).

36 Sorokin, S. P. Reconstructions of centriole formation and ciliogenesis in mammalian lungs. *J Cell Sci* **3**, 207-230 (1968).

37 Sedmak, T. & Wolfrum, U. Intraflagellar transport proteins in ciliogenesis of photoreceptor cells. *Biol Cell* **103**, 449-466, doi:10.1042/bc20110034 (2011).

38 Pedersen, L. B., Veland, I. R., Schrøder, J. M. & Christensen, S. T. Assembly of primary cilia. *Developmental Dynamics* **237**, 1993-2006, doi:https://doi.org/10.1002/dvdy.21521 (2008).

39 Obata, S. & Usukura, J. Morphogenesis of the photoreceptor outer segment during postnatal development in the mouse (BALB/c) retina. *Cell Tissue Res* **269**, 39-48, doi:10.1007/bf00384724 (1992).

40 Sjostrand, F. S. The ultrastructure of the outer segments of rods and cones of the eye as revealed by the electron microscope. *J Cell Comp Physiol* **42**, 15-44, doi:10.1002/jcp.1030420103 (1953).

41 Mustafi, D., Engel, A. H. & Palczewski, K. Structure of cone photoreceptors. *Progress in retinal and eye research* **28**, 289-302, doi:10.1016/j.preteyeres.2009.05.003 (2009).

42 Anderson, D. H., Fisher, S. K. & Steinberg, R. H. Mammalian cones: disc shedding, phagocytosis, and renewal. *Invest Ophthalmol Vis Sci* **17**, 117-133 (1978).

43 Besharse, J. C., Hollyfield, J. G. & Rayborn, M. E. Photoreceptor outer segments: accelerated membrane renewal in rods after exposure to light. *Science* **196**, 536-538, doi:10.1126/science.300504 (1977).

44 Carter-Dawson, L. D. & LaVail, M. M. Rods and cones in the mouse retina. I. Structural analysis using light and electron microscopy. *J Comp Neurol* **188**, 245-262, doi:10.1002/cne.901880204 (1979).

45 Kinney, M. S. & Fisher, S. K. The photoreceptors and pigment epithelim of the adult Xenopus retina: morphology and outer segment renewal. *Proc R Soc Lond B Biol Sci* **201**, 131-147, doi:10.1098/rspb.1978.0036 (1978).

46 Kinney, M. S. & Fisher, S. K. The photoreceptors and pigment epithelium of the larval Xenopus retina: morphogenesis and outer segment renewal. *Proc R Soc Lond B Biol Sci* **201**, 149-167, doi:10.1098/rspb.1978.0037 (1978).

47 Steinberg, R. H., Fisher, S. K. & Anderson, D. H. Disc morphogenesis in vertebrate photoreceptors. *J Comp Neurol* **190**, 501-508, doi:10.1002/cne.901900307 (1980).

48 Burgoyne, T. *et al.* Rod disc renewal occurs by evagination of the ciliary plasma membrane that makes cadherin-based contacts with the inner segment. *Proceedings of the National Academy of Sciences* **112**, 15922, doi:10.1073/pnas.1509285113 (2015).

49 Ding, J.-D., Salinas, R. Y. & Arshavsky, V. Y. Discs of mammalian rod photoreceptors form through the membrane evagination mechanism. *Journal of Cell Biology* **211**, 495-502, doi:10.1083/jcb.201508093 (2015).

50 Volland, S. *et al.* Three-dimensional organization of nascent rod outer segment disk membranes. *Proceedings of the National Academy of Sciences* **112**, 14870, doi:10.1073/pnas.1516309112 (2015).

51 Arikawa, K., Molday, L. L., Molday, R. S. & Williams, D. S. Localization of peripherin/rds in the disk membranes of cone and rod photoreceptors: relationship to disk membrane morphogenesis and retinal degeneration. *The Journal of cell biology* **116**, 659-667, doi:10.1083/jcb.116.3.659 (1992).

52 Tokuyasu, K. & Yamada, E. The fine structure of the retina studied with the electron microscope. IV. Morphogenesis of outer segments of retinal rods. *J Biophys Biochem Cytol* **6**, 225-230, doi:10.1083/jcb.6.2.225 (1959).

53 Pugh, E. N., Jr. Photoreceptor disc morphogenesis: The classical evagination model prevails. *J Cell Biol* **211**, 491-493, doi:10.1083/jcb.201510067 (2015).

54 Chuang, J.-Z., Zhao, Y. & Sung, C.-H. SARA-regulated vesicular targeting underlies formation of the light-sensing organelle in mammalian rods. *Cell* **130**, 535-547, doi:10.1016/j.cell.2007.06.030 (2007).

55 Young, R. W. The renewal of photoreceptor cell outer segments. *J Cell Biol* **33**, 61-72, doi:10.1083/jcb.33.1.61 (1967).

56 Young, R. W. & Bok, D. Participation of the retinal pigment epithelium in the rod outer segment renewal process. *J Cell Biol* **42**, 392-403, doi:10.1083/jcb.42.2.392 (1969).

57 Young, R. W. & Droz, B. The renewal of protein in retinal rods and cones. *J Cell Biol* **39**, 169-184, doi:10.1083/jcb.39.1.169 (1968).

58 Anderson, D. H. & Fisher, S. K. Disc shedding in rodlike and conelike photoreceptors of tree squirrels. *Science* **187**, 953, doi:10.1126/science.1145180 (1975).

59 Skiba, N. P. *et al.* Proteomic identification of unique photoreceptor disc components reveals the presence of PRCD, a protein linked to retinal degeneration. *J Proteome Res* **12**, 3010-3018, doi:10.1021/pr4003678 (2013).

60 Cheng, T. *et al.* The effect of peripherin/rds haploinsufficiency on rod and cone photoreceptors. *J Neurosci* **17**, 8118-8128, doi:10.1523/JNEUROSCI.17-21-08118.1997 (1997).

61 Connell, G. *et al.* Photoreceptor peripherin is the normal product of the gene responsible for retinal degeneration in the rds mouse. *Proc Natl Acad Sci U S A* **88**, 723-726, doi:10.1073/pnas.88.3.723 (1991).

62 Démant, P., Iványi, D. & van Nie, R. The map position of the rds gene on the 17th chromosome of the mouse. *Tissue Antigens* **13**, 53-55, doi:10.1111/j.1399-0039.1979.tb01136.x (1979).

63 Hawkins, R. K., Jansen, H. G. & Sanyal, S. Development and degeneration of retina in rds mutant mice: photoreceptor abnormalities in the heterozygotes. *Exp Eye Res* **41**, 701-720, doi:10.1016/0014-4835(85)90179-4 (1985).

64 Sanyal, S., De Ruiter, A. & Hawkins, R. K. Development and degeneration of retina in rds mutant mice: light microscopy. *J Comp Neurol* **194**, 193-207, doi:10.1002/cne.901940110 (1980).

65 Sanyal, S. & Jansen, H. G. Absence of receptor outer segments in the retina of rds mutant mice. *Neurosci Lett* **21**, 23-26, doi:10.1016/0304-3940(81)90051-3 (1981).

66 Molday, R. S., Hicks, D. & Molday, L. Peripherin. A rim-specific membrane protein of rod outer segment discs. *Invest Ophthalmol Vis Sci* **28**, 50-61 (1987).

67 Chang, B. *et al.* Retinal degeneration mutants in the mouse. *Vision Res* **42**, 517-525, doi:10.1016/s0042-6989(01)00146-8 (2002).

68 van Nie, R., Iványi, D. & Démant, P. A new H-2-linked mutation, rds, causing retinal degeneration in the mouse. *Tissue Antigens* **12**, 106-108, doi:10.1111/j.1399-0039.1978.tb01305.x (1978).

69 Travis, G. H., Brennan, M. B., Danielson, P. E., Kozak, C. A. & Sutcliffe, J. G. Identification of a photoreceptor-specific mRNA encoded by the gene responsible for retinal degeneration slow (rds). *Nature* **338**, 70-73, doi:10.1038/338070a0 (1989).

70 Ma, J. *et al.* Retinal degeneration slow (rds) in mouse results from simple insertion of a t haplotype-specific element into protein-coding exon II. *Genomics* **28**, 212-219, doi:10.1006/geno.1995.1133 (1995).

71 Travis, G. H. *et al.* The human retinal degeneration slow (RDS) gene: chromosome assignment and structure of the mRNA. *Genomics* **10**, 733-739, doi:10.1016/0888-7543(91)90457-p (1991).

72 Travis, G. H., Sutcliffe, J. G. & Bok, D. The retinal degeneration slow (rds) gene product is a photoreceptor disc membrane-associated glycoprotein. *Neuron* **6**, 61-70, doi:10.1016/0896-6273(91)90122-g (1991).

73 Stuck, M. W., Conley, S. M. & Naash, M. I. PRPH2/RDS and ROM-1: Historical context, current views and future considerations. *Progress in retinal and eye research* **52**, 47-63, doi:10.1016/j.preteyeres.2015.12.002 (2016).

74 Clarke, G. *et al.* Rom-1 is required for rod photoreceptor viability and the regulation of disk morphogenesis. *Nat Genet* **25**, 67-73, doi:10.1038/75621 (2000).

75 Humphries, M. M. *et al.* Retinopathy induced in mice by targeted disruption of the rhodopsin gene. *Nature Genetics* **15**, 216-219, doi:10.1038/ng0297-216 (1997).

76 Lem, J. *et al.* Morphological, physiological, and biochemical changes in rhodopsin knockout mice. *Proceedings of the National Academy of Sciences* **96**, 736, doi:10.1073/pnas.96.2.736 (1999).

77 Papermaster, D. S. & Dreyer, W. J. Rhodopsin content in the outer segment membranes of bovine and frog retinal rods. *Biochemistry* **13**, 2438-2444, doi:10.1021/bi00708a031 (1974).

78 Fotiadis, D. *et al.* Rhodopsin dimers in native disc membranes. *Nature* **421**, 127-128, doi:10.1038/421127a (2003).

79 Rakshit, T., Senapati, S., Sinha, S., Whited, A. M. & Park, P. S. H. Rhodopsin Forms Nanodomains in Rod Outer Segment Disc Membranes of the Cold-Blooded Xenopus laevis. *PLOS ONE* **10**, e0141114, doi:10.1371/journal.pone.0141114 (2015).

80 Liang, Y. *et al.* Organization of the G Protein-coupled Receptors Rhodopsin and Opsin in Native Membranes. *Journal of Biological Chemistry* **278**, 21655-21662, doi:10.1074/jbc.M302536200 (2003).

81 Wen, X. H. *et al.* Overexpression of rhodopsin alters the structure and photoresponse of rod photoreceptors. *Biophys J* **96**, 939-950, doi:10.1016/j.bpj.2008.10.016 (2009).

82 Makino, C. L. *et al.* Rhodopsin expression level affects rod outer segment morphology and photoresponse kinetics. *PLoS One* **7**, e37832, doi:10.1371/journal.pone.0037832 (2012).

83 Liang, Y. *et al.* Rhodopsin Signaling and Organization in Heterozygote Rhodopsin Knockout Mice. *J Biol Chem* **279**, 48189-48196 (2004).

84 Rakshit, T. & Park, P. S. Impact of reduced rhodopsin expression on the structure of rod outer segment disc membranes. *Biochemistry* **54**, 2885-2894, doi:10.1021/acs.biochem.5b00003 (2015).

85 Arshavsky, V. Y., Lamb, T. D. & Pugh, E. N., Jr. G proteins and phototransduction. *Annu Rev Physiol* **64**, 153-187, doi:10.1146/annurev.physiol.64.082701.102229 (2002).

86 Fu, Y. in *Webvision: The Organization of the Retina and Visual System* (eds H. Kolb, E. Fernandez, & R. Nelson) (University of Utah Health Sciences Center Copyright: © 2021 Webvision . 1995).

87 Lamb, T. D. & Pugh, E. N., Jr. Phototransduction, Dark Adaptation, and Rhodopsin Regeneration The Proctor Lecture. *Investigative Ophthalmology & Visual Science* **47**, 5138-5152, doi:10.1167/iovs.06-0849 (2006).

88 Baker, S. A. & Kerov, V. in *Current Topics in Membranes* Vol. 72 (ed Vann Bennett) 231-265 (Academic Press, 2013).

89 MacLeish, P. R. & Nurse, C. A. Ion Channel Compartments in Photoreceptors: Evidence From Salamander Rods With Intact and Ablated Terminals. *Journal of Neurophysiology* **98**, 86-95, doi:10.1152/jn.00775.2006 (2007).

90 Hubbard, R. & Wald, G. Cis-trans isomers of vitamin A and retinene in the rhodopsin system. *J Gen Physiol* **36**, 269-315, doi:10.1085/jgp.36.2.269 (1952).

91 Wald, G. The Chemistry of Rod Vision. *Science* **113**, 287, doi:10.1126/science.113.2933.287 (1951).

92 Kawamura, S. & Tachibanaki, S. in *Vertebrate Photoreceptors: Functional Molecular Bases* (eds Takahisa Furukawa, James B. Hurley, & Satoru Kawamura) 23-45 (Springer Japan, 2014).

93 Noel, J. P., Hamm, H. E. & Sigler, P. B. The 2.2 Å crystal structure of transducin-α complexed with GTPγS. *Nature* **366**, 654-663, doi:10.1038/366654a0 (1993).

94 Srivastava, D. *et al.* Transducin Partners Outside the Phototransduction Pathway. *Frontiers in Cellular Neuroscience* **14**, doi:10.3389/fncel.2020.589494 (2020).

95 Kuksa, V., Imanishi, Y., Batten, M., Palczewski, K. & Moise, A. R. Retinoid cycle in the vertebrate retina: experimental approaches and mechanisms of isomerization. *Vision Research* **43**, 2959-2981, doi:https://doi.org/10.1016/S0042-6989(03)00482-6 (2003).

96 Wald, G. Molecular basis of visual excitation. *Science* **162**, 230-239, doi:10.1126/science.162.3850.230 (1968).

97 Palczewski, K. & Kiser, P. D. Shedding new light on the generation of the visual chromophore. *Proceedings of the National Academy of Sciences* **117**, 19629, doi:10.1073/pnas.2008211117 (2020).

98 Parker, R. O. & Crouch, R. K. Retinol dehydrogenases (RDHs) in the visual cycle. *Experimental eye research* **91**, 788-792, doi:10.1016/j.exer.2010.08.013 (2010).

99 Baehr, W., Wu, S. M., Bird, A. C. & Palczewski, K. The retinoid cycle and retina disease. *Vision Research* **43**, 2957-2958, doi:https://doi.org/10.1016/j.visres.2003.10.001 (2003).

100 Lenis, T. L. *et al.* Expression of ABCA4 in the retinal pigment epithelium and its implications for Stargardt macular degeneration. *Proceedings of the National Academy of Sciences* **115**, E11120, doi:10.1073/pnas.1802519115 (2018).

101 Ruiz, A. *et al.* Molecular and Biochemical Characterization of Lecithin Retinol Acyltransferase *. *Journal of Biological Chemistry* **274**, 3834-3841, doi:10.1074/jbc.274.6.3834 (1999).

102 Jin, M., Li, S., Moghrabi, W. N., Sun, H. & Travis, G. H. Rpe65 is the retinoid isomerase in bovine retinal pigment epithelium. *Cell* **122**, 449-459, doi:10.1016/j.cell.2005.06.042 (2005).

103 Kühn, H. & Wilden, U. Deactivation of photoactivated rhodopsin by rhodopsin-kinase and arrestin. *J Recept Res* **7**, 283-298, doi:10.3109/10799898709054990 (1987).

104 Ohguro, H., Van Hooser, J. P., Milam, A. H. & Palczewski, K. Rhodopsin phosphorylation and dephosphorylation in vivo. *J Biol Chem* **270**, 14259-14262, doi:10.1074/jbc.270.24.14259 (1995).

105 Makino, E. R., Handy, J. W., Li, T. & Arshavsky, V. Y. The GTPase activating factor for transducin in rod photoreceptors is the complex between RGS9 and type 5 G protein beta subunit. *Proc Natl Acad Sci U S A* **96**, 1947-1952, doi:10.1073/pnas.96.5.1947 (1999).

106 He, W., Cowan, C. W. & Wensel, T. G. RGS9, a GTPase accelerator for phototransduction. *Neuron* **20**, 95-102, doi:10.1016/s0896-6273(00)80437-7 (1998).

107 Hu, G. & Wensel, T. G. R9AP, a membrane anchor for the photoreceptor GTPase accelerating protein, RGS9-1. *Proc Natl Acad Sci U S A* **99**, 9755-9760, doi:10.1073/pnas.152094799 (2002).

108 Molday, R. S. & Kaupp, U. B. in *Handbook of Biological Physics* Vol. 3 (eds D. G. Stavenga, W. J. DeGrip, & E. N. Pugh) 143-181 (North-Holland, 2000).

109 Nakatani, K. & Yau, K. W. Calcium and magnesium fluxes across the plasma membrane of the toad rod outer segment. *The Journal of Physiology* **395**, 695-729, doi:https://doi.org/10.1113/jphysiol.1988.sp016942 (1988).

110 Kang, K. *et al.* Assembly of retinal rod or cone Na(+)/Ca(2+)-K(+) exchanger oligomers with cGMP-gated channel subunits as probed with heterologously expressed cDNAs. *Biochemistry* **42**, 4593-4600, doi:10.1021/bi027276z (2003).

111 Reiländer, H. *et al.* Primary structure and functional expression of the Na/Ca,K-exchanger from bovine rod photoreceptors. *The EMBO Journal* **11**, 1689-1695, doi:https://doi.org/10.1002/j.1460-2075.1992.tb05219.x (1992).

112 Ames, A., 3rd, Li, Y. Y., Heher, E. C. & Kimble, C. R. Energy metabolism of rabbit retina as related to function: high cost of Na+ transport. *J Neurosci* **12**, 840-853, doi:10.1523/jneurosci.12-03-00840.1992 (1992).

113 Bader, C. R., Bertrand, D. & Schwartz, E. A. Voltage-activated and calcium-activated currents studied in solitary rod inner segments from the salamander retina. *The Journal of Physiology* **331**, 253-284, doi:https://doi.org/10.1113/jphysiol.1982.sp014372 (1982).

114 Maricq, A. V. & Korenbrot, J. I. Potassium currents in the inner segment of single retinal cone photoreceptors. *J Neurophysiol* **64**, 1929-1940, doi:10.1152/jn.1990.64.6.1929 (1990).

115 Barrow, A. J. & Wu, S. M. Low-Conductance HCN1 Ion Channels Augment the Frequency Response of Rod and Cone Photoreceptors. *The Journal of Neuroscience* **29**, 5841, doi:10.1523/JNEUROSCI.5746-08.2009 (2009).

116 Seeliger, M. W. *et al.* Modulation of rod photoreceptor output by HCN1 channels is essential for regular mesopic cone vision. *Nature Communications* **2**, 532, doi:10.1038/ncomms1540 (2011).

117 Barrow, A. J. & Wu, S. M. Complementary conductance changes by Ikx and Ih contribute to membrane impedance stability during the rod light response. *Channels* **3**, 301-307, doi:10.4161/chan.3.5.9454 (2009).

118 Cordeiro, S., Guseva, D., Wulfsen, I. & Bauer, C. K. Expression Pattern of Kv11 (Ether à-go-go-Related Gene; erg) K+ Channels in the Mouse Retina. *PLOS ONE* **6**, e29490, doi:10.1371/journal.pone.0029490 (2011).

119 Klumpp, D. J., Song, E. J. & Pinto, L. H. Identification and localization of K+ channels in the mouse retina. *Visual Neuroscience* **12**, 1177-1190, doi:10.1017/S0952523800006805 (1995).

120 Zhang, X., Yang, D. & Hughes, B. A. KCNQ5/Kv7.5 potassium channel expression and subcellular localization in primate retinal pigment epithelium and neural retina.

American Journal of Physiology-Cell Physiology **301**, C1017-C1026, doi:10.1152/ajpcell.00185.2011 (2011).

121 Czirják, G., Tóth, Z. E. & Enyedi, P. Characterization of the Heteromeric Potassium Channel Formed by Kv2.1 and the Retinal Subunit Kv8.2 in Xenopus Oocytes. *Journal of Neurophysiology* **98**, 1213-1222, doi:10.1152/jn.00493.2007 (2007).

122 Frings, S. *et al.* Characterization of Ether-à-go-go Channels Present in Photoreceptors Reveals Similarity to IKx, a K+ Current in Rod Inner Segments. *Journal of General Physiology* **111**, 583-599, doi:10.1085/jgp.111.4.583 (1998).

123 Mercer, A. J., Chen, M. & Thoreson, W. B. Lateral Mobility of Presynaptic L-Type Calcium Channels at Photoreceptor Ribbon Synapses. *The Journal of Neuroscience* **31**, 4397, doi:10.1523/JNEUROSCI.5921-10.2011 (2011).

124 Thoreson, W. B., Nitzan, R. O. N. & Miller, R. F. Chloride efflux inhibits single calcium channel open probability in vertebrate photoreceptors: Chloride imaging and cell-attached patch-clamp recordings. *Visual Neuroscience* **17**, 197-206, doi:10.1017/S0952523800172025 (2000).

125 Thoreson, W. B. & Stella, S. L. Anion modulation of calcium current voltage dependence and amplitude in salamander rods. *Biochim Biophys Acta* **1464**, 142-150, doi:10.1016/s0005-2736(99)00257-6 (2000).

126 Singh, N. *et al.* Prevention of Age-Related Macular Degeneration. *The Asia-Pacific Journal of Ophthalmology* **6** (2017).

127 Veltel, S., Gasper, R., Eisenacher, E. & Wittinghofer, A. The retinitis pigmentosa 2 gene product is a GTPase-activating protein for Arf-like 3. *Nature Structural & Molecular Biology* **15**, 373-380, doi:10.1038/nsmb.1396 (2008).

128 Daiger, S., Rossiter, B., Greenberg, J., Christoffels, A. & Hide, W. Data services and software for identifying genes and mutations causing retinal degeneration. *Invest Ophthalmol Vis Sci* **39** (1998).

129 Newton, F. & Megaw, R. Mechanisms of Photoreceptor Death in Retinitis Pigmentosa. *Genes* **11**, doi:10.3390/genes11101120 (2020).

130 O'Neal, T. B. & Luther, E. E. in *StatPearls* (StatPearls Publishing Copyright © 2020, StatPearls Publishing LLC., 2020).

131 den Hollander, A. I., Roepman, R., Koenekoop, R. K. & Cremers, F. P. M. Leber congenital amaurosis: Genes, proteins and disease mechanisms. *Progress in Retinal and Eye Research* **27**, 391-419, doi:https://doi.org/10.1016/j.preteyeres.2008.05.003 (2008).

132 Cremers, F. P. M., van den Hurk, J. A. J. M. & den Hollander, A. I. Molecular genetics of Leber congenital amaurosis. *Hum Mol Genet* **11**, 1169-1176, doi:10.1093/hmg/11.10.1169 (2002).

133 Mitchell, P., Liew, G., Gopinath, B. & Wong, T. Y. Age-related macular degeneration. *The Lancet* **392**, 1147-1159, doi:https://doi.org/10.1016/S0140-6736(18)31550-2 (2018).

134 Kolb, H. in *Webvision: The Organization of the Retina and Visual System* (eds H. Kolb, E. Fernandez, & R. Nelson) (University of Utah Health Sciences Center Copyright: © 2021 Webvision . 1995).

135 Storti, F. *et al.* Impaired ABCA1/ABCG1-mediated lipid efflux in the mouse retinal pigment epithelium (RPE) leads to retinal degeneration. *eLife* **8**, e45100, doi:10.7554/eLife.45100 (2019).

136 Huang, S. S. Future Vision 2020 and Beyond-5 Critical Trends in Eye Research. *Asia Pac J Ophthalmol (Phila)* **9**, 180-185, doi:10.1097/APO.0000000000000299 (2020).

137 Ziccardi, L. *et al.* Gene Therapy in Retinal Dystrophies. *Int J Mol Sci* **20**, 5722, doi:10.3390/ijms20225722 (2019).

138 Allon, G. *et al.* PRCD is concentrated at the base of photoreceptor outer segments and is involved in outer segment disc formation. *Hum Mol Genet* **28**, 4078-4088, doi:10.1093/hmg/ddz248 (2019).

139 Spencer, W. J. *et al.* PRCD is essential for high-fidelity photoreceptor disc formation. *Proc Natl Acad Sci U S A* **116**, 13087-13096, doi:10.1073/pnas.1906421116 (2019).

140 Murphy, J. & Kolandaivelu, S. Palmitoylation of Progressive Rod-Cone Degeneration (PRCD) Regulates Protein Stability and Localization. *J Biol Chem* **291**, 23036-23046, doi:10.1074/jbc.M116.742767 (2016).

141 Spencer, W. J. *et al.* Progressive Rod–Cone Degeneration (PRCD) Protein Requires N-Terminal S-Acylation and Rhodopsin Binding for Photoreceptor Outer Segment Localization and Maintaining Intracellular Stability. *Biochemistry* **55**, 5028-5037, doi:10.1021/acs.biochem.6b00489 (2016).

142 Gelabert-Baldrich, M. *et al.* Dynamics of KRas on endosomes: involvement of acidic phospholipids in its association. *Faseb j* **28**, 3023-3037, doi:10.1096/fj.13-241158 (2014).

143 Williams, C. L. The polybasic region of Ras and Rho family small GTPases: a regulator of protein interactions and membrane association and a site of nuclear localization signal sequences. *Cell Signal* **15**, 1071-1080, doi:10.1016/s0898-6568(03)00098-6 (2003).

144 Matt, L., Kim, K., Chowdhury, D. & Hell, J. W. Role of Palmitoylation of Postsynaptic Proteins in Promoting Synaptic Plasticity. *Frontiers in Molecular Neuroscience* **12**, doi:10.3389/fnmol.2019.00008 (2019).

145 Mazelova, J. *et al.* Ciliary targeting motif VxPx directs assembly of a trafficking module through Arf4. *Embo j* **28**, 183-192, doi:10.1038/emboj.2008.267 (2009).

146 Spencer, W. J. *The Role of PRCD in Building the Photoreceptor Outer Segment*, Dissertation, Duke University, (2017).

147 Zangerl, B. *et al.* Identical mutation in a novel retinal gene causes progressive rod-cone degeneration in dogs and retinitis pigmentosa in humans. *Genomics* **88**, 551-563, doi:10.1016/j.ygeno.2006.07.007 (2006).

148 Pach, J., Kohl, S., Gekeler, F. & Zobor, D. Identification of a novel mutation in the PRCD gene causing autosomal recessive retinitis pigmentosa in a Turkish family. *Mol Vis* **19**, 1350-1355 (2013).

149 Nevet, M. J., Shalev, S. A., Zlotogora, J., Mazzawi, N. & Ben-Yosef, T. Identification of a prevalent founder mutation in an Israeli Muslim Arab village confirms the role of PRCD in the aetiology of retinitis pigmentosa in humans. *J Med Genet* **47**, 533-537, doi:10.1136/jmg.2009.073619 (2010).

150 Remez, L., Zobor, D., Kohl, S. & Ben-Yosef, T. The progressive rod-cone degeneration (PRCD) protein is secreted through the conventional ER/Golgi-

dependent pathway. *Exp Eye Res* **125**, 217-225, doi:10.1016/j.exer.2014.06.017 (2014).

151 Aguirre, G., Alligood, J., O'Brien, P. & Buyukmihci, N. Pathogenesis of progressive rod-cone degeneration in miniature poodles. *Investigative Ophthalmology & Visual Science* **23**, 610-630 (1982).

152 Aguirre, G. & O'Brien, P. Morphological and biochemical studies of canine progressive rod-cone degeneration. 3H-fucose autoradiography. *Investigative Ophthalmology & Visual Science* **27**, 635-655 (1986).

153 Aguirre, G. D. & Acland, G. M. Variation in retinal degeneration phenotype inherited at the prcd locus. *Experimental Eye Research* **46**, 663-687, doi:https://doi.org/10.1016/S0014-4835(88)80055-1 (1988).

154 Aguirre, G. D. & Rubin, L. F. Progressive retinal atrophy in the Miniature Poodle: an electrophysiologic study. *Journal of the American Veterinary Medical Association* **160**, 191-201 (1972).

155 Goldstein, O. *et al.* Linkage disequilibrium mapping in domestic dog breeds narrows the progressive rod-cone degeneration interval and identifies ancestral disease-transmitting chromosome. *Genomics* **88**, 541-550, doi:10.1016/j.ygeno.2006.05.013 (2006).

156 Downs, L. M., Hitti, R., Pregnolato, S. & Mellersh, C. S. Genetic screening for PRA-associated mutations in multiple dog breeds shows that PRA is heterogeneous within and between breeds. *Veterinary Ophthalmology* **17**, 126-130, doi:10.1111/vop.12122 (2014).

157 Huang, J. C., Chesselet, M.-F. & Aguirre, G. D. Decreased Opsin mRNA and Immunoreactivity in Progressive Rod-Cone Degeneration (prcd): Cytochemical Studies of Early Disease and Degeneration. *Experimental Eye Research* **58**, 17-30, doi:https://doi.org/10.1006/exer.1994.1191 (1994).

158 Gropp, K. E., Huang, J. C. & Aguirre, G. D. Differential Expression of Photoreceptor-Specific Proteins During Disease and Degeneration in the Progressive Rod-Cone Degeneration (prcd) Retina. *Experimental Eye Research* **64**, 875-886, doi:https://doi.org/10.1006/exer.1996.0257 (1997).

159 Mieziewska, K., van Veen, T. & Aguirre, G. D. Structural changes of the interphotoreceptor matrix in an inherited retinal degeneration: a lectin cytochemical study of progressive rod-cone degeneration. *Invest Ophthalmol Vis Sci* **34**, 3056-3067 (1993).

160 Resh, M. D. Fatty acylation of proteins: The long and the short of it. *Prog Lipid Res* **63**, 120-131, doi:10.1016/j.plipres.2016.05.002 (2016).

161 Aicart-Ramos, C., Valero, R. A. & Rodriguez-Crespo, I. Protein palmitoylation and subcellular trafficking. *Biochim Biophys Acta* **1808**, 2981-2994, doi:10.1016/j.bbamem.2011.07.009 (2011).

162 Linder, M. E. & Deschenes, R. J. Palmitoylation: policing protein stability and traffic. *Nature Reviews Molecular Cell Biology* **8**, 74-84, doi:10.1038/nrm2084 (2007).

163 Munday, A. D. & López, J. A. Posttranslational protein palmitoylation: promoting platelet purpose. *Arterioscler Thromb Vasc Biol* **27**, 1496-1499, doi:10.1161/atvbaha.106.136226 (2007).

164 Mitchell, D. A., Vasudevan, A., Linder, M. E. & Deschenes, R. J. Thematic review series: Lipid Posttranslational Modifications. Protein palmitoylation by a family of DHHC protein S-acyltransferases. *Journal of Lipid Research* **47**, 1118-1127, doi:10.1194/jlr.R600007-JLR200 (2006).

165 Baekkeskov, S. & Kanaani, J. Palmitoylation cycles and regulation of protein function (Review). *Mol Membr Biol* **26**, 42-54, doi:10.1080/09687680802680108 (2009).

166 Plain, F. *et al.* Control of protein palmitoylation by regulating substrate recruitment to a zDHHC-protein acyltransferase. *Communications Biology* **3**, 411, doi:10.1038/s42003-020-01145-3 (2020).

167 Camp, L. A., Verkruyse, L. A., Afendis, S. J., Slaughter, C. A. & Hofmann, S. L. Molecular cloning and expression of palmitoyl-protein thioesterase. *Journal of Biological Chemistry* **269**, 23212-23219 (1994).

168 Soyombo, A. A. & Hofmann, S. L. Molecular Cloning and Expression of Palmitoyl-protein Thioesterase 2 (PPT2), a Homolog of Lysosomal Palmitoyl-protein

Thioesterase with a Distinct Substrate Specificity. *Journal of Biological Chemistry* **272**, 27456-27463, doi:10.1074/jbc.272.43.27456 (1997).

169 Clausen, M. V., Hilbers, F. & Poulsen, H. The Structure and Function of the Na,K-ATPase Isoforms in Health and Disease. *Front Physiol* **8**, 371, doi:10.3389/fphys.2017.00371 (2017).

170 Geering, K. The functional role of beta subunits in oligomeric P-type ATPases. *J Bioenerg Biomembr* **33**, 425-438, doi:10.1023/a:1010623724749 (2001).

171 Ackermann, U. & Geering, K. Mutual dependence of Na,K-ATPase alpha- and beta-subunits for correct posttranslational processing and intracellular transport. *FEBS Lett* **269**, 105-108, doi:10.1016/0014-5793(90)81130-g (1990).

172 Tokhtaeva, E., Sachs, G. & Vagin, O. Assembly with the Na,K-ATPase alpha(1) subunit is required for export of beta(1) and beta(2) subunits from the endoplasmic reticulum. *Biochemistry* **48**, 11421-11431, doi:10.1021/bi901438z (2009).

173 Tokhtaeva, E., Clifford, R. J., Kaplan, J. H., Sachs, G. & Vagin, O. Subunit Isoform Selectivity in Assembly of Na,K-ATPase α-β Heterodimers *. *Journal of Biological Chemistry* **287**, 26115-26125, doi:10.1074/jbc.M112.370734 (2012).

174 Blanco, G. & Mercer, R. W. Isozymes of the Na-K-ATPase: heterogeneity in structure, diversity in function. *American Journal of Physiology-Renal Physiology* **275**, F633-F650, doi:10.1152/ajprenal.1998.275.5.F633 (1998).

175 Vagin, O., Tokhtaeva, E. & Sachs, G. The role of the beta1 subunit of the Na,K-ATPase and its glycosylation in cell-cell adhesion. *J Biol Chem* **281**, 39573-39587, doi:10.1074/jbc.M606507200 (2006).

176 Tokhtaeva, E., Munson, K., Sachs, G. & Vagin, O. N-glycan-dependent quality control of the Na,K-ATPase beta(2) subunit. *Biochemistry* **49**, 3116-3128, doi:10.1021/bi100115a (2010).

177 Sweadner, K. J. & Rael, E. The FXYD gene family of small ion transport regulators or channels: cDNA sequence, protein signature sequence, and expression. *Genomics* **68**, 41-56, doi:10.1006/geno.2000.6274 (2000).

178 Geering, K. Function of FXYD proteins, regulators of Na, K-ATPase. *J Bioenerg Biomembr* **37**, 387-392, doi:10.1007/s10863-005-9476-x (2005).

179 Aperia, A., Akkuratov, E. E., Fontana, J. M. & Brismar, H. Na+-K+-ATPase, a new class of plasma membrane receptors. *American Journal of Physiology-Cell Physiology* **310**, C491-C495, doi:10.1152/ajpcell.00359.2015 (2016).

180 Plössl, K. *et al.* Retinoschisin is linked to retinal Na/K-ATPase signaling and localization. *Mol Biol Cell* **28**, 2178-2189, doi:10.1091/mbc.E17-01-0064 (2017).

181 Li, Z. & Langhans, S. A. Transcriptional regulators of Na,K-ATPase subunits. *Frontiers in Cell and Developmental Biology* **3**, doi:10.3389/fcell.2015.00066 (2015).

182 Vagin, O., Dada, L. A., Tokhtaeva, E. & Sachs, G. The Na-K-ATPase α1β1 heterodimer as a cell adhesion molecule in epithelia. *American Journal of Physiology-Cell Physiology* **302**, C1271-C1281, doi:10.1152/ajpcell.00456.2011 (2012).

183 Schneider, B. G. & Kraig, E. Na+, K(+)-ATPase of the photoreceptor: selective expression of alpha 3 and beta 2 isoforms. *Exp Eye Res* **51**, 553-564, doi:10.1016/0014-4835(90)90086-a (1990).

184 Schneider, B. G., Shyjan, A. W. & Levenson, R. Co-localization and polarized distribution of Na,K-ATPase alpha 3 and beta 2 subunits in photoreceptor cells. *J Histochem Cytochem* **39**, 507-517, doi:10.1177/39.4.1848572 (1991).

185 Wetzel, R. K., Arystarkhova, E. & Sweadner, K. J. Cellular and Subcellular Specification of Na,K-ATPase α and β Isoforms in the Postnatal Development of Mouse Retina. *The Journal of Neuroscience* **19**, 9878, doi:10.1523/JNEUROSCI.19-22-09878.1999 (1999).

186 Stahl, W. L. & Baskin, D. G. Immunocytochemical localization of Na+,K+ adenosine triphosphatase in the rat retina. *J Histochem Cytochem* **32**, 248-250, doi:10.1177/32.2.6319483 (1984).

187 Antonicek, H., Persohn, E. & Schachner, M. Biochemical and functional characterization of a novel neuron-glia adhesion molecule that is involved in neuronal migration. *Journal of Cell Biology* **104**, 1587-1595, doi:10.1083/jcb.104.6.1587 (1987).

188 Gloor, S. *et al.* The adhesion molecule on glia (AMOG) is a homologue of the beta subunit of the Na,K-ATPase. *J Cell Biol* **110**, 165-174, doi:10.1083/jcb.110.1.165 (1990).

189 Mobasheri, A. *et al.* Na+, K+-ATPase isozyme diversity; comparative biochemistry and physiological implications of novel functional interactions. *Biosci Rep* **20**, 51-91, doi:10.1023/a:1005580332144 (2000).

190 Pagliusi, S. *et al.* Identification of a cDNA clone specific for the neural cell adhesion molecule AMOG. *Journal of Neuroscience Research* **22**, 113-119, doi:https://doi.org/10.1002/jnr.490220202 (1989).

191 Antonicek, H. & Schachner, M. The adhesion molecule on glia (AMOG) incorporated into lipid vesicles binds to subpopulations of neurons. *J Neurosci* **8**, 2961-2966, doi:10.1523/jneurosci.08-08-02961.1988 (1988).

192 Müller-Husmann, G., Gloor, S. & Schachner, M. Functional characterization of beta isoforms of murine Na,K-ATPase. The adhesion molecule on glia (AMOG/beta 2), but not beta 1, promotes neurite outgrowth. *J Biol Chem* **268**, 26260-26267 (1993).

193 Magyar, J. P. *et al.* Degeneration of neural cells in the central nervous system of mice deficient in the gene for the adhesion molecule on Glia, the beta 2 subunit of murine Na,K-ATPase. *J Cell Biol* **127**, 835-845, doi:10.1083/jcb.127.3.835 (1994).

194 Weber, P., Bartsch, U., Schachner, M. & Montag, D. Na,K-ATPase subunit beta1 knock-in prevents lethality of beta2 deficiency in mice. *J Neurosci* **18**, 9192-9203, doi:10.1523/jneurosci.18-22-09192.1998 (1998).

195 Friedrich, U. *et al.* The Na/K-ATPase is obligatory for membrane anchorage of retinoschisin, the protein involved in the pathogenesis of X-linked juvenile retinoschisis. *Hum Mol Genet* **20**, 1132-1142, doi:10.1093/hmg/ddq557 (2011).

196 Molday, L. L., Wu, W. W. & Molday, R. S. Retinoschisin (RS1), the protein encoded by the X-linked retinoschisis gene, is anchored to the surface of retinal photoreceptor and bipolar cells through its interactions with a Na/K ATPase-SARM1 complex. *J Biol Chem* **282**, 32792-32801, doi:10.1074/jbc.M706321200 (2007).

197 Gehrig, A. E., Warneke-Wittstock, R., Sauer, C. G. & Weber, B. H. F. Isolation and characterization of the murine X-linked juvenile retinoschisis (Rs1h) gene. *Mammalian Genome* **10**, 303-307, doi:10.1007/s003359900991 (1999).

198 Sauer, C. G. *et al.* Positional cloning of the gene associated with X-linked juvenile retinoschisis. *Nature Genetics* **17**, 164-170, doi:10.1038/ng1097-164 (1997).

199 George, N. D., Yates, J. R., Bradshaw, K. & Moore, A. T. Infantile presentation of X linked retinoschisis. *British Journal of Ophthalmology* **79**, 653, doi:10.1136/bjo.79.7.653 (1995).

200 Rao, P., Dedania, V. S. & Drenser, K. A. Congenital X-Linked Retinoschisis: An Updated Clinical Review. *The Asia-Pacific Journal of Ophthalmology* **7** (2018).

201 Tantri, A. *et al.* X-linked retinoschisis: A clinical and molecular genetic review. *Survey of Ophthalmology* **49**, 214-230, doi:https://doi.org/10.1016/j.survophthal.2003.12.007 (2004).

202 Molday, L. L., Hicks, D., Sauer, C. G., Weber, B. H. F. & Molday, R. S. Expression of X-Linked Retinoschisis Protein RS1 in Photoreceptor and Bipolar Cells. *Investigative Ophthalmology & Visual Science* **42**, 816-825 (2001).

203 Plössl, K. *et al.* Identification of the retinoschisin-binding site on the retinal Na/K-ATPase. *PLOS ONE* **14**, e0216320, doi:10.1371/journal.pone.0216320 (2019).

204 Plössl, K., Weber, B. H. F. & Friedrich, U. The X-linked juvenile retinoschisis protein retinoschisin is a novel regulator of mitogen-activated protein kinase signalling and apoptosis in the retina. *J Cell Mol Med* **21**, 768-780, doi:10.1111/jcmm.13019 (2017).

205 Carecchio, M., Zorzi, G., Ragona, F., Zibordi, F. & Nardocci, N. ATP1A3-related disorders: An update. *Eur J Paediatr Neurol* **22**, 257-263, doi:10.1016/j.ejpn.2017.12.009 (2018).

206 Heinzen, E. L. *et al.* Distinct neurological disorders with ATP1A3 mutations. *Lancet Neurol* **13**, 503-514, doi:10.1016/s1474-4422(14)70011-0 (2014).

207 Holm, T. H. & Lykke-Hartmann, K. Insights into the Pathology of the α3 Na(+)/K(+)-ATPase Ion Pump in Neurological Disorders; Lessons from Animal Models. *Frontiers in physiology* **7**, 209-209, doi:10.3389/fphys.2016.00209 (2016).

208 Maas, R. P., Schieving, J. H., Schouten, M., Kamsteeg, E. J. & van de Warrenburg, B. P. The Genetic Homogeneity of CAPOS Syndrome: Four New Patients With the c.2452G>A (p.Glu818Lys) Mutation in the ATP1A3 Gene. *Pediatr Neurol* **59**, 71-75.e71, doi:10.1016/j.pediatrneurol.2016.02.010 (2016).

209 Zhou, G. H. *et al.* ATP1A3 mutation as a candidate cause of autosomal dominant cone-rod dystrophy. *Hum Genet* **139**, 1391-1401, doi:10.1007/s00439-020-02182-y (2020).

Chapter 2 – Loss of PRCD alters number and packaging density of rhodopsin in rod photoreceptor disc membranes

Original article – *Scientific Reports*

Emily R. Sechrest[1,2], Joseph Murphy[2,3], Subhadip Senapati[4], Andrew F.X. Goldberg[5], Paul S.-H. Park[4], Saravanan Kolandaivelu[2,3,*]

[1]Department of Pharmaceutical Sciences, [2]Department of Ophthalmology and Visual Sciences, [3]Department of Biochemistry, West Virginia University, Morgantown, WV 26506, USA.

[4]Department of Ophthalmology and Visual Sciences, Case Western Reserve University, Cleveland, OH 44106, USA.

[5]Eye Research Institute, Oakland University, Rochester, MI 48309, USA.

***Corresponding author:** Saravanan Kolandaivelu, Departments of Ophthalmology and Visual Sciences and Biochemistry; Eye Institute, One Medical Center Drive, West Virginia University, Morgantown, WV 26506-9193, USA. Email: kolandaivelus@wvumedicine.org; Tel: 304 598 5484; Fax: 304 598 6928.

2.1 Abstract

Progressive rod-cone degeneration (PRCD) is a small protein localized to photoreceptor outer segment (OS) disc membranes. Several mutations in PRCD are linked to retinitis pigmentosa (RP) in canines and humans, and while recent studies have established that PRCD is required for high fidelity disc morphogenesis, its precise role in this process remains a mystery. To better understand the part which PRCD plays in disease progression as well as its contribution to photoreceptor OS disc morphogenesis, we generated a *Prcd*-KO animal model using CRISPR/Cas9. Loss of PRCD from the retina results in reduced visual function accompanied by slow rod photoreceptor degeneration. We observed a significant decrease in rhodopsin levels in *Prcd*-KO retina prior to photoreceptor degeneration. Furthermore, ultrastructural analysis demonstrates that rod photoreceptors lacking PRCD display disoriented and dysmorphic OS disc membranes. Strikingly, atomic force microscopy reveals that many disc membranes in *Prcd*-KO rod photoreceptor neurons are irregular, containing fewer rhodopsin molecules and decreased rhodopsin packing density compared to wild-type discs. This study strongly suggests an important role for PRCD in regulation of rhodopsin incorporation and packaging density into disc membranes, a process which, when dysregulated, likely gives rise to the visual defects observed in patients with PRCD-associated RP.

2.2 Introduction

Rod and cone photoreceptor neurons contain a distinct membrane-rich structure at the cilium known as the outer segment (OS). Each rod OS (ROS) is packed with over 1,000 tightly stacked, double membranous discs which house phototransduction proteins required for normal photoreceptor function and structural stability[1-6]. In this study, we focus on progressive rod-cone degeneration (PRCD), a small 54 amino acid (53 amino acid in mice) protein which is specifically localized to OS disc membranes[7]. The most common mutation in PRCD is a C2Y mutation, which is linked to retinitis pigmentosa (RP) in humans and progressive retinal atrophy (PRA) in over 29 dog breeds[8-10]. RP and PRA are both hereditary retinal disorders which result in degeneration of rods followed by cones, leading eventually to complete blindness[11-13]. In canines and humans, PRCD-associated disease is characterized by progressive loss of vision and severe disorganization of OS disc membranes [10,14-16].

Previous studies, including ours, have demonstrated that PRCD undergoes palmitoylation, a post-translational lipid modification. Loss of palmitoylation in PRCD-C2Y results in mislocalization of PRCD to the inner segment (IS), where it is rapidly degraded[17,18]. Additionally, PRCD has been shown to interact with rhodopsin, a highly abundant ROS protein which is responsible for initiation of phototransduction[18-20]. While the significance of this interaction is not well understood, many animal models containing mutations in rhodopsin have demonstrated the crucial role rhodopsin plays in ROS maintenance and disc morphogenesis[21-27]. Within the ROS disc membranes, rhodopsin

forms oligomers which are further organized into densely packed nanoscale domains[28-30]. Atomic force microscopy (AFM) imaging can achieve nanoscale resolution adequate to visualize these nanodomains[31]. Strikingly, these AFM studies demonstrate that there are biological mechanisms in place to ensure the density of rhodopsin in ROS disc membranes is kept constant, suggesting that regulation of proper rhodopsin density is crucial for photoreceptor disc formation and health[32,33].

Although PRCD's specific role within the photoreceptor remains elusive, recent studies in a PRCD knockout mouse model have identified a requirement for PRCD in high fidelity disc morphogenesis. In this model, it is observed that discs do not flatten or form properly in the absence of PRCD. Consequently, membrane bulges containing rhodopsin appear to separate into extracellular vesicles and accrue within the interphotoreceptor space[34]. A second PRCD knockout mouse model has also shown accumulation of these vesicles and observed a reduced rate of phagocytosis of OS discs by the retinal pigmented epithelium (RPE)[35]. Along with evidence of retinal degeneration in these models and structural defects exacerbated by microglia recruitment to clear these vesicles, it is clear that PRCD is required for proper OS maintenance and disc morphogenesis; however further studies are needed to clarify the precise mechanistic role which PRCD plays in these processes.

To further understand the interaction between PRCD and rhodopsin, as well as PRCD's role in photoreceptor OS disc morphogenesis and maintenance, we utilized our *Prcd*-KO mouse model. In this study, we demonstrate that *Prcd*-KO retina display dramatic

disorganization of the photoreceptor OS. Most importantly, using AFM imaging, we observe that loss of PRCD leads to decreased rhodopsin number and packaging density in ROS disc membranes, likely associated with the observed morphological changes in *Prcd*-KO retina.

2.3 Results

2.3.1 Generation of *Prcd*-KO mice using CRISPR/Cas9 genome editing

To better understand the importance of PRCD in the maintenance and stability of the photoreceptor outer segment (OS), we generated a global *Prcd*-KO mouse model using CRISPR/Cas9 genome editing. Among 48 founder mice, we found 12 contained INDEL deletions in exon 1. For this study, we collected data from the 1738 founder, whose *Prcd* gene contains a single nucleotide deletion in exon 1 at cytosine 61 (c61x), resulting in a frameshift mutation (Fig. 2.1A and Supplementary Fig. S2.1). To rule out off-target effects, additional founder lines were tested, including mice with a 14 bp deletion (1734) and 71 bp deletion in *Prcd* (1748) (Supplementary Fig. S2.1). All lines exhibited similar phenotypes, were comparable in weight and development to wild-type (WT) littermates and are fertile with no detectable health issues. Western blot analysis demonstrated that lysate from *Prcd*-KO retina does not contain PRCD protein (Fig. 2.1B). Co-immunofluorescent labeling of retinal cross sections with antibodies against PRCD and the OS marker anti-cyclic-nucleotide gated channel A (CNGA) revealed expected PRCD OS localization in WT retina, whereas PRCD labeling was absent in *Prcd*-KO retinal

sections (Fig. 2.1C). Altogether, these data validate the absence of PRCD protein in the *Prcd*-KO animal model used in this study.

2.3.2 Loss of PRCD leads to progressive loss of visual function and slow photoreceptor degeneration

To evaluate the visual response of rod and cone photoreceptor neurons, we assessed scotopic (rod) and photopic (cone) responses in *Prcd*-KO and WT littermates by electroretinography (ERG). A light-evoked ERG response is comprised of an “a-wave” (photoreceptor) and a “b-wave” (inner retinal neurons), which result from hyperpolarization of photoreceptors and depolarization of downstream retinal neurons, respectively[36]. At postnatal day (P) 30, *Prcd*-KO mice present with an approximate 30% reduction in rod response compared to WT littermate controls in bright light conditions (Fig. 2.2A). At low light intensities (0.00025 and 0.001 cd*s/m^2), we were unable to identify any discernable differences in scotopic rod response between WT and *Prcd*-KO animals. However, at brighter flash intensities 0.158 (p = 0.009424), 0.995 (p = 0.001771), and 2.5 cd*s/m^2 (p = 0.001363), rod a-waves were significantly reduced in *Prcd*-KO animals compared to WT littermate controls (Fig. 2.2B). Furthermore, we observed a slow decrease in visual response over time at various ages (P30, P60, P100, and P200); by P200, *Prcd*-KO animals demonstrate an approximate 50% reduction in rod photoresponse compared to WT littermate controls (Fig. 2.2C). In contrast, *Prcd*-KO photopic ERGs demonstrated no noticeable changes compared to WT responses at any tested ages or flash intensities (Fig. 2.2D). The evident impairment and gradual reduction in rod visual function of *Prcd*-KO animals suggests a possible defect in the morphology

or survival of photoreceptor cells. We utilized hematoxylin and eosin (H&E) staining of WT and *Prcd*-KO retina at P30, P120, and P250 in order to analyze retinal morphology. No significant defects in retinal lamination or morphology were observed in P30 *Prcd*-KO mice (Fig. 2.2E). To determine if retinal degeneration was evident at P30, where we observed significant loss of rod function in bright light conditions, we counted photoreceptor nuclei at 10 different locations in the same H&E sections. No significant reduction in photoreceptor nuclei was apparent in retina lacking PRCD until after P120. At P250, we observed a significant reduction in photoreceptor nuclei, with approximately 23.8% fewer nuclei in *Prcd*-KO retina compared to WT (p = 0.001332; Fig. 2.2F). Based on these data, the early rod ERG defects observed in bright light conditions were likely not due to loss of rod photoreceptors.

2.3.3 *Prcd*-KO retina exhibit reduced levels of rhodopsin and increased structural disorganization of rod OS as disease progresses

As *Prcd*-KO retina do not undergo degeneration until after P120, it is possible that the observed defect in visual function is due to changes in major photoreceptor or disc-resident proteins, as PRCD is localized exclusively to the OS disc membrane. Therefore, we analyzed retinal lysate from WT and *Prcd*-KO mice at P30 and P100 by western blot and found no significant changes in any tested proteins (Supplementary Fig. S2.3). However, due to the reported interaction between rhodopsin and PRCD, we measured the concentration of rhodopsin in WT and *Prcd*-KO retina with spectrophotometric analysis, a technique which has been widely used to measure and calculate picomolar concentrations of rhodopsin in the retina[37,38]. At P30, total rhodopsin concentration was

similar between *Prcd*-KO and WT retina (Fig. 2.3A). However, by P120, we observed a 20.4% decrease (p = 0.000072) in the amount of rhodopsin per *Prcd*-KO retina compared to age-matched WT controls (Fig. 2.3B). Despite the observed decrease in rhodopsin protein at P120, rhodopsin mRNA levels were comparable between WT and *Prcd*-KO animals at P30 and P120 (Supplementary Fig. S2.4). Furthermore, no mislocalization of rhodopsin is evident at P120 in *Prcd*-KO retinal sections when analyzed by immunofluorescent staining (Supplementary Fig. S2.5).

To gain further insight into the observed reduction in rod photoreceptor function at P30, we investigated photoreceptor ultrastructure at various ages (P30, P60, and P120) using transmission electron microscopy (TEM). At the earliest tested age (P30), many *Prcd*-KO rod photoreceptors contained discs that were disoriented and vertically aligned, although rod OS had an overall normal shape (Fig. 2.3D; arrowhead). Ultrastructural analysis of *Prcd*-KO rods at P60 showed the OS layer to be disorganized compared to WT. Outer segments had irregular diameters, included frequent examples of overgrown and misoriented disc membranes, and occasionally shed OS fragments and whorls of membrane packets into the OS layer. Closer inspection revealed a distinct population of *Prcd*-KO rods containing small packets of overgrown discs (10-40 discs), which were aligned abnormally, having grown along the long axis of the photoreceptors (Fig. 2.3E and Supplementary Fig. S2.6B-E). Although these defects were observed in *Prcd*-KO rods, there were still many rods which were comparable to WT, with no apparent differences in gross OS ultrastructure and contained nicely stacked, correctly sized, and properly aligned disc membranes (Supplementary Fig. S2.6A, B, and F). Additionally, our

evaluation of *Prcd*-KO retina ultrastructure found no apparent difference in the connecting cilium, inner segment (IS), mitochondria, or adjacent RPE layer compared to WT littermates. With increased age, *Prcd*-KO mice showed an increased frequency of defective photoreceptor cells with incorrectly stacked discs, further disorganization of ROS, and more space between discs at P120 compared to age-matched WT (Fig. 2.3C and F).

2.3.4 Disc membranes in *Prcd*-KO rod photoreceptors contain reduced packaging density and number of rhodopsin molecules

To investigate the interplay between rhodopsin and the observed defects in the *Prcd*-KO ROS ultrastructure, we evaluated ROS disc membranes isolated from *Prcd*-KO mice and age matched WT controls by atomic force microscopy (AFM). Previous studies have successfully used AFM to visualize rhodopsin nanodomains in the disc membranes[39]. Rhodopsin nanodomains are formed by oligomers of rhodopsin of various size and are not an artifact of phase separation of lipids or those related to the AFM procedure[28,30,40]. To further our confidence in this detection method, ROS disc membranes from WT mice at P30 and P120 exhibited properties similar to those reported previously[30,32] (Fig. 2.4A-C). In these discs, rhodopsin was arranged into nanodomains and the nanodomains were largely densely packed within the disc (Fig. 2.4A-C). *Prcd*-KO mice at P30 and P120 exhibited some ROS disc membranes which resembled those from WT mice with rhodopsin nanodomains densely packed within the membrane (Fig. 2.4D and G); however, they also exhibited ROS disc membranes that were irregular. Irregular ROS disc membranes from *Prcd*-KO discs had fewer rhodopsin nanodomains with larger areas

devoid of rhodopsin nanodomains (Fig. 2.4E, F, H, and I; asterisks). Irregular ROS disc membranes were also observed for WT mice; however, they were only sporadically observed, representing 6% or less of the ROS disc membranes analyzed. The proportion of regular and irregular ROS disc membranes were quantified for P30 and P120 *Prcd*-KO mice. In P30 KO mice, about one-third of the ROS disc membranes were irregular, and this increased for P120 mice, where about half of the ROS disc membranes were irregular (Fig. 2.5A, Table 2.2). Thus, the proportion of irregular ROS disc membranes increased with age for *Prcd*-KO mice. Since ROS discs from photoreceptor cells are heterogeneous, quantitative analysis is required[32]. The number of rhodopsin contained within a ROS disc membrane was estimated from the size of nanodomains and the density of rhodopsin was computed presuming single rhodopsin molecules homogenously distribute throughout the area of the lamellar region of the discs[39]. The number and density of rhodopsin nanodomains and molecules of rhodopsin in the irregular ROS disc membranes of both P30 and P120 mice were lower compared to that of regular ROS disc membranes (Fig 2.5B-E). The regular ROS disc membranes of both P30 and P120 *Prcd*-KO mice contained a similar number and density of rhodopsin as that of WT ROS disc membranes (Table 2.3). Altogether, these data demonstrate that *Prcd*-KO mice have an impaired ability to form proper ROS disc membranes with sufficient rhodopsin number and packaging density.

2.4 Discussion

In the current study, we sought to further understand the role of PRCD, a small disc-resident protein, in photoreceptor disc morphogenesis. Mutations in PRCD are associated

with dramatic misalignment of disc membranes and disorganization of the OS, followed by slow retinal degeneration. The most common PRCD mutation (C2Y) has been extensively characterized in several dog breeds[16]. Recent studies in additional mouse models have shown that high fidelity disc morphogenesis is compromised when PRCD is not present[34,35]. However, the precise role PRCD plays in this process remains unclear. In this study, we demonstrate that loss of PRCD disrupts rhodopsin packaging into ROS disc membranes, leading to defects in visual function and compromised OS structure, phenotypes consistent with clinical findings in humans and dogs with a PRCD-C2Y mutation[10].

Previous studies in canines demonstrate that PRCD-associated disease is heterogeneous, with spatial and temporal differences in disease onset and progression between dog breeds[14,15,41] In these models, it is reported that changes in ERG response correspond to the presence of morphological defects in affected animals[16]. In our *Prcd*-KO mouse model, retina appear to develop normally, exhibiting proper lamination. Our ERG studies demonstrate that loss of PRCD impairs mass rod photoreceptor response in bright light conditions as early as P30. At P30, ultrastructural analysis reveals *Prcd*-KO rod photoreceptors with defects in OS morphology, including focal misalignment of discs and imperfect disc stacking. As mice age, ERG response continues to decline and more pronounced morphological defects are observed. Importantly, all tested disc-resident and phototransduction proteins appear normal in *Prcd*-KO retina at P30, suggesting the observed reduction in *Prcd*-KO rod response at this age is due to morphological defects rather than loss of crucial phototransduction proteins[34].

Similar to two recently published mouse models lacking PRCD, photoreceptor degeneration in our *Prcd*-KO mice occurs well after disease onset, as we only see significant degeneration after P120. However, it seems that disease onset occurs earlier in our mouse model compared to others. In one model, Spencer *et al* report that single cell recording of rods shows no differences in visual response compared to WT at P40-P45. Additionally, *Prcd*$^{-/-}$ rods appear relatively normal compared to WT at 2 months, with only a few deformed ROS[34]. In another model, Allon *et al* report that mass rod response was not reduced until after 20 weeks of age and do not mention disorganized disc membranes until 30 weeks[35]. We believe these discrepancies can be explained by mouse strain differences and genetic heterogeneity, as our *Prcd*-KO model is in a 129/SV-E background and the other two are in a C57BL/6J background. If the characterized correlation between ERG response and morphology in canines with a PRCD-C2Y mutation holds true in *Prcd*-KO animals, it explains why we see reductions in ERG response at P30 when we also observe morphological defects. Additionally, it may explain why ERG response is not affected in these other knockout models, when ROS appear normal.

These models also show that retina lacking PRCD develop an abundance of extracellular vesicles (EV) containing rhodopsin, which phagocytic microglia cannot manage to clear properly[34,35]. Spencer *et al* demonstrates that discs lacking PRCD do not form properly and that prior to flattening, membrane bulges containing rhodopsin separate into EV in the interphotoreceptor space[34]. We were able to identify several examples of EV in our

model, but they often appear in the same areas as fixation artifacts and were also observed in WT retina. These newly formed EV are likely labile structures which require cardiac perfusion to retain their ultrastructure. It is important to note that the presence of vesicular profiles is also a hallmark of PRCD-associated disease in miniature poodles[14]. However, these vesicular profiles were reported to be missing or sparsely distributed in retina of English cocker spaniels with PRCD-C2Y mutations[16]. Therefore, while the traditional TEM fixation protocols used in this study may not have captured these vesicles properly, it is also possible that formation of these vesicles is just another phenotypic variation that can be attributed to genetic differences in mouse strain, as demonstrated in canine models. We plan to investigate this possibility in our future studies. In general, the variable phenotypes observed in canines and mice with PRCD-associated disease underscores the importance of continued study of this protein in multiple model systems.

In contrast to other published studies, we furthered our analysis of *Prcd*-KO disc membranes using AFM. PRCD is identified as one of 11 proteins exclusively present in the disc membrane and has been shown to interact with rhodopsin[7,18]. As mentioned, rhodopsin is organized into nanoscale domains and AFM has been extensively used to visualize these nanodomains in various studies[28,30,32,42,43]. Rhodopsin protein is reduced by half in Rho+/- retina and AFM analysis of Rho+/- discs demonstrates that although disc size decreases in response to availability of rhodopsin, at 6 weeks of age, Rho+/- disc membranes contain a density of rhodopsin comparable to WT[22,32]. With an average density of about 20,000 μm^{-2} in murine discs, rhodopsin is likely maintained at this density in order for rods to retain high sensitivity to light[23,30,33,39,44,45]. In fact, high rhodopsin

packaging density appears very important for proper visual function, as mice housed in constant dark display increased rhodopsin packing density within ROS disc membranes and show improved visual function compared to mice housed in cyclic light conditions[33]. In contrast to tight regulation of rhodopsin packaging density, our *Prcd*-KO mice demonstrate a population (~33%) of "irregular" discs at P30 which contain both fewer molecules of rhodopsin and decreased density of rhodopsin in comparison to WT "regular" discs. By P120, the relative proportion of these irregular discs increases to ~50%, corresponding with worsening retinal defects as assessed by ERG and TEM. Thus, if there do exist mechanisms to maintain consistent rhodopsin packaging density in ROS disc membranes, our data suggest that PRCD may be involved in regulation of this process.

Although rhodopsin levels and availability appear relatively normal in *Prcd*-KO retina at P30, there is an apparent inability for rod photoreceptor neurons lacking PRCD to maintain the proper density of rhodopsin within ROS disc membranes. Furthermore, the presence of these irregular discs strongly suggests a possible explanation for the observed reduction in *Prcd*-KO rod ERG response and ROS ultrastructural defects at P30 and subsequent ages. By P120, we detect an approximate 20.4% reduction in total rhodopsin protein. We speculate that this decrease is related to the disrupted incorporation of rhodopsin into these aforementioned irregular discs.

In all PRCD knockout models to date, cones appear unaffected until rods degenerate. As cones rely on opsins other than rhodopsin for phototransduction, the specific role for

PRCD in rod photoreceptors through packaging of rhodopsin into disc membranes is compelling. Considering PRCD's small size, one hypothesis is that PRCD works by anchoring nascent discs in place to ensure that the proper density of rhodopsin is packed into each disc before flattening and enclosure. Investigation of this possibility, as well as determining why *Prcd*-KO rods are still able to form a population of phenotypically normal discs, are topics of future study.

Altogether, our data provide further insight into PRCD's involvement in proper rhodopsin packaging density in ROS disc membranes, a process which is crucial for OS maintenance and disc morphogenesis.

2.5 Methods

2.5.1 Generation of *Prcd* knockout model

Prcd-KO mice were generated using CRISPR/Cas9 genome editing at the transgenic core facility at West Virginia University. Small guide RNA (sgRNA) were designed as described in earlier studies[46,47]. Two sgRNA target sequences were created for exon 1 of *Prcd*, both upstream (CCGTAGATTTACCAACCGAG*TGG*) and downstream (CCACTCGGTTGGTAAATCTA*CGG*) of the 5'-NGG "PAM" (protospacer adjacent motif). These sequences were annealed and ligated into a pX330 vector (pSpCas9). Using PCR amplification, a T7 promoter (TTAATACGACTCACTATAGGG) was added to the sgRNA template and purified using an RNA purification kit from Ambion. After confirming the specificity and efficacy of the sgRNA/Cas9 cutting by *in-vitro* assays, both sgRNA (17ng/μl) and Cas9 (34 ng/μl) mRNA (Invitrogen) were injected into the pronuclei of FVB blastocysts. The correctly targeted founder mice were identified by sequencing and backcrossed with 129/SV-E mice (Charles River Laboratories) to eliminate the *rd1* allele, which naturally occurs in FVB mice. Furthermore, *Prcd*-KO mice were confirmed to lack the *rd8* mutation and were extensively backcrossed for more than 6 generations with 129/SV-E mice to rule out "off-target" effects sometimes associated with CRISPR/Cas9 gene editing. Genotyping was performed by PCR amplification followed by sequencing. All experimental procedures involving animals in this study were approved and conducted in strict accordance with relevant guidelines and regulations by the Institutional Animal Care and Use Committee at West Virginia University.

2.5.2 Electroretinography

Prior to measuring light dependent electrical response, mice were dark-adapted overnight before testing and ERGs were performed under dim red light. Animals were anesthetized with isoflurane (5% in 2.5% oxygen) and eyes were dilated (1:1 Phenylephrine : Tropicamide) for 10 minutes and placed on a stage heated to 37ºC with a nose cone supplying isoflurane (1.5% in 2.5% oxygen) for testing. After lubrication with GenTeal gel (0.3% Hypromellose), silver electrodes were placed above the cornea to measure ERG response. A reference electrode was placed between the ears on top of the animal's head. ERG recordings were conducted using the UTAS Visual Diagnostic System with BigShot Ganzfeld, UBA-4200 amplifier and interface, and EMWIN software (version 9.0.0, LKC Technologies, Gaithersburg, MD, USA). Scotopic (rod) ERGs were performed in the dark with flashes of white light at increasing intensities. Photopic (cone) responses were performed with flashes of increasing intensities of white light with a 30 cd/m^2 white background light for 10 minutes to saturate rods.

2.5.3 Immunoblotting

To evaluate protein expression by immunoblot, two retinas were homogenized by sonication (Microson Ultrasonic cell disruptor, 3 pulses 5 s at power setting 10) in 200 μl of urea sample buffer (USB) containing 6M, 4% SD0S, and 125 mM Tris-HCl, pH 6.8 in1.5-ml microcentrifuge tube on ice. Protein concentration was determined using a NanoDrop spectrophotometer (ND-1000, Thermo Fisher Scientific). Samples were normalized to 5 mg/ml with additional USB and 5% 2-mercaptoethanol and bromophenol blue were added prior to SDS-PAGE. Equal concentration of each sample was loaded

and separated by SDS-PAGE in a 4-15% tris-glycine precast gel (4–20% Mini-PROTEAN TGX, Bio-Rad, Hercules, CA, USA) and subsequently transferred to an Immobilon-FL PVDF membrane (Immobilon-FL, Millipore, Burlington, MA, USA). After blocking membranes with blocking buffer (Odyssey Blocking Buffer; LI-COR Biosciences, Lincoln, NE, USA) for 1 hour at room temperature (RT) and incubated with primary antibodies for 2 hours at RT or overnight at 4°C on a bidirectional rotator. After primary antibody incubation (***see Table 2.1***), immunoblots were washed three times in 1X PBST (1X PBS/0.1% Tween-20) for 5 minutes each at RT and incubated with secondary antibody, goat anti-rabbit Alexa Fluor 680, goat anti-mouse DyLight 800 or donkey anti-sheep Alexa Fluor 680 (Thermo Fisher Scientific) for 30 minutes at RT. After washing three additional times in 1X PBST, membranes were scanned using an Odyssey Infrared Imaging System and protein density was measured according to manufacturer's instruction (LI-COR Biosciences, Lincoln, NE, USA).

2.5.4 Immunohistochemistry

Whole eyes from P30, P120, and P250 were enucleated, immersed, and fixed in Excalibur's Z-fix. Embedding, sectioning, and hematoxylin and eosin (H&E) staining was carried out on WT and *Prcd*-KO eyes by Excalibur Pathology, Inc. (Norman, OK, USA). Images were collected using a Nikon C2 confocal microscope. Five points were chosen to count the number of photoreceptor nuclei in the outer nuclear layer (every 350 μm) above and below the optic nerve. Counts were completed for three independent eyes (n=3) and averaged to determine the amount of photoreceptor degeneration at each age. Images were processed using ImageJ software along with the Bio-Formats plugin[48,49].

2.5.5 Immunofluorescent staining

After enucleation, mouse eyes were prepared as described previously[17]. Using a Leica CM1850 Cyrostat, 16 μM cross-sections were cut and placed on Superfrost plus slides (Fisher Scientific). Slides were washed with 1X PBS to hydrate tissue and to remove OCT. To prevent non-specific antibody labeling, slides were blocked for 1 hour. After blocking, primary antibodies were added at a 1:1000 dilution and incubated overnight at 4 °C (***see Table 2.1***). After primary antibody incubation, sections were washed in 1X PBST (1X PBS/0.1% Triton X-100) three times and incubated with the nuclear stain DAPI (1:5,000; Molecular Probes) and secondary antibody (Thermo Fisher Scientific goat anti-mouse Alexa Fluor-488 or goat anti-rabbit Alexa Fluor-568) at a 1:1,000 dilution for 1 hour at RT. Slides were mounted with Prolong Gold antifade reagent (Thermo Fisher Scientific) and coverslipped (1 mm). Slides were imaged using a Nikon C2 confocal microscope. Images were processed using ImageJ software along with the Bio-Formats plugin[48,49].

2.5.6 Transmission electron microscopy

Enucleated eyes were placed in freshly prepared buffer containing 2% paraformaldehyde, 2.5% glutaraldehyde, and 0.1M cacodylate buffer, pH 7.5. After 30 minutes of fixation, cornea and lens were removed, and eyecups were fixed for an additional 48 hours at RT with constant rotation on a nutator. Dissection, embedding, and transmission electron microscopy were performed as described previously[50].

2.5.7 Rod outer segment and disc membrane isolation

Retina from 15 age-matched WT (129/SV-E) and *Prcd*-KO mice were collected. Retinal tissues were suspended in 300 μl of 8% (vol/vol) Optiprep (Sigma-Aldrich, St. Louis, MO, USA) in Ringer's buffer (10 mM HEPES, 130 mM NaCl, 3.6 mM KCl, 2.4 mM $MgCl_2$, 1.2 mM $CaCl_2$, and 0.02 mM EDTA) and vortexed for 1 minute. Next, samples were centrifuged at 238 *x g* for 1 min at 4ºC and the supernatant was collected into a clean tube. This was repeated four additional times and the subsequent supernatant was pooled and placed on top of a 10-30% Optiprep in Ringer's buffer gradient. The gradient containing the sample was then centrifuged at 26,500 *x g* for 50 minutes at 4ºC with no brakes (Beckman Coulter Optima LE-80K; SW-41Ti). A dense band approximately two-thirds from the top of the gradient was collected and diluted fourfold in Ringer's buffer. After a 3 minute centrifugation at 627 *x g* at 4ºC, the supernatant was next transferred to a high-speed centrifuge tube and centrifuged at 26,500 *x g* for 30 minutes at 4ºC (Beckman Coulter Optima TLX; rotor-TLA55). The resulting pellet was then resuspended in 2 mM Tris-HCl and used for AFM studies.

2.5.8 Atomic force microscopy

All experimental procedures were conducted under dim red light conditions to avoid photobleaching. ROS disc membranes were diluted in Ringer's buffer (10 mM HEPES, 130 mM NaCl, 3.6 mM KCl, 2.4 mM $MgCl_2$, 1.2 mM $CaCl_2$, and 0.02 mM EDTA, pH 7.4), immobilized on freshly cleaved mica and imaged by AFM in imaging buffer (20 mM Tris, 150 mM KCl, 25 mM $MgCl_2$, pH 7.8), as described previously[32]. Contact mode AFM imaging was performed using Bruker Multimode II atomic force microscope equipped with

an E scanner (13 μm scan size) and silicon nitride cantilevers with a nominal spring constant of 0.06 N/m (DNP-S, Bruker, Santa Barbara, CA). Deflection images were analyzed using SPIP (version 6.5, Image Metrology A/S, Hørsholm, Denmark) to determine the number and density of rhodopsin, as described previously[32,39]. Graphs and statistical analyses were done using Prism 7 (GraphPad Software, San Diego, CA).

2.5.9 Rhodopsin measurement

The amount of rhodopsin (picomoles per retina) was assessed using a modified protocol[37,38]. The concentration of rhodopsin was determined by measuring the difference in absorbance using a spectrophotometer before and after bleaching of the sample with a known light intensity. Individual retina were dissected in the dark under dim red light and placed in 200 μl of water containing 10% n-octyl-β-d-glucopyranoside and 50 μl of 200 mM hydroxylamine, pH 7.5. After sonication, the sample was centrifuged at 14,000 rpm in a tabletop centrifuge for 30 seconds and 150 μl of sample was measured by spectrophotometer before and after light exposure. Absorbance and a molar extinction coefficient of 40,500 were used to calculate the concentration of rhodopsin per retina[37,38].

2.5.10 Statistical analysis

Data are expressed as means ± S.E.M., unless otherwise indicated. The differences between littermate or age matched control (WT) and experimental animals (*Prcd*-KO) were analyzed with a two-tailed student *t* test (online version, https://www.socscistatistics.com/).

2.6 References

1 Burns, M. E. & Arshavsky, V. Y. Beyond Counting Photons: Trials and Trends in Vertebrate Visual Transduction. *Neuron* **48**, 387-401, doi:10.1016/j.neuron.2005.10.014 (2005).

2 Goldberg, A. F. X. in *International Review of Cytology* Vol. 253 131-175 (Academic Press, 2006).

3 Sung, C.-H. & Chuang, J.-Z. The cell biology of vision. *The Journal of Cell Biology* **190**, 953, doi:10.1083/jcb.201006020 (2010).

4 Goldberg, A. F., Moritz, O. L. & Williams, D. S. Molecular basis for photoreceptor outer segment architecture. *Prog Retin Eye Res* **55**, 52-81, doi:10.1016/j.preteyeres.2016.05.003 (2016).

5 Palczewski, K. Chemistry and Biology of Vision. *Journal of Biological Chemistry* **287**, 1612-1619 (2012).

6 Wensel, T. G. *et al.* Structural and molecular bases of rod photoreceptor morphogenesis and disease. *Prog Retin Eye Res* **55**, 32-51, doi:10.1016/j.preteyeres.2016.06.002 (2016).

7 Skiba, N. P. *et al.* Proteomic identification of unique photoreceptor disc components reveals the presence of PRCD, a protein linked to retinal degeneration. *J Proteome Res* **12**, 3010-3018, doi:10.1021/pr4003678 (2013).

8 Downs, L. M., Hitti, R., Pregnolato, S. & Mellersh, C. S. Genetic screening for PRA-associated mutations in multiple dog breeds shows that PRA is heterogeneous within and between breeds. *Veterinary Ophthalmology* **17**, 126-130, doi:10.1111/vop.12122 (2014).

9 Goldstein, O. *et al.* Linkage disequilibrium mapping in domestic dog breeds narrows the progressive rod-cone degeneration interval and identifies ancestral disease-transmitting chromosome. *Genomics* **88**, 541-550, doi:10.1016/j.ygeno.2006.05.013 (2006).

10 Zangerl, B. *et al.* Identical mutation in a novel retinal gene causes progressive rod-cone degeneration in dogs and retinitis pigmentosa in humans. *Genomics* **88**, 551-563, doi:10.1016/j.ygeno.2006.07.007 (2006).

11 Hartong, D. T., Berson, E. L. & Dryja, T. P. Retinitis pigmentosa. *The Lancet* **368**, 1795-1809, doi:10.1016/S0140-6736(06)69740-7 (2006).

12 Verbakel, S. K. *et al.* Non-syndromic retinitis pigmentosa. *Prog Retin Eye Res* **66**, 157-186, doi:10.1016/j.preteyeres.2018.03.005 (2018).

13 Parry, H. B. Degenerations of the Dog Retina. *British Journal of Ophthalmology* **37**, 487, doi:10.1136/bjo.37.8.487 (1953).

14 Aguirre, G., Alligood, J., O'Brien, P. & Buyukmihci, N. Pathogenesis of progressive rod-cone degeneration in miniature poodles. *Investigative Ophthalmology & Visual Science* **23**, 610-630 (1982).

15 Aguirre, G. & O'Brien, P. Morphological and biochemical studies of canine progressive rod-cone degeneration. 3H-fucose autoradiography. *Investigative Ophthalmology & Visual Science* **27**, 635-655 (1986).

16 Aguirre, G. D. & Acland, G. M. Variation in retinal degeneration phenotype inherited at the prcd locus. *Experimental Eye Research* **46**, 663-687, doi:https://doi.org/10.1016/S0014-4835(88)80055-1 (1988).

17 Murphy, J. & Kolandaivelu, S. Palmitoylation of Progressive Rod-Cone Degeneration (PRCD) Regulates Protein Stability and Localization. *J Biol Chem* **291**, 23036-23046, doi:10.1074/jbc.M116.742767 (2016).

18 Spencer, W. J. *et al.* Progressive Rod–Cone Degeneration (PRCD) Protein Requires N-Terminal S-Acylation and Rhodopsin Binding for Photoreceptor Outer Segment Localization and Maintaining Intracellular Stability. *Biochemistry* **55**, 5028-5037, doi:10.1021/acs.biochem.6b00489 (2016).

19 Papermaster, D. S. & Dreyer, W. J. Rhodopsin content in the outer segment membranes of bovine and frog retinal rods. *Biochemistry* **13**, 2438-2444, doi:10.1021/bi00708a031 (1974).

20 Palczewski, K. G Protein–Coupled Receptor Rhodopsin. *Annual Review of Biochemistry* **75**, 743-767, doi:10.1146/annurev.biochem.75.103004.142743 (2006).

21 Chakraborty, D., Conley, S. M., Al-Ubaidi, M. R. & Naash, M. I. Initiation of Rod Outer Segment Disc Formation Requires RDS. *PLOS ONE* **9**, e98939, doi:10.1371/journal.pone.0098939 (2014).

22 Liang, Y. *et al.* Rhodopsin Signaling and Organization in Heterozygote Rhodopsin Knockout Mice. *J Biol Chem* **279**, 48189-48196 (2004).

23 Makino, C. L. *et al.* Rhodopsin expression level affects rod outer segment morphology and photoresponse kinetics. *PLoS One* **7**, e37832, doi:10.1371/journal.pone.0037832 (2012).

24 Sakami, S., Kolesnikov, A. V., Kefalov, V. J. & Palczewski, K. P23H opsin knock-in mice reveal a novel step in retinal rod disc morphogenesis. *Hum Mol Genet* **23**, 1723-1741, doi:10.1093/hmg/ddt561 (2014).

25 Wen, X. H. *et al.* Overexpression of rhodopsin alters the structure and photoresponse of rod photoreceptors. *Biophys J* **96**, 939-950, doi:10.1016/j.bpj.2008.10.016 (2009).

26 Humphries, M. M. *et al.* Retinopathy induced in mice by targeted disruption of the rhodopsin gene. *Nature Genetics* **15**, 216-219, doi:10.1038/ng0297-216 (1997).

27 Lem, J. *et al.* Morphological, physiological, and biochemical changes in rhodopsin knockout mice. *Proceedings of the National Academy of Sciences* **96**, 736, doi:10.1073/pnas.96.2.736 (1999).

28 Liang, Y. *et al.* Organization of the G Protein-coupled Receptors Rhodopsin and Opsin in Native Membranes. *Journal of Biological Chemistry* **278**, 21655-21662, doi:10.1074/jbc.M302536200 (2003).

29 Fotiadis, D. *et al.* Rhodopsin dimers in native disc membranes. *Nature* **421**, 127-128, doi:10.1038/421127a (2003).

30 Rakshit, T., Senapati, S., Sinha, S., Whited, A. M. & Park, P. S. H. Rhodopsin Forms Nanodomains in Rod Outer Segment Disc Membranes of the Cold-Blooded Xenopus laevis. *PLOS ONE* **10**, e0141114, doi:10.1371/journal.pone.0141114 (2015).

31 Whited, A. M. & Park, P. S. Atomic force microscopy: a multifaceted tool to study membrane proteins and their interactions with ligands. *Biochim Biophys Acta* **1838**, 56-68, doi:10.1016/j.bbamem.2013.04.011 (2014).

32 Rakshit, T. & Park, P. S. Impact of reduced rhodopsin expression on the structure of rod outer segment disc membranes. *Biochemistry* **54**, 2885-2894, doi:10.1021/acs.biochem.5b00003 (2015).

33 Rakshit, T. *et al.* Adaptations in rod outer segment disc membranes in response to environmental lighting conditions. *Biochim Biophys Acta Mol Cell Res* **1864**, 1691-1702, doi:10.1016/j.bbamcr.2017.06.013 (2017).

34 Spencer, W. J. *et al.* PRCD is essential for high-fidelity photoreceptor disc formation. *Proc Natl Acad Sci U S A* **116**, 13087-13096, doi:10.1073/pnas.1906421116 (2019).

35 Allon, G. *et al.* PRCD is Concentrated at the Base of Photoreceptor Outer Segments and is Involved in Outer Segment Disc Formation. *Hum Mol Genet*, doi:10.1093/hmg/ddz248 (2019).

36 Pinto, L. H., Invergo, B., Shimomura, K., Takahashi, J. S. & Troy, J. B. Interpretation of the mouse electroretinogram. *Doc Ophthalmol* **115**, 127-136, doi:10.1007/s10633-007-9064-y (2007).

37 Sokolov, M. *et al.* Massive Light-Driven Translocation of Transducin between the Two Major Compartments of Rod Cells: A Novel Mechanism of Light Adaptation. *Neuron* **34**, 95-106, doi:https://doi.org/10.1016/S0896-6273(02)00636-0 (2002).

38 Strissel, K. J., Sokolov, M., Trieu, L. H. & Arshavsky, V. Y. Arrestin translocation is induced at a critical threshold of visual signaling and is superstoichiometric to bleached rhodopsin. *J Neurosci* **26**, 1146-1153, doi:10.1523/JNEUROSCI.4289-05.2006 (2006).

39 Senapati S., P. P. S. Investigating the Nanodomain Organization of Rhodopsin in Native Membranes by Atomic Force Microscopy. *Methods Mol Biol* **1886**, 61-74, doi:10.1007/978-1-4939-8894-5_4 (2019).

40 Gunkel, M. *et al.* Higher-order architecture of rhodopsin in intact photoreceptors and its implication for phototransduction kinetics. *Structure* **23**, 628-638, doi:10.1016/j.str.2015.01.015 (2015).

41 Aguirre, G. D. & Rubin, L. F. Progressive retinal atrophy in the Miniature Poodle: an electrophysiologic study. *Journal of the American Veterinary Medical Association* **160**, 191-201 (1972).

42 Buzhynskyy, N., Salesse, C. & Scheuring, S. Rhodopsin is spatially heterogeneously distributed in rod outer segment disk membranes. *Journal of Molecular Recognition* **24**, 483-489, doi:10.1002/jmr.1086 (2011).

43 Whited, A. M. & Park, P. S. H. Nanodomain organization of rhodopsin in native human and murine rod outer segment disc membranes. *Biochimica et biophysica acta* **1848**, 26-34, doi:10.1016/j.bbamem.2014.10.007 (2015).

44 Nickell, S., Park, P. S., Baumeister, W. & Palczewski, K. Three-dimensional architecture of murine rod outer segments determined by cryoelectron tomography. *J Cell Biol* **177**, 917-925, doi:10.1083/jcb.200612010 (2007).

45 Calvert, P. D. *et al.* Membrane protein diffusion sets the speed of rod phototransduction. *Nature* **411**, 90-94, doi:10.1038/35075083 (2001).

46 Cong, L. *et al.* Multiplex genome engineering using CRISPR/Cas systems. *Science* **339**, 819-823, doi:10.1126/science.1231143 (2013).

47 Ran, F. A. *et al.* Genome engineering using the CRISPR-Cas9 system. *Nature Protocols* **8**, 2281, doi:10.1038/nprot.2013.143 https://www.nature.com/articles/nprot.2013.143#supplementary-information (2013).

48 Schneider, C. A., Rasband, W. S. & Eliceiri, K. W. NIH Image to ImageJ: 25 years of image analysis. *Nature Methods* **9**, 671-675, doi:10.1038/nmeth.2089 (2012).

49 Linkert, M. *et al.* Metadata matters: access to image data in the real world. *Journal of Cell Biology* **189**, 777-782, doi:10.1083/jcb.201004104 (2010).

50 Goldberg, A. F. X. *et al.* An Intramembrane Glutamic Acid Governs Peripherin/rds Function for Photoreceptor Disk Morphogenesis. *Investigative Ophthalmology & Visual Science* **48**, 2975-2986, doi:10.1167/iovs.07-0049 (2007).

2.7 Figures and Figure Legends

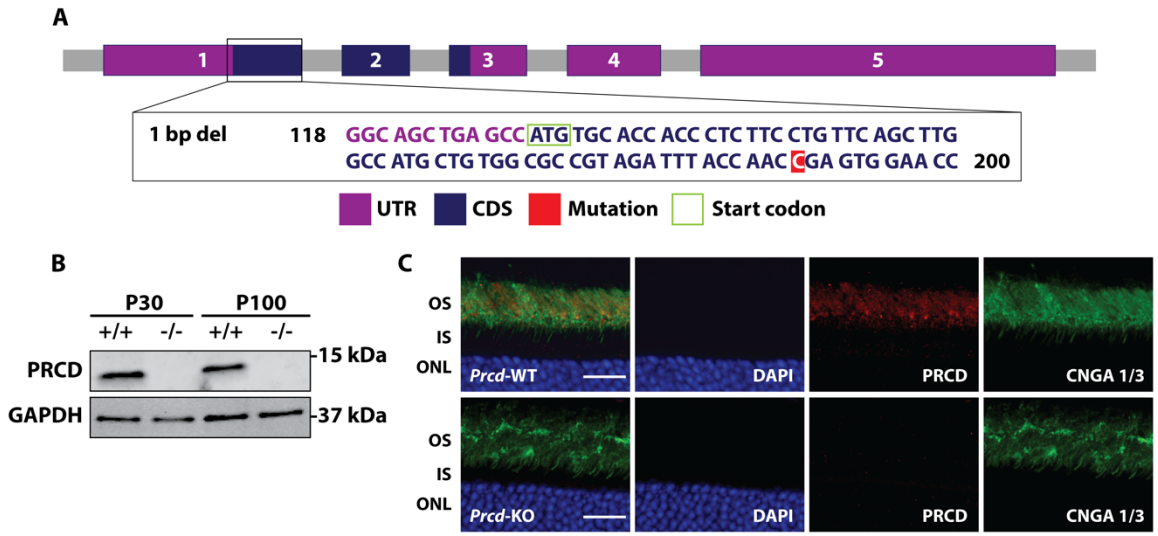

Figure 2.1. (A) Scheme demonstrating the generation of the *Prcd*-KO animal model using CRISPR/Cas9 technology. In this study, we used the 1738 founder line, which has a single base pair deletion in exon 1 of *Prcd*. UTR = untranslated region, CDS = coding sequence. **(B)** Immunoblot analysis shows loss of PRCD protein from *Prcd*-KO retinal lysate at postnatal (P) 30 and P100, whereas wild-type (WT) retinal lysates demonstrate PRCD immunoreactivity (n=4). Please note that immunoblot data is cropped; full-length, raw data is available in Supplementary Fig. S2.2. **(C)** Immunofluorescent staining of P30 retinal cross-sections from WT and *Prcd*-KO mice, probing with antibodies against PRCD (red) and the OS marker cGMP-gated cation channel alpha-1 and alpha-3 (CNGA 1/3; green) to demonstrate proper localization of PRCD to the OS in WT retina and loss of PRCD from *Prcd*-KO retina (n=3). Scale bar = 20 μm. All experiments were conducted with littermate controls.

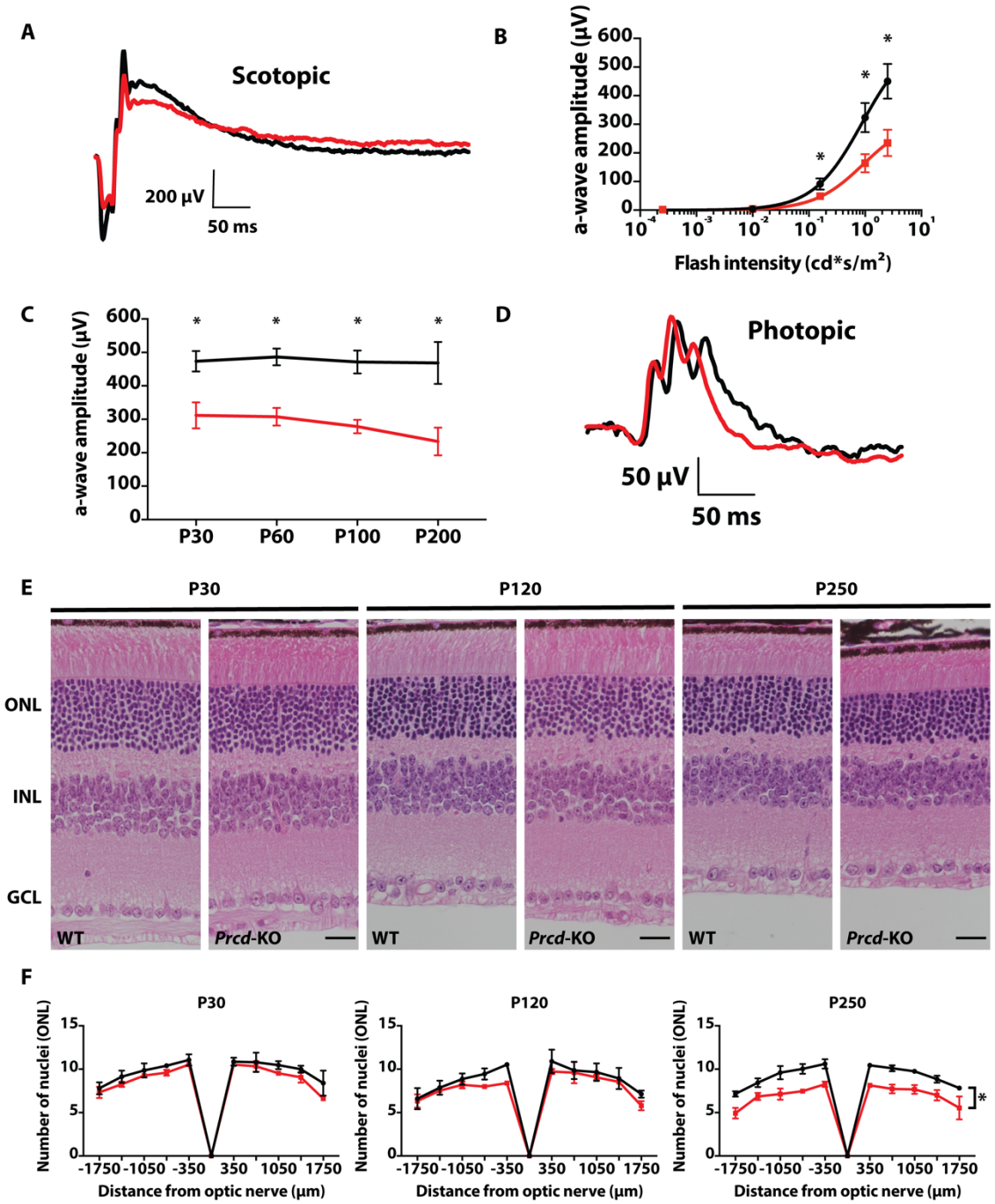

Figure 2.2. Reduced rod photoreceptor function and slow retinal degeneration in animals lacking *Prcd*. (A) Representative waveform from scotopic ERGs of WT (black) and *Prcd*-KO (grey) animals at P30 (0.995 cd*s/m^2). **(B)** Significant loss of rod

photoreceptor function at higher light intensities (0.158, 0.995, and 2.5 cd*s/m^2) compared with low light conditions (0.00025 and 0.001 cd*s/m^2) (n=4, data from B and C stats are unpaired two-tailed t-test; higher light intensities were statistically significant, *$p < 0.01$; Low light intensities were not significant). **(C)** Maximum a-wave amplitude of Prcd-KO animals at different ages compared to WT controls from P30 to P200. **(D)** Representative waveform from photopic (cone) ERGs of Prcd-KO and WT animals at P200 (7.9 cd*s/m2) (n=4). **(E)** *Prcd*-KO and WT littermate control cross-sections stained with hematoxylin and eosin (H&E), imaged by light microscopy, at P30, P120, and P250. Scale bar = 20 μm. **(F)** Quantification of number of photoreceptor nuclei in the outer nuclear layer (ONL) from both *Prcd*-KO (grey) and WT littermate controls (black), every 350 μm from the optic nerve, at P30, P120, and P250. Data are represented as mean (n=3, unpaired two-tailed t-test; *$p < 0.01$).

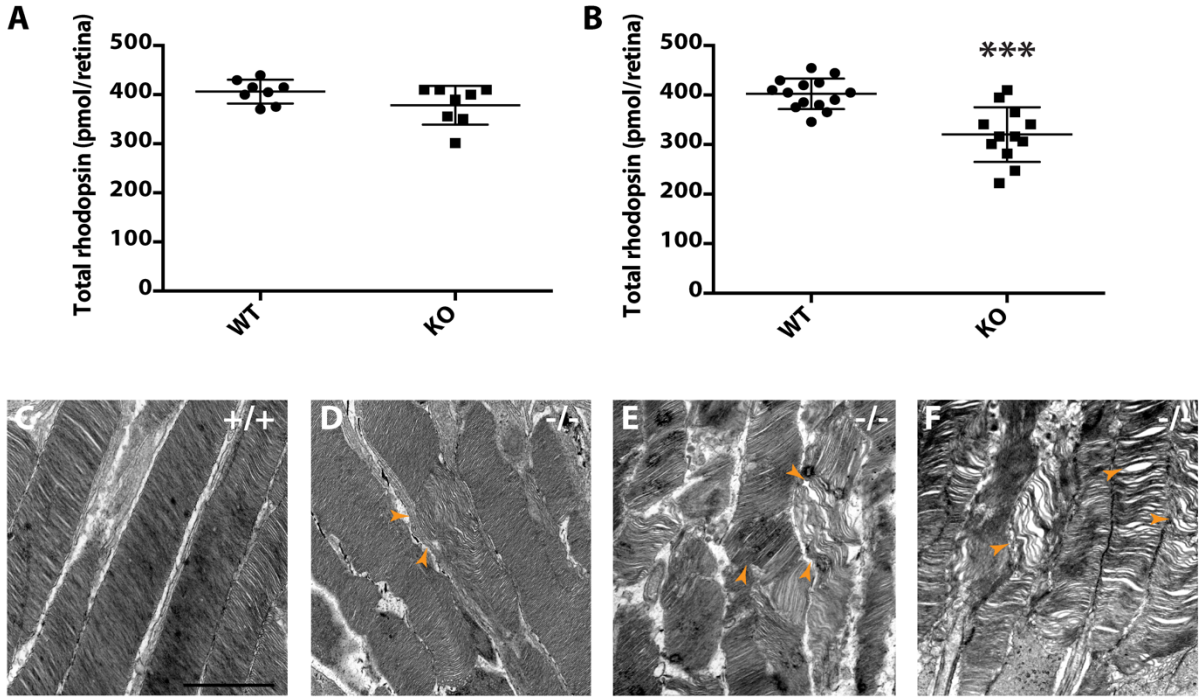

Figure 2.3. Reduced rhodopsin concentration and aberrant ultrastructure of photoreceptor OS during disease progression in *Prcd*-KO mice. (A) Quantification of total rhodopsin (pmol rhodopsin/retina) in WT and *Prcd*-KO retina at P30. **(B)** Quantification of total rhodopsin (pmol rhodopsin/retina) in WT and *Prcd*-KO retina at P120. Data is reported as the mean (unpaired, two-tailed t-test; ***p = .000072). **(C)** TEM image of the photoreceptor OS and well organized disc membranes at P120 (WT). **(D-F)** TEM ultrastructure of photoreceptor OS at various ages in *Prcd*-KO retina show the progressive disruption of OS structure from **(D)** P30, **(E)** P60, and **(F)** P120. Arrowheads indicate the defective and disorganized disc membranes. Scale bar = 500 nm.

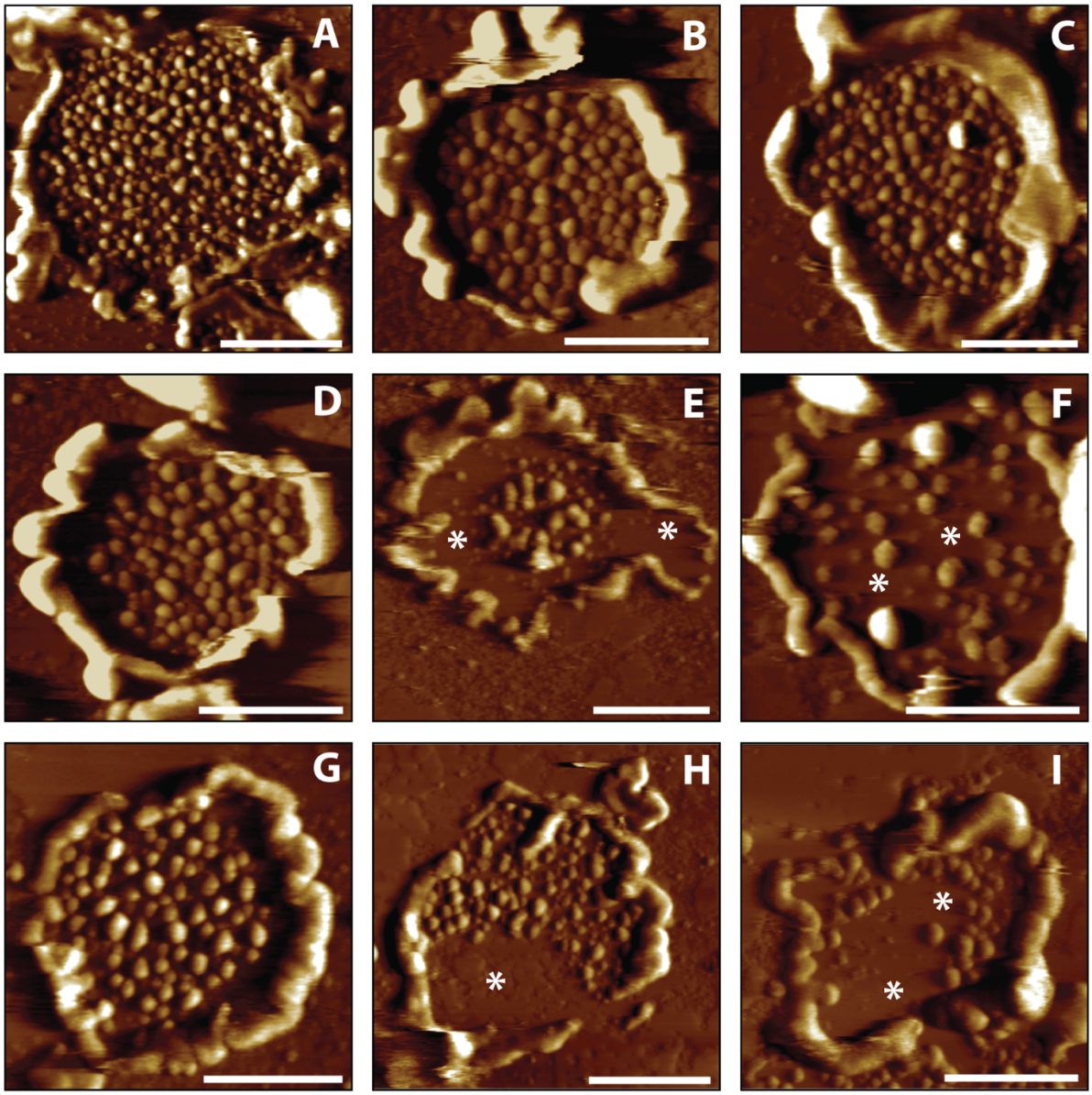

Figure 2.4. Representative AFM images of ROS disc membranes isolated from WT and *Prcd*-KO retina. Representative AFM images of ROS disc membranes isolated from **(A-C)** WT retina at P120, **(D-F)** *Prcd*-KO retina at P30, and **(G-I)** *Prcd*-KO retina at P120. Asterisks indicate large areas without rhodopsin nanodomains. Scale bar = 500 nm.

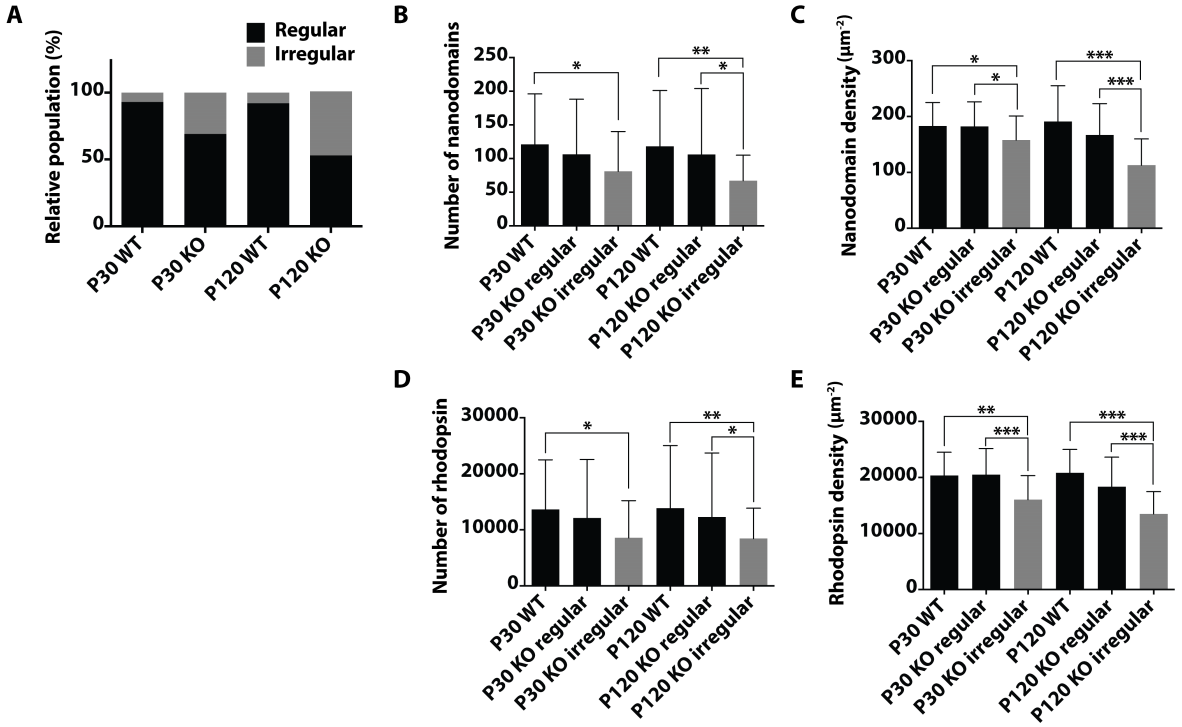

Figure 2.5. Quantification of ROS disc membrane properties of WT and *Prcd-KO* mice. (A) Relative population of regular (black) and irregular discs (grey). **(B)** Number of rhodopsin nanodomains packed into a ROS disc membrane. **(C)** Density of rhodopsin nanodomains within a ROS disc membrane. **(D)** Number of rhodopsin molecules packed into a ROS disc membrane. **(E)** Density of rhodopsin molecules within a ROS disc membrane. The number of ROS disc membranes analyzed are as follows: P30 WT, n=48; P30 KO regular, n=61; P30 KO irregular, n=27; P120 WT, n=47; P120 KO regular, n=53; P120 KO irregular, n=48. Mean values are reported with the standard deviation (unpaired, two-tailed t-test; *$p \leq 0.05$, **$p \leq 0.01$, ***$p \leq .00001$).

2.8 Tables

Table 2.1. List of primary antibodies used in this study.

Antibody	Source	Dilution
Rabbit anti-PRCD	Lab generated	1:1,000
Mouse anti-Rhodopsin (4D2)	Gift from R. Molday, Univ. British Columbia	1:2,000
Mouse anti-GAPDH	Proteintech, 60004-1-Ig	1:10,000
Rabbit anti-PDE6β	Thermo Fisher Scientific, PA 1-722	1:2,000
Rabbit anti-GNAT1	Proteintech, 55167-1-AP	1:2,000
Rabbit anti-ROM1	Gift from G. Travis, UCLA	1:2,000
Rabbit anti-PRPH2	Gift from G. Travis, UCLA	1:2,000
Sheep anti-RGS9	Gift from M. Sokolov, WVU	1:5,000
Rabbit anti-GC-1	Gift from V. Ramamurthy, WVU	1:2,000

Table 2.2. Relative population of regular and irregular discs observed in WT and *Prcd*-KO mice across ages (P30 and P120).

Mice	Regular disc (%)	Irregular disc (%)
WT (P30)	93	7
WT (P120)	92	8
Prcd-KO (P30)	69	31
Prcd-KO (P120)	52	48

Table 2.3. ROS disc properties of 129/SV-E wild-type (WT) and *Prcd*-KO mice across ages (P30 and P120).

	Nanodomains of rhodopsin		**Rhodopsin molecules**	
Parameter value	**Number**	**Density (μm^{-2})**	**Number**	**Density (μm^{-2})**
P30 WT (n = 42)	121 ± 75	183 ± 42	13642 ± 8848	20346 ± 4171
P120 WT (n = 47)	118 ± 83	191 ± 64	13857 ± 11177	20828 ± 4171
P30 *Prcd*-KO, regular (n = 61)	106 ± 82	182 ± 44	12089 ± 10465	20494 ± 4658
P30 *Prcd*-KO, irregular (n = 27)	81 ± 59	158 ± 43	8582 ± 6621	16059 ± 4276
P120 *Prcd*-KO, regular (n = 53)	106 ± 98	167 ± 56	12290 ± 11434	18345 ± 5297
P120 *Prcd*-KO, irregular (n = 48)	67 ± 38	113 ± 47	8454 ± 5417	13497 ± 3991

2.9 Supplementary information

Supplementary methods

RNA extraction, cDNA synthesis, and quantitative RT-PCR

Total RNA from P30 and P120 retina from WT and *Prcd*-KO animals was purified with TRIzol reagent (Thermo Fisher Scientific) according to manufacturer's protocols. RNA concentration was evaluated using a NanoDrop spectrophotometer (ND-1000, Thermo Fisher Scientific). First strand cDNA synthesis was carried out using the RevertAid First Strand cDNA Synthesis Kit (Thermo Fisher Scientific) using Oligo (dT)18 primer and 2.5 μg of purified total RNA per 20 μl of reaction volume. Each cDNA was diluted 10-fold with nuclease-free water before qRT-PCR. The qRT-PCR reactions were prepared using qPCR Brilliant II SYBR mastermix with ROX (Agilent), 150 nM of each primer, and cDNA from reverse transcription. To prime the cDNA synthesis, the reactions were performed according to the manufacturing instructions using a Stratagene Mx3000P real-time PCR system. Data was acquired using the MxPro QPCR software (Agilent). Each sample (n = 3) was run in triplicate and averaged to produce a single data point. Rhodopsin mRNA levels were analyzed using the primers SK254F (GAATCACGCTATCATGGGTGTGG) and SK255R (ATGACAAAGGATTCGTTGTTGACC). Relative rhodopsin gene expression was evaluated by normalization to the levels of the reference genes *Hmbs* (hydroxymethylbilane synthase) and *Ywhaz* (tyrosine 3-monooxygenase/tryptophan 5-monooxygenase activation protein, zeta polypeptide). *Hmbs* levels were quantified using the primers SK258F (GTTTACCAAGGAGCTAGAAAACGC) and SK259R

(GTGAAAGACAACAGCATCACAAGG). *Ywhaz* transcript was amplified using the primers SK260F (GTTGTAGGAGCCCGTAGGTCATCG) and SK261R (GCTTTCTGGTTGCGAAGCATTGGG).

```
                                1         10        20        30        40        50
(a) PRCD WT - 129/SV-E          MCTTLFLFSLAMLWRRRFTNRVEPEPSRVDGTVVGSGSDTDLQSTGREKGPVK
(b) PRCD Δ1bp - #1738           MCTTLFLFSLAMLWRRRFTNEWNQSPAEWTGQSWAAAQTQTFNLPAGRKDL*
(c) PRCD Δ14bp - #1734          MCTTLFLFSLAMLWRRRFTRAQQSGRDSRGQRGQRLRHRPSIYRQGERTCEV
(d) PRCD Δ71bp - #1748          ----------------SGTRAQQSGRDSRGQRGQRLRHRPSIYRQGERTCEV
```

Supplementary Figure S2.1. Depiction of mutations in *Prcd*-KO mice by CRISPR/Cas9 genome editing. The amino acid sequence of (a) WT PRCD protein from 129/SV-E mice compared to *Prcd*-KO founder lines (b) 1738 with a 1 bp deletion, (c) 1734 with a 14 bp deletion, and (d) 1748 with a 71 bp deletion. Red represents the frameshift mutation, green represents a start codon, and asterisks represent an early stop codon.

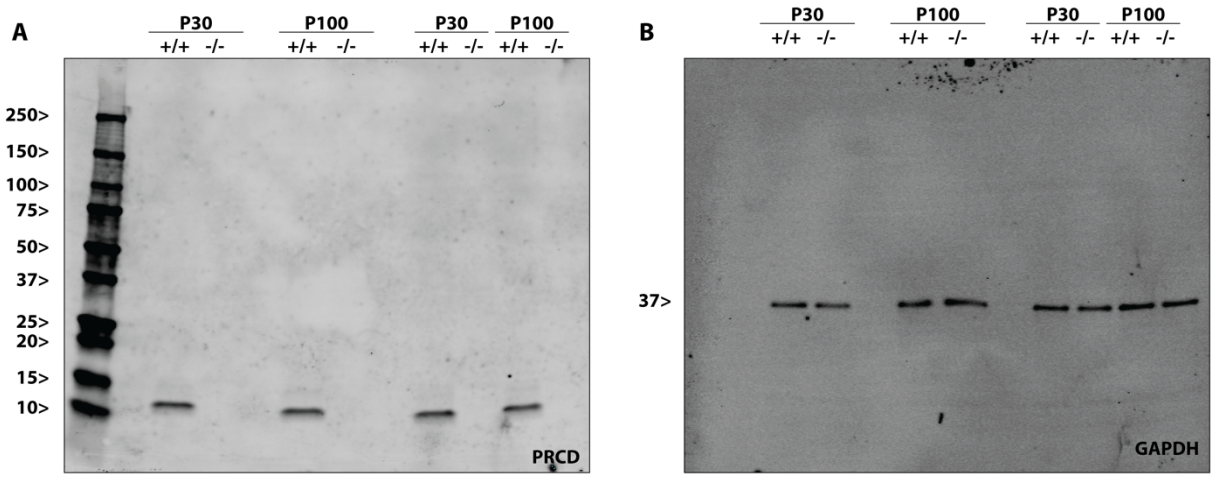

Supplementary Figure S2.2. Uncropped data corresponding to Figure 1B. Validation of *Prcd*-KO animal model. Lysate from both *Prcd*-KO and WT littermate control retina at P30 and P100 were subjected to western blot analysis and probed for **(A)** PRCD, progressive rod-cone degeneration and **(B)** GAPDH (served as a loading control). Please note that samples were loaded in duplicate.

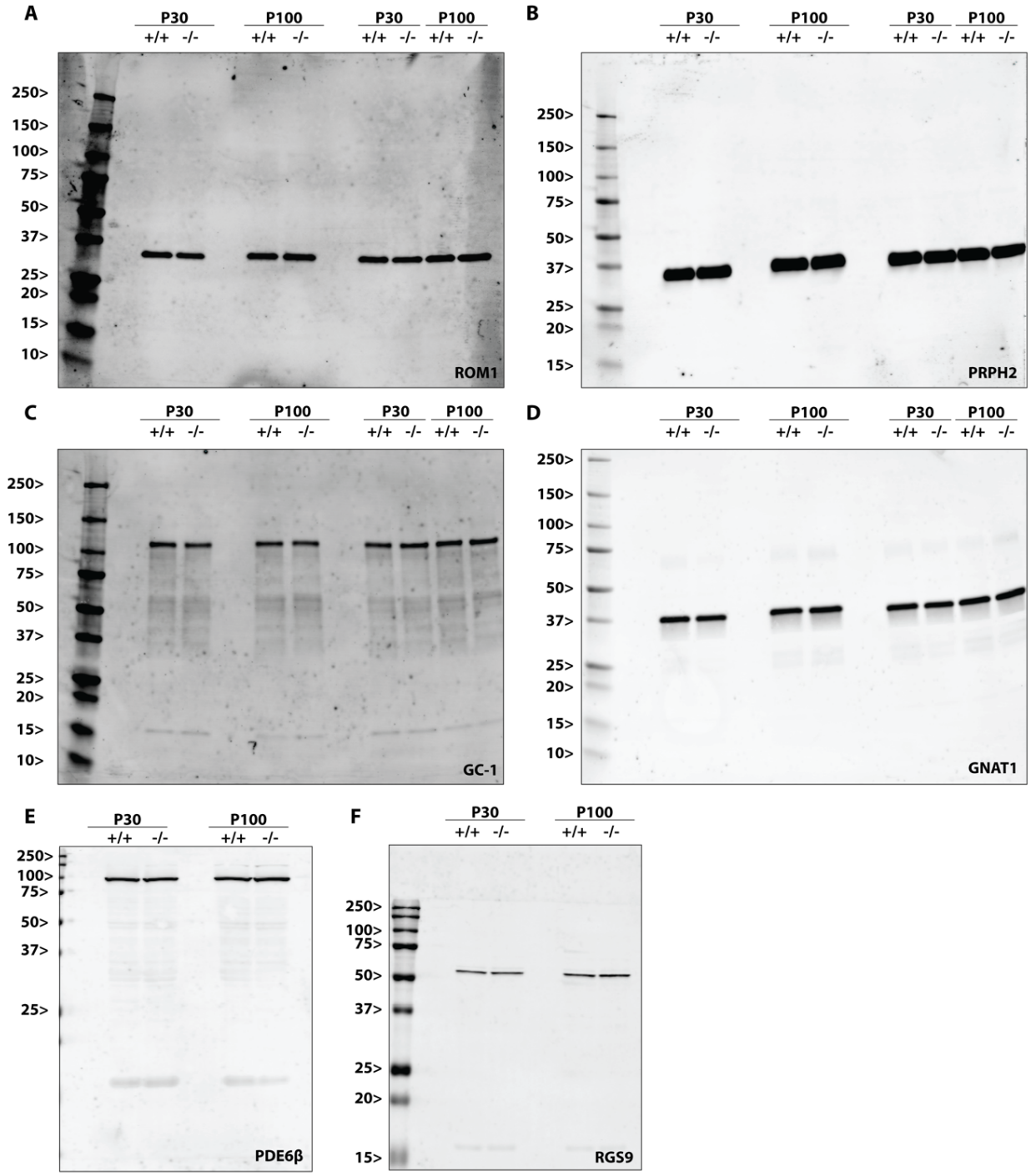

Supplementary Figure S2.3. Normal levels of major photoreceptor specific proteins in *Prcd*-KO retina. Lysate from both *Prcd*-KO and WT littermate control retina were subjected to western blot analysis. Blots were probed for several phototransduction

and OS-disc specific proteins at P30 and P100 with antibodies against **(A)** ROM1, rod outer segment membrane protein-1, **(B)** PRPH2, peripherin 2, **(C)** GC-1, guanylate cyclase-1, **(D)** GNAT1, rod transducin α, **(E)** PDE6β, phosphodiesterase-6 subunit beta, **(F)** RGS9, regulator of G-protein signaling-9. GAPDH served as a loading control (as shown in Supplementary Fig. S2.2). Please note that Supplementary Fig. S2.4A-D were loaded in duplicate.

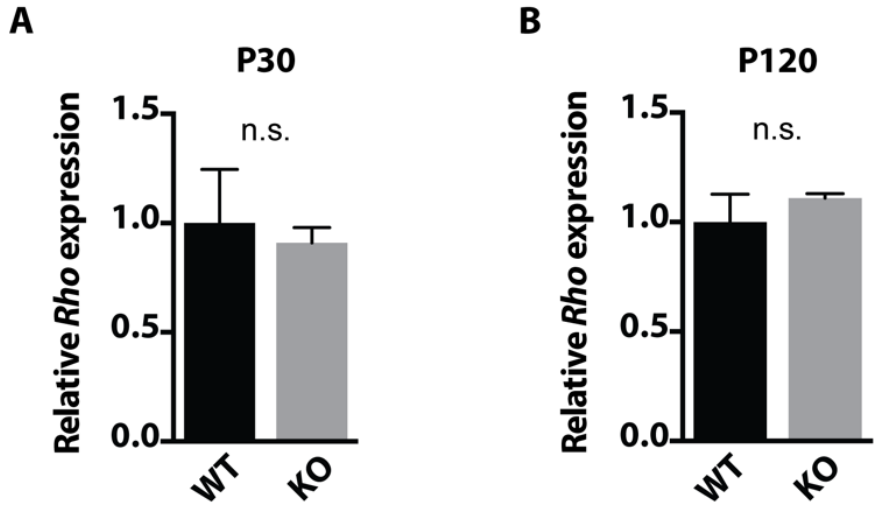

Supplementary Figure S2.4. No alteration in rhodopsin gene expression at P30 and P120. WT and *Prcd*-KO rhodopsin mRNA levels are comparable at **(A)** P30 and **(B)** P120. *Rho* gene expression was normalized to mRNA levels of the reference genes *Ywhaz* and *Hmbs*. Data are represented as mean relative *Rho* expression (*n*=3, unpaired two-tailed t-test). (*Ymhaz;* tyrosine 3-monooxygenase/tryptophan 5-monooxygenase activation protein, zeta polypeptide, and *Hmbs;* hydroxymethylbilane synthase).

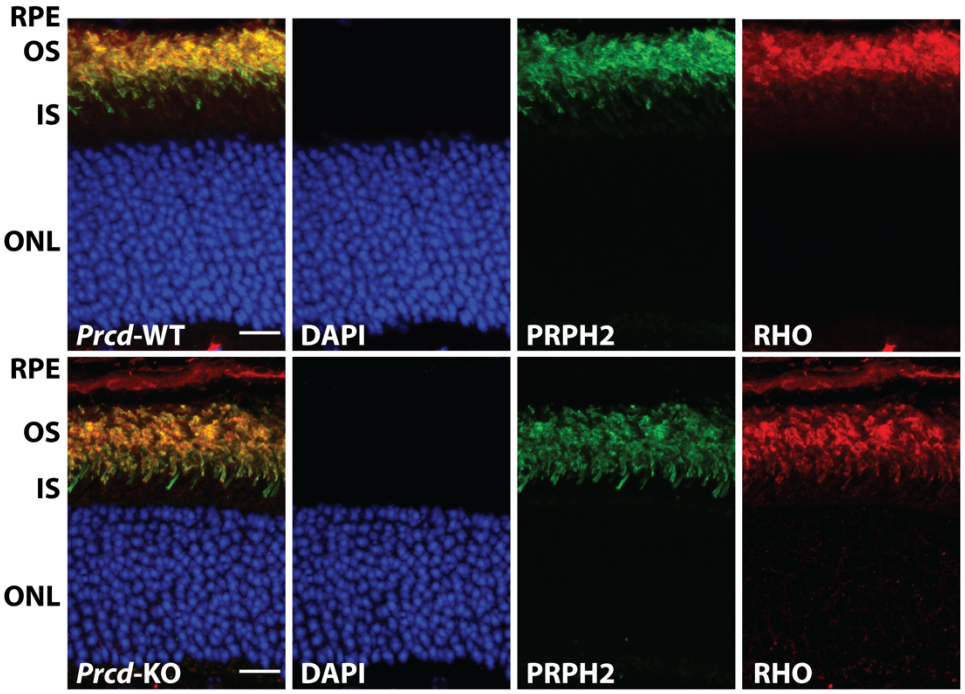

Supplementary Figure S2.5. Localization of rhodopsin and peripherin-2 in *Prcd*-KO retina at P30. Cross-sections from *Prcd*-KO and WT littermate controls were subjected to immunofluorescent staining with antibodies against the OS disc rim-specific protein PRPH2 (green) and the OS disc lamellae protein RHO (red) at P30. Scale bar = 20 μm

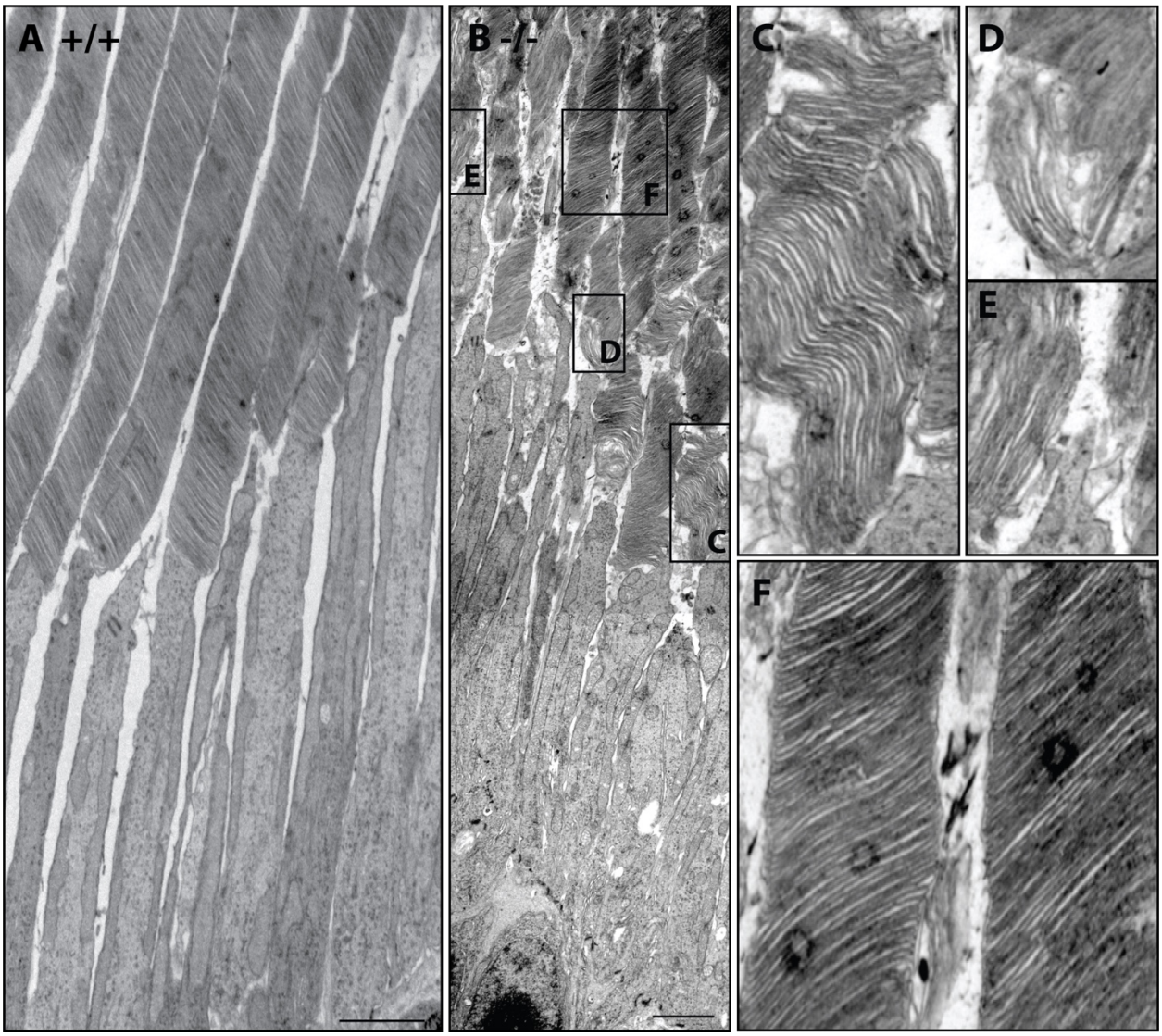

Supplementary Figure S2.6. Defective photoreceptor OS ultrastructure of *Prcd*-KO retina at P60. (A) Representative TEM images of WT and **(B)** *Prcd*-KO photoreceptor OS cross-sections at P60. (**C-E)** *Prcd*-KO ROS displayed some disorganized disc membranes, vertically aligned stacks of enlarged disc membranes, and disrupted OS with disc membranes aligned in a vertical and perpendicular shape. **(F)** *Prcd*-KO cross sections also revealed many photoreceptors with normal OS structure with properly stacked disc membranes. Inlet boxes enlarged from Supplementary Fig. S2.6B **(C-F)**. Scale bar = 2 μm.

Chapter 3 – The β2-subunit of the retinal Na^+, K^+-ATPase is post-translationally lipid modified by palmitoylation

Emily R. Sechrest[1,2], David Sokolov[2], Connor Nevin[2], Joseph Murphy[2], Saravanan Kolandaivelu[2,3,*]

[1]Department of Pharmaceutical Sciences, [2]Department of Ophthalmology and Visual Sciences, [3]Department of Biochemistry, West Virginia University, Morgantown, WV 26506, USA.

***Corresponding author:** Saravanan Kolandaivelu, Departments of Ophthalmology and Visual Sciences and Biochemistry; Eye Institute, One Medical Center Drive, West Virginia University, Morgantown, WV 26506-9193, USA. Email: kolandaivelus@wvumedicine.org; Tel: 304 598 5484; Fax: 304 598 6928.

3.1 Abstract

The photoreceptor outer segment (OS) is a highly modified primary cilium, which serves as the light-sensing compartment of the cell. The OS contains stacks of double membranous discs which house proteins required for phototransduction. Many of these proteins must undergo lipidation in order to properly traffic and associate with the disc membranes in the OS, such as the rod-specific G-protein coupled receptor complex, rhodopsin, and the phosphodiesterase-6 (PDE6) heteromeric complex. Unlike other post-translational lipid modifications, S-palmitoylation is reversible. This means that in addition to general roles of lipidation such as membrane association, trafficking, and protein-protein interactions, cycles of palmitoylation and depalmitoylation of a protein can be implicated in dynamic processes such as ion channel activity or signal transduction. In this study, we have utilized acyl resin-assisted capture (acyl-RAC) and mass spectrometry in order to isolate and identify novel proteins in the retina which undergo S-palmitoylation. From the pool of candidate proteins, we have found and validated that the β2-subunit of the Na^+, K^+-ATPase (ATP1B2) is post-translationally lipid modified by palmitoylation. Furthermore, we evaluated ATP1B2 palmitoylation using mass-tag labeling (acyl-PEG exchange). Using palmitoylation prediction software (GPS-Palm) and mass spectrometry, we were able to identify that ATP1B2 is palmitoylated on its 10th amino acid, Cys^{10}. Plasmid constructs expressing WT and C10A mutant ATP1B2 were injected into the subretinal space of neonatal mice. Injected retina subjected to acyl-RAC and western blot analysis show that a C10A mutation leads to loss of palmitoylation of ATP1B2. Altogether, this study utilizes a myriad of well-established techniques in order to identify novel proteins which undergo palmitoylation, including ATP1B2.

3.2 Introduction

Many photoreceptor-specific proteins involved in phototransduction are post-translationally lipidated, including transducin, phosphodiesterase 6 (PDE6), and rhodopsin[1,2]. Lipidation of proteins has proven to be an important regulator of protein-membrane and protein-protein interactions, protein stability, trafficking, and enzymatic activity[3]. Several types of lipids can be covalently linked to proteins, including isoprenoids (prenylation and geranylgeranylation), phospholipids, sterols, glycosylphosphatidyl inositol (GPI) anchors, and fatty acids (N-myristoylation and S-palmitoylation)[4].

The α-subunit of rod transducin ($G\alpha_{t1}$) is acylated on its N-terminus by various fatty acids including myristate[5,6]. Interestingly, the level of hydrophobicity of the attached fatty acid alters the light-induced mobility of $G\alpha_{t1}$ from the photoreceptor OS to the inner segment (IS), a process known as transducin translocation[7]. Additionally, the catalytic subunits of rod PDE6 are heterogeneously prenylated. The α-subunit is farnesylated while the β-subunit is geranylgeranylated at the C-terminal CaaX motif[8]. Both of these lipid modifications are important for efficient trafficking and membrane attachment of PDE6 in the outer segment (OS)[8]. Rhodopsin, the highly abundant G-protein coupled receptor (GPCR) in rod photoreceptors, is S-palmitoylated on two neighboring cysteine residues(Cys^{322} and Cys^{323})[2,9]; these lipids are important for stabilization and dimerization-dependent raftophilicity of rhodopsin[10,11].

Palmitoylation is a post-translational lipid modification which involves attachment of a 16-carbon fatty acid (palmitate) to cysteine residues on a protein[12]. Unlike many lipid

modifications, palmitoylation is unique in that it is reversible. A family of DHHC-motif containing palmitoyl acyl-transferases (DHHC-PATs) catalyze the addition of palmitate to cysteine residues on a protein, while palmitoyl-protein thioesterases (PPTs) de-palmitoylate proteins[13,14,15]. Palmitoylation is important for myriad biological functions, including membrane association, protein-protein interactions, protein maturation, and localization to the plasma membrane or specific membrane microdomains[14-17]. Due to its reversible nature, palmitoylation plays a role in several dynamic processes including signaling and ion channel activity[18,19]. Several experimental methods for the detection and quantification of protein palmitoylation have been developed[20-24].

Due to the dynamic nature of protein palmitoylation and the high number of processes which must be tightly regulated in the extremely metabolically active retina, our lab was interested in identifying retinal proteins which undergo S-palmitoylation. In the current study, our lab utilizes acyl-resin-assisted capture (acyl-RAC) and mass spectrometry to isolate and identify palmitoylated proteins in the retina. From the pool of candidate palmitoylated proteins, we have discovered and validated through several additional methods that the β2-subunit of the retinal Na^+,K^+-ATPase is palmitoylated.

The Na^+,K^+-ATPase is an integral membrane protein which exists as a heterodimer comprised of an α- and a β- subunit and functions as an ion pump in all cells[25,26]. The α-subunit is the catalytic subunit, whereas the β-subunit facilitates the maturation and trafficking of the holoenzyme to the plasma membrane[27]. The predominantly expressed subunit isoforms of the Na^+,K^+-ATPase in the retina are α3 (ATP1A3) and β2 (ATP1B2),

and are together often referred to as the retinal Na^+,K^+-ATPase[28,29]. ATP1B2 has been shown to play a crucial role in photoreceptor maintenance, although this role still remains unclear[29-33]. Here, we show that ATP1B2 is palmitoylated on Cys^{10}, a cysteine residue and post-translational lipid modification unique to ATP1B2 when compared to the other Na^+,K^+-ATPase β-subunit isoforms. Although we identify a novel post-translational modification of ATP1B2 in the retina, further work must be done to determine the specific functional consequences of retinal ATP1B2 palmitoylation.

3.3 Results

3.3.1 Identification of palmitoylated proteins in the retina using acyl-RAC followed by mass spectrometry

In order to comprehensively identify retinal proteins which are palmitoylated, we utilized an assay known as acyl resin-assisted capture (acyl-RAC), which takes advantage of the reversible thioester linkage between palmitate and the modified cysteine residue (Fig. 1A)[20]. As the reagent used to bind and capture palmitoylated cysteines is Thiopropyl Sepharose-6B (TPS-6B) resin, which binds free thiol groups, the first step in the assay is to incubate retinal lysate under denaturing conditions with methylmethanethiosulfonate (MMTS) to block any free thiol groups. These free thiol groups represent non-palmitoylated cysteine residues on proteins.

In the second step after blocking free thiols, palmitoylated cysteine residues are subjected to treatment with hydroxylamine (NH_2OH), which removes palmitate from the protein,

through cleavage of the thioester bond which holds it to the cysteine residue, creating a new free thiol group. The third step is to incubate the samples with the TPS-6B resin in order to capture the newly formed free thiol groups formed after cleavage of palmitate by NH_2OH. Finally, in the fourth step, proteins which bind to the resin are eluted with a reducing agent such as dithiothreitol (DTT). To ensure proper blocking and to serve as a negative control, a portion of retinal lysate was not treated with hydroxylamine (-NH_2OH). Both treated (+NH_2OH) and negative control (-NH_2OH) samples were sent for mass spectrometry (LC-MS/MS) to identify candidate proteins which are palmitoylated in the retina.

A total of 803 proteins which were present in the palmitoylated fraction (+NH_2OH elute) were chosen from the mass spectrometry data based on their spectral counts to analyze further. These proteins were cross-referenced with SwissPalm, a comprehensive online database which compiles data concerning palmitoylation of proteins and proteins appearing in proteomic studies[34]. Of our candidate proteins, 64.3% have been identified in palmitoyl proteome studies but not independently validated, 0.9% have been independently validated as palmitoylated but not identified in any palmitoyl proteomes, and 13.2% of proteins have been both validated and reported in palmitoyl proteome studies previously. Interestingly, 17.8% of proteins identified in our study have not previously been identified as palmitoylated (Fig. 1B).

To validate our mass spectrometry data, we chose several proteins whose palmitoylation status is well-documented and confirmed their statuses using western blot.

Synaptotagmin-2 (SYT2), rhodopsin (RHO), and ADP-ribosylation factor-like protein 13B (ARL13B) are all proteins which have been validated as palmitoylated or appeared in other mouse palmitoyl proteomes[9,35-37]. These proteins all appeared in our mass spectrometry results as palmitoylated and were also detectable via western blot (Fig. 1C). As a negative control, we blotted for rod PDE6α, a farnesylated protein (Fig. 1C). Collectively, these data suggest that acyl-RAC is an effective method to use for the identification of palmitoylated retinal proteins.

3.3.2 The β2 subunit of the Na^+, K^+-ATPase (ATP1B2) is palmitoylated in the retina

Of the other candidate proteins which appear in our acyl-RAC/mass spectrometry data, the one that is of most interest to this study is the β2 subunit of the Na^+, K^+-ATPase (ATP1B2). First, we used acyl-RAC and western blot analysis to confirm palmitoylation of ATP1B2 (Fig. 2A). In this study, GOα, a known palmitoylated protein localized to bipolar cells, was used as a positive control[37]. Importantly, when the amino acid sequence of ATP1B2 is analyzed using a palmitoylation prediction algorithm (GPS-Palm), the 10th amino acid (Cys^{10}) is predicted to be palmitoylated with a medium confidence score (Fig. 2B)[38]. Interestingly, when compared to the other β-subunit isoforms of the Na^+,K^+-ATPase, Cys^{10} is unique to ATP1B2 (Fig. 2C). As expected, ATP1B1 was not found to be palmitoylated (Fig. 2A). Furthermore, Cys^{10} is conserved across several mammalian species (Fig. 2C). Although ATP1B2 is heavily glycosylated on the extracellular portion of the protein and has six additional cysteines implicated in disulfide bonds, palmitoylation appears to be the only known post-translational modification located on the N-terminus of the protein (Fig. 2D).

An additional method known as acyl-PEG exchange was also used to validate the palmitoylation of ATP1B2 in retina (Fig. 3A)[24]. In this method, Bond-Breaker™ TCEP is used to break any disulfide bonds and N-ethylmaleimide (NEM) is used to block all free cysteines. Once again, hydroxylamine (NH_2OH) is used to cleave the thioester bond attaching palmitate to the palmitoylated cysteine on the protein. Once a new free thiol group is formed, lysate is incubated with mPEG-maleimide 5kDa. This PEGylated chemical will then attach to the free thiol group, giving the palmitoylated protein an additional 5 kDa shift for every residue which is modified when analyzed by western blot. Our data from retinal lysate reveal a 5 kDa shift of a portion of ATP1B2 in only the treated (+NH_2OH) sample, indicating selective PEGylation and denoted by an asterisk (Fig. 3B). A fraction of total ATP1B2 is non-PEGylated (denoted as "apo"), indicating the portion of the retinal pool of ATP1B2 which is not palmitoylated. As a negative control, a sample not treated with hydroxylamine (-NH_2OH) is run alongside the treated sample (Fig. 3B, lanes 1 and 3). PEGylation of the known palmitoylated protein (GOα) and non-PEGylation of a negative control (PDE6α) confirm the specificity of the acyl-PEG exchange assay. Collectively, mass-tag labeling of retinal proteins by acyl-PEG exchange further confirms that Cys^{10} in ATP1B2 is modified by palmitoylation.

3.3.3 ATP1B2 is palmitoylated on Cys^{10}

Interestingly, aside from the predicted palmitoylated Cys^{10} residue, all other cysteines in ATP1B2 have been shown to participate in disulfide bonds (Fig. 2C). To determine the ATP1B2 residue which is palmitoylated, we utilized mass spectrometry in conjunction with

carbamidomethylation labeling, a method which has been widely used for identifying palmitoylated cysteines[23]. Retinal lysate was subjected to acyl-RAC and eluted samples were then treated with iodoacetamide, which binds free thiol groups. Alkylation of iodoacetamide results in covalent addition of a carbamidomethyl group, which gives a mass difference of 57 Da. Analysis of treated samples by mass spectrometry can visualize these carbamidomethylated cysteines as residues with increased mass (C+57). As expected, our mass spectrometry analysis reveals that Cys^{10} in ATP1B2 is modified (Fig. 4).

3.3.4 A C10A mutation in ATP1B2 results in loss of palmitoylation *in vivo*

In order to confirm palmitoylation of ATP1B2 on its N-terminal Cys^{10} residue *in vivo*, we generated two plasmid constructs in a pCAG vector under a chicken β-actin promoter. One construct expresses wild-type mouse HA-tagged ATP1B2, while the other expresses mouse HA-tagged ATP1B2 with a cysteine to alanine mutation at Cys^{10} (C10A) (Fig. 5A, B). Both of these constructs feature an HA tag on the C-terminal end of the protein. Additionally, our construct has a separate IRES driven EGFP reporter to evaluate transfection efficiency and protein stability. We injected these constructs into the subretinal space of neonatal mice at P0 and collected retinal tissue at P21. Uninjected (contralateral eye), ATP1B2, and ATP1B2-C10A injected retinal lysates were analyzed using acyl-RAC. Western blot analysis clearly shows that endogenous ATP1B2 and ectopically-expressed ATP1B2 is palmitoylated, while ATP1B2-C10A is not (Fig. 5C). These data confirm that ATP1B2 is palmitoylated on Cys^{10} and that a C10A mutation results in loss of palmitoylation *in vivo*.

3.4 Discussion

Many photoreceptor proteins involved in phototransduction, OS maintenance, and photoreceptor function require lipidation to participate in their required functions, the original focus of the current study was to identify a pool of proteins in the metabolically active retina which undergo palmitoylation. By taking advantage of the unique chemistry of palmitoylation, our lab employed acyl-RAC and mass spectrometry in order to isolate and identify proteins in the retina which undergo this post-translational lipid modification. We utilized the SwissPalm database in order to individually cross reference 803 candidate proteins from our data against proteins which had been identified in other palmitoyl proteome studies and proteins which had been validated as palmitoylated.

As expected, many proteins which are ubiquitously expressed in different tissues are also expressed in the retina, so we did identify a large population of proteins (64.3%) which had been identified in other palmitoyl proteome studies. There was also a population of proteins which have not been identified in other palmitoyl proteome studies, but have been validated (0.9%), likely proteins which are expressed in tissues which have not had palmitoyl proteomes characterized. Two examples of proteins which fit into this category would be progressive rod-cone degeneration (PRCD) and rhodopsin. Additionally, there were proteins which had been both validated and identified in other palmitoyl proteome studies (13.2%), as well as proteins which have not been placed into either of these categories (17.8%). From these candidate proteins, we decided to choose one protein which has also been identified in other palmitoyl proteome studies, but has not yet been validated – the β-subunit of the retinal Na^+,K^+-ATPase, ATP1B2. Additionally, we were

able to determine that ATP1B2 is palmitoylated on its N-terminal cysteine residue at the 10th amino acid position (Cys^{10}) using palmitoylation prediction software and mass spectrometry.

All isoforms of the β-subunit of the Na^+,K^+-ATPase (ATP1B1, ATP1B2, and ATP1B3) contain six cysteine residues located on the extracellular portion of the protein, all of which have been shown to participate in disulfide bonds[27]. Two of these disulfide bonds are crucial for binding the α-subunit, while the other is required for proper enzymatic activity of the holoenzyme[39]. Although both ATP1B1 and ATP1B2 contain one additional cysteine, the extra cysteine in ATP1B1 is located within the transmembrane domain at the 45th amino acid position (Cys^{45}) and has been shown to undergo glutathionylation[40]. The additional cysteine residue located near the N-terminus of ATP1B2 (Cys^{10}) is not only unique to ATP1B2, but is conserved across several different mammalian species. Therefore, it is possible that palmitoylation of ATP1B2 plays an important role in modulating one or more of its functions.

In the retina, the predominantly expressed subunits of the Na^+,K^+-ATPase are ATP1A3 and ATP1B2[28,29]. Although photoreceptors express ATP1A3, ATP1B2, and ATP1B3, ATP1B2 has been shown to play a crucial role in photoreceptor maintenance, as 50% of photoreceptors degenerate by P17 in retina lacking ATP1B2[31-35]. Furthermore, another animal model has been characterized which lacks ATP1B2, but expresses ATP1B1 in its place (β1/β2 knock-in). While expression of ATP1B1 in photoreceptors helps to delay degeneration, 50% of photoreceptors still degenerate by 4 months of age in the absence

ATP1B2[33]. These studies outline an apparent requirement of ATP1B2 expression in the retina to ensure photoreceptor maintenance and survival, yet the unique requirement of this β-subunit isoform of the Na^+,K^+-ATPase remains unclear. While there are structural similarities between the β-isoforms of the Na^+,K^+-ATPase, the overall sequence homology between the three is relatively low. These differences in structure give unique properties to each isoform, granting variety in their involvement in different cellular functions. Palmitoylation provides a unique feature to the β2-subunit isoform which the other isoforms lack.

One possible role for palmitoylation of ATP1B2 is proper targeting and subcellular localization of the Na^+,K^+-ATPase to the IS. In photoreceptors, the Na^+,K^+-ATPase exclusively localizes to the IS, where proteins are synthesized. Due to the high amount of ATP utilized by the Na^+,K^+-ATPase, it is believed that this specific localization to the IS is required in order to ensure that ATP can be funneled to and utilized by the OS during light stimulus[41,42]. In the dark when phototransduction is dormant, the Na^+,K^+-ATPase uses the majority of ATP, but this trend shifts in the light when phototransduction is actively cycling in the OS[41]. Many phototransduction proteins, such as rhodopsin, are synthesized in the IS and must be trafficked to the OS to participate in their proper function. However, the connecting cilium bridging the IS and OS restricts which proteins are able to pass. Studies in frog photoreceptors have shown that rhodopsin is able to diffuse from the OS to the IS when this barrier is compromised, yet the Na^+,K^+-ATPase remains confined to the IS[43]. To date, only one other protein (ankyrin-B) has been shown to interact with ATP1B2 and demonstrate a role in securing the Na^+,K^+-ATPase to the IS

cytoskeleton, however only a small amount of ankyrin-B has been shown to immunoprecipitate with the Na^+,K^+-ATPase in retina[41,44]. Due to the implication of palmitoylation in localization to specific membrane microdomains and subcellular trafficking, it is possible that palmitoylation of ATP1B2 in photoreceptors could be important to tether the Na^+,K^+-ATPase to the IS plasma membrane, ensuring proper localization to the IS compartment.

As mentioned, the amino acid sequences and post-translational modifications of the β-subunit isoforms (β1, β2, and β3) vary greatly, contributing to their unique cellular functions. Interestingly, of the β-subunit isoforms, the transmembrane alpha helix in ATP1B2 has been shown to have a tilt angle which is 5° different compared to ATP1B1 and ATP1B3[45]. This tilt angle is thought to alter the interaction between ATP1B2 and its bound catalytic (α-) subunit, which may influence Na^+,K^+-ATPase activity[45]. In fact, studies show that pumps containing ATP1B2 have a lower affinity for K^+ ions[46]. Due to the reversibility of S-palmitoylation, this post-translational lipid modification carries implications in dynamic biological processes such as signaling and ion channel activity. Considering the unusually high activity of the Na^+,K^+-ATPase in photoreceptors and the fact that loss of the β2-subunit of the retinal Na^+,K^+-ATPase leads to photoreceptor degeneration, it is apparent that regulation of Na^+,K^+-ATPase activity would be extremely important for retinal health.

Interestingly, many tissues express a γ-subunit of the Na^+,K^+-ATPase which binds the Na^+,K^+-ATPase holoenzyme and alters the pump's ion affinities or its kinetic properties,

yet no γ-subunit has yet been identified in the retina[47]. It is quite possible that palmitoylation of ATP1B2 could also alter the structural conformation of the retinal Na^+,K^+-ATPase enough to alter its affinities for Na^+ and K^+, or otherwise modulate the kinetic properties of pump activity. In this role, palmitoylation would essentially serve as a quasi-γ-subunit for the retinal Na^+,K^+-ATPase.

In conclusion, we have identified a previously unknown post-translation modification of ATP1B2 by palmitoylation in the retina. Using several experimental approaches, we have verified this modification and identified it on Cys^{10}, which we provide evidence is palmitoylated *in vivo*. We also employed a palmitoylation gel-shift assay to observe that a significant portion of retinal ATP1B2 is likely palmitoylated, which likely contributes a role to one or multiple functions of ATP1B2. While there are several enticing hypotheses concerning the mechanistic role of ATP1B2 palmitoylation, this specific role remains to be delineated and is a subject of ongoing and future studies. In general, continued study of ATP1B2 and other palmitoylated proteins in the mammalian retina promises to increase our collective understanding of this unique post-translational modification and its ever-growing list of important biological roles.

3.5 Methods

3.5.1 Animals

All experimental procedures involving animals in this study were approved and conducted in strict accordance with relevant guidelines and regulations by the Institutional Animal Care and Use Committee at West Virginia University.

3.5.2 Cloning

Plasmid constructs encoding wild type and mutant (C10A) mouse ATP1B2 with a C-terminal epitope hemagglutinin-tag (HA) were synthesized as followed. Epitope-tagged gene fragments were generated using PCR and custom-made primers (***see Table 3.1***) and subsequently ligated into a SalI-HF/BamHI digested (New England BioLabs) pCAG vector containing a CAG promoter and in-frame IRES-EGFP sequence.

3.5.3 Acyl-RAC Isolation of Palmitoylated Proteins

Palmitoylated proteins or transiently transfected hRPE1 cells were assessed by acyl-RAC as described previously[20,37]. Retinas were homogenized in ice-cold lysis buffer (25 mM HEPES, pH 7.5, 150 mM NaCl, 1 mM EDTA, 1 mM HDSF, plus protease and phosphatase inhibitors) by sonication. Lysate was then treated with 1% Triton-X-100 for 20 minutes at 4°C on a rotator. Next, lysate was centrifuged at 500 *xg* for 3 minutes and supernatant was transferred to a new tube to block free cysteine residues with blocking buffer (100 mM HEPES, pH 7.5, 1 mM EDTA, 2.5% SDS, and S-methyl methanethiosulfonate). Blocking was carried out for 18 minutes at 40°C by vortexing

every 2 minutes. Proteins were precipitated using ice-cold acetone for 30 minutes at -20°C and subsequently centrifuged for 20 minutes at 4°C. Protein pellets were washed four times with 70% ice-cold acetone and then air dried at room temperature for 15-20 minutes. After resuspension with 600 μl of binding buffer (100 mM HEPES, pH 7.5, 1 mM EDTA, 1% SDS), the lysate was split into two fractions. Both fractions were added to 40 μl of pre-washed Thiopropyl Sepharose 6B beads (GE Healthcare). One fraction (+NH_2OH) was treated with 40 μl of 2M hydroxylamine, pH 7.5 (Sigma), while the other (-NH_2OH) was treated with 40 μl of NaCl (control). Samples were incubated for 2 hours at room temperature and beads were washed with binding buffer four times. Bound proteins were then eluted with 10 mM DTT and further analyzed by LC/MS mass spectrometry and western blotting.

3.5.4 Proteomic analysis

As described earlier, retinal lysate was subjected to acyl-RAC and samples were eluted with 100 µl of elution buffer containing 10 mM DTT. Two samples treated with and without hydroxylamine (NH_2OH) were concentrated by lyophilization. The lyophilized protein samples were reconstituted with 1X PBS at an equal concentration for both treated and untreated (+/- NH_2OH) for LC-MS/MS mass spec analysis. Three independent analyses from two different places, 1) Protea Biosciences, (Morgantown, WV) and 2) Harvard University mass spectrometry facility were performed.

3.5.5 Western blotting

To assess protein levels, retina or cells were homogenized on ice by sonication (Microson Ultrasonic cell disruptor; 3 pulses, 3 seconds at power setting 10) in 1X phosphate buffered saline (PBS) with protease and phosphatase inhibitors. A NanoDrop spectrophotometer (ND-1000, Thermo Fisher Scientific) was utilized to quantify protein concentration. To each sample before boiling for 5 minutes, 5X Laemmli buffer was added with 5% β-mercaptoethanol. An equal concentration of each sample was loaded and separated by SDS-PAGE in a 4-20% tris-glycine precast gel (4–20% Mini-PROTEAN TGX, Bio-Rad, Hercules, CA, USA) and then transferred to an Immobilon-FL PVDF membrane (Immobilon-FL, Millipore, Burlington, MA, USA). Membranes were then blocked for 1 hour at room temperature using Odyssey Blocking Buffer (LI-COR Biosciences, Lincoln, NE, USA) prior to being incubated with primary antibodies (see ***Table 3.2*** for full list of antibodies used). Primary antibody was left on membranes for 2 hours at RT or overnight at 4°C on a bidirectional rotator. Membranes were then washed three times in 1X PBST (1X PBS/0.1% Tween-20) for 5 minutes each at room temperature prior to being incubated with secondary antibody, goat anti-rabbit Alexa Fluor 680, goat anti-mouse DyLight 800 or donkey anti-sheep Alexa Fluor 680 (Thermo Fisher Scientific) for 30 minutes at RT. Blots were washed 3 times in 1X PBST before being scanned using an Odyssey Infrared Imaging System. Protein density was measured according to manufacturer's instruction (LI-COR Biosciences, Lincoln, NE, USA).

3.5.6 Carbamidomethylation of acyl-RAC retinal samples

This process was completed at Protea Biosciences, Inc. Morgantown, WV. The concentrated samples from acyl-RAC treated with or without NH_2OH were incubated with

50 mM iodoacetamide in 50 mM ammonium bicarbonate for 10 min at RT. The reaction was stopped by addition of matrix (sinapinic acid in 30% acetonitril, 0.3% TFA) and analyzed by MALDI-TOF, and LC-MS/MS. The peptides were identified by MS/MS spectra searched against using the Scaffold4 software search engine. The samples were processed to identify cysteines modified by carbamidomethylation. The precursor mass tolerance for carbamidomethylation or palmitoylation on Cys, Acetyl on Protein N-terminus and oxidation of Met were used by setting fragment ion mass tolerance to 0.5 Da. Iodoacetamide only affected the peak corresponding to the deacylated ATP1B2 at N-terminal cysteine 10, with an expected increase of 57 Da corresponding to a carbamidomethylation of the free sulfhydryl group.

3.5.7 Acyl-PEG exchange

Experiment was conducted using a modified protocol which was previously described[24]. 2 retina were suspended in 150 μl lysis buffer (1X TEA buffer [5 mM Triethanolamine, 15 mM NaCl, pH 7.3], 4% SDS, protease inhibitor, Pierce universal nuclease, and PMSF) and sonicated. After addition of EDTA (final concentration 5 mM), total protein concentration was assessed using a NanoDrop spectrophotometer (ND-1000, Thermo Fisher Scientific). Next, 2 μg of total protein was transferred to a clean tube and treated with neutralized Bond-Breaker™ TCEP (Thermo Fisher Scientific) for 30 minutes at room temperature under constant rotation in order to break any disulfide bonds. Lysate was next treated with 25 mM N-ethyl maleimide (NEM) for 2 hours at room temperature with nutation in order to block any exposed cysteine residues. To remove TCEP and NEM, protein was next precipitated three sequential times as described by Percher *et al* using

methanol, chloroform, and water at a 4:1.5:3 ratio relative to sample volume[24]. After precipitation, precipitated protein was dried using a vacuum centrifuge (Vacufuge, Eppendorf*) for 10 minutes at room temperature and then resuspended in 60 μl of 1X TEA buffer with 4% SDS and 4 mM EDTA. Next, the sample was split into two-30 μl fractions. One fraction (+NH_2OH) was treated with 90 μl of hydroxylamine (prepared in 1X TEA buffer with 0.2% Triton-X-100), while the other (-NH_2OH) was treated with 90 μl of 1X TEA buffer with 0.2% Triton-X-100 (control). Samples incubated for 1 hour at room temperature under nutation with hydroxylamine in order to cleave thioester bond (remove palmitoylation). After incubation, proteins were precipitated (see above) in order to remove all traces of hydroxylamine present. Next, samples were resuspended in 30 μl of 1X TEA buffer with 4% SDS and 4 mM EDTA and treated with 1 mM mPEG-maleimide (5 kDa) for 1 hour at room temperature (under nutation) to give a mass shift difference to any cysteine residues which were modified by palmitoylation. After a final protein precipitation, samples were resuspended in 1X Laemmli buffer (200 μl 5X Laemmli in 800 μl 1X TEA buffer/4% SDS) with 5% b-mercaptoethanol and incubated at 95°C for 5 minutes. Samples were then analyzed by SDS-PAGE electrophoresis and western blot.

3.5.8 Subretinal injection

Wild-type and mutant (C10A) *Atp1b2* plasmid DNA (5.0 μg/μl) was purified and prepared for injection by adding 0.1% fluorescein sodium (100 mg/ml; AK-FLUOR). Surgery was performed under a Leica M80 microscope (Leica Microsystems). Neonatal mice (postnatal day 0) were anesthetized by hypothermia and an incision was made using a $25^{5/8}$-gauge needle (BD Biosciences) to open the future eyelid. Next, a $30^{1/2}$-gauge needle

is used to make a small hole in the sclera, just outside the border of the cornea. Using a Hamilton syringe, 33-gauge blunt end needle (Hamilton Company) is placed through the hole which was made and 0.25-0.5 μl of plasmid DNA was injected into the subretinal space. Plasmid DNA was next electroporated (five pulses of 80V, 50 ms duration, 950 ms interval) by Tweezer-type electrodes (BTX model 520, 7mm diameter). Injected and contralateral (control) retina were collected 21 days later and subjected to acyl-RAC followed by western blot analysis.

3.6 References

1 Pearring, J. N., Salinas, R. Y., Baker, S. A. & Arshavsky, V. Y. Protein sorting, targeting and trafficking in photoreceptor cells. *Prog Retin Eye Res* **36**, 24-51, doi:10.1016/j.preteyeres.2013.03.002 (2013).

2 Palczewski, K. G protein-coupled receptor rhodopsin. *Annu Rev Biochem* **75**, 743-767, doi:10.1146/annurev.biochem.75.103004.142743 (2006).

3 Jiang, H. *et al.* Protein Lipidation: Occurrence, Mechanisms, Biological Functions, and Enabling Technologies. *Chemical Reviews* **118**, 919-988, doi:10.1021/acs.chemrev.6b00750 (2018).

4 Resh, M. D. Covalent lipid modifications of proteins. *Curr Biol* **23**, R431-R435, doi:10.1016/j.cub.2013.04.024 (2013).

5 Kokame, K., Fukada, Y., Yoshizawa, T., Takao, T. & Shimonishi, Y. Lipid modification at the N terminus of photoreceptor G-protein α-subunit. *Nature* **359**, 749-752, doi:10.1038/359749a0 (1992).

6 Neubert, T. A., Johnson, R. S., Hurley, J. B. & Walsh, K. A. The rod transducin alpha subunit amino terminus is heterogeneously fatty acylated. *J Biol Chem* **267**, 18274-18277 (1992).

7 Lobanova, E. S. *et al.* Transducin translocation in rods is triggered by saturation of the GTPase-activating complex. *J Neurosci* **27**, 1151-1160, doi:10.1523/JNEUROSCI.5010-06.2007 (2007).

8 Anant, J. S. *et al.* In vivo differential prenylation of retinal cyclic GMP phosphodiesterase catalytic subunits. *J Biol Chem* **267**, 687-690 (1992).

9 Ovchinnikov Yu, A., Abdulaev, N. G. & Bogachuk, A. S. Two adjacent cysteine residues in the C-terminal cytoplasmic fragment of bovine rhodopsin are palmitylated. *FEBS Lett* **230**, 1-5, doi:10.1016/0014-5793(88)80628-8 (1988).

10 Maeda, A. *et al.* Palmitoylation stabilizes unliganded rod opsin. *Proc Natl Acad Sci U S A* **107**, 8428-8433, doi:10.1073/pnas.1000640107 (2010).

11 Seno, K. & Hayashi, F. Palmitoylation is a prerequisite for dimerization-dependent raftophilicity of rhodopsin. *The Journal of biological chemistry* **292**, 15321-15328, doi:10.1074/jbc.M117.804880 (2017).

12 Resh, M. D. Fatty acylation of proteins: The long and the short of it. *Prog Lipid Res* **63**, 120-131, doi:10.1016/j.plipres.2016.05.002 (2016).

13 Mitchell, D. A., Vasudevan, A., Linder, M. E. & Deschenes, R. J. Thematic review series: Lipid Posttranslational Modifications. Protein palmitoylation by a family of DHHC protein S-acyltransferases. *Journal of Lipid Research* **47**, 1118-1127, doi:10.1194/jlr.R600007-JLR200 (2006).

14 Aicart-Ramos, C., Valero, R. A. & Rodriguez-Crespo, I. Protein palmitoylation and subcellular trafficking. *Biochim Biophys Acta* **1808**, 2981-2994, doi:10.1016/j.bbamem.2011.07.009 (2011).

15 Linder, M. E. & Deschenes, R. J. Palmitoylation: policing protein stability and traffic. *Nature Reviews Molecular Cell Biology* **8**, 74-84, doi:10.1038/nrm2084 (2007).

16 Matt, L., Kim, K., Chowdhury, D. & Hell, J. W. Role of Palmitoylation of Postsynaptic Proteins in Promoting Synaptic Plasticity. *Frontiers in Molecular Neuroscience* **12**, doi:10.3389/fnmol.2019.00008 (2019).

17 Munday, A. D. & López, J. A. Posttranslational protein palmitoylation: promoting platelet purpose. *Arterioscler Thromb Vasc Biol* **27**, 1496-1499, doi:10.1161/atvbaha.106.136226 (2007).

18 Shipston, M. J. Ion channel regulation by protein palmitoylation. *J Biol Chem* **286**, 8709-8716, doi:10.1074/jbc.R110.210005 (2011).

19 Smotrys, J. E. & Linder, M. E. Palmitoylation of intracellular signaling proteins: regulation and function. *Annu Rev Biochem* **73**, 559-587, doi:10.1146/annurev.biochem.73.011303.073954 (2004).

20 Forrester, M. T. *et al.* Site-specific analysis of protein S-acylation by resin-assisted capture. *J Lipid Res* **52**, 393-398, doi:10.1194/jlr.D011106 (2011).

21 Roth, A. F. *et al.* Global Analysis of Protein Palmitoylation in Yeast. *Cell* **125**, 1003-1013, doi:https://doi.org/10.1016/j.cell.2006.03.042 (2006).

22 Drisdel, R. C. & Green, W. N. Labeling and quantifying sites of protein palmitoylation. *BioTechniques* **36**, 276-285, doi:10.2144/04362rr02 (2004).

23 Thinon, E., Fernandez, J. P., Molina, H. & Hang, H. C. Selective Enrichment and Direct Analysis of Protein S-Palmitoylation Sites. *J Proteome Res* **17**, 1907-1922, doi:10.1021/acs.jproteome.8b00002 (2018).

24 Percher, A., Thinon, E. & Hang, H. Mass-Tag Labeling Using Acyl-PEG Exchange for the Determination of Endogenous Protein S-Fatty Acylation. *Curr Protoc Protein Sci* **89**, 14.17.11-14.17.11, doi:10.1002/cpps.36 (2017).

25 Craig, W. S. & Kyte, J. Stoichiometry and molecular weight of the minimum asymmetric unit of canine renal sodium and potassium ion-activated adenosine triphosphatase. *J Biol Chem* **255**, 6262-6269 (1980).

26 Pedersen, P. L. & Carafoli, E. Ion motive ATPases. I. Ubiquity, properties, and significance to cell function. *Trends in Biochemical Sciences* **12**, 146-150, doi:10.1016/0968-0004(87)90071-5 (1987).

27 Clausen, M. V., Hilbers, F. & Poulsen, H. The Structure and Function of the Na,K-ATPase Isoforms in Health and Disease. *Front Physiol* **8**, 371, doi:10.3389/fphys.2017.00371 (2017).

28 Schneider, B. G. & Kraig, E. Na+, K(+)-ATPase of the photoreceptor: selective expression of alpha 3 and beta 2 isoforms. *Exp Eye Res* **51**, 553-564, doi:10.1016/0014-4835(90)90086-a (1990).

29 Wetzel, R. K., Arystarkhova, E. & Sweadner, K. J. Cellular and Subcellular Specification of Na,K-ATPase α and β Isoforms in the Postnatal Development of Mouse Retina. *The Journal of Neuroscience* **19**, 9878, doi:10.1523/JNEUROSCI.19-22-09878.1999 (1999).

30 Friedrich, U. *et al.* The Na/K-ATPase is obligatory for membrane anchorage of retinoschisin, the protein involved in the pathogenesis of X-linked juvenile retinoschisis. *Hum Mol Genet* **20**, 1132-1142, doi:10.1093/hmg/ddq557 (2011).

31 Magyar, J. P. *et al.* Degeneration of neural cells in the central nervous system of mice deficient in the gene for the adhesion molecule on Glia, the beta 2 subunit of murine Na,K-ATPase. *J Cell Biol* **127**, 835-845, doi:10.1083/jcb.127.3.835 (1994).

32 Molday, L. L., Wu, W. W. & Molday, R. S. Retinoschisin (RS1), the protein encoded by the X-linked retinoschisis gene, is anchored to the surface of retinal photoreceptor and bipolar cells through its interactions with a Na/K ATPase-SARM1 complex. *J Biol Chem* **282**, 32792-32801, doi:10.1074/jbc.M706321200 (2007).

33 Weber, P., Bartsch, U., Schachner, M. & Montag, D. Na,K-ATPase subunit beta1 knock-in prevents lethality of beta2 deficiency in mice. *J Neurosci* **18**, 9192-9203, doi:10.1523/jneurosci.18-22-09192.1998 (1998).

34 Blanc, M. *et al.* SwissPalm: Protein Palmitoylation database [version 1; peer review: 3 approved]. *F1000Research* **4**, doi:10.12688/f1000research.6464.1 (2015).

35 Wan, J. *et al.* Tracking brain palmitoylation change: predominance of glial change in a mouse model of Huntington's disease. *Chem Biol* **20**, 1421-1434, doi:10.1016/j.chembiol.2013.09.018 (2013).

36 Roy, K. *et al.* Palmitoylation of the ciliary GTPase ARL13b is necessary for its stability and its role in cilia formation. *J Biol Chem* **292**, 17703-17717, doi:10.1074/jbc.M117.792937 (2017).

37 Murphy, J. & Kolandaivelu, S. Palmitoylation of Progressive Rod-Cone Degeneration (PRCD) Regulates Protein Stability and Localization. *J Biol Chem* **291**, 23036-23046, doi:10.1074/jbc.M116.742767 (2016).

38 Ning, W. *et al.* GPS-Palm: a deep learning-based graphic presentation system for the prediction of S-palmitoylation sites in proteins. *Brief Bioinform*, doi:10.1093/bib/bbaa038 (2020).

39 Noguchi, S., Mutoh, Y. & Kawamura, M. The functional roles of disulfide bonds in the beta-subunit of (Na,K)ATPase as studied by site-directed mutagenesis. *FEBS Lett* **341**, 233-238, doi:10.1016/0014-5793(94)80463-x (1994).

40 Figtree, G. A. *et al.* Reversible oxidative modification: a key mechanism of Na+-K+ pump regulation. *Circ Res* **105**, 185-193, doi:10.1161/circresaha.109.199547 (2009).

41 Baker, S. A. & Kerov, V. in *Current Topics in Membranes* Vol. 72 (ed Vann Bennett) 231-265 (Academic Press, 2013).

42 Ames, A., 3rd, Li, Y. Y., Heher, E. C. & Kimble, C. R. Energy metabolism of rabbit retina as related to function: high cost of Na+ transport. *J Neurosci* **12**, 840-853, doi:10.1523/jneurosci.12-03-00840.1992 (1992).

43 Spencer, M., Detwiler, P. B. & Bunt-Milam, A. H. Distribution of membrane proteins in mechanically dissociated retinal rods. *Investigative Ophthalmology & Visual Science* **29**, 1012-1020 (1988).

44 Kizhatil, K., Sandhu, N. K., Peachey, N. S. & Bennett, V. Ankyrin-B is required for coordinated expression of beta-2-spectrin, the Na/K-ATPase and the Na/Ca exchanger in the inner segment of rod photoreceptors. *Exp Eye Res* **88**, 57-64, doi:10.1016/j.exer.2008.09.022 (2009).

45 Hilbers, F. *et al.* Tuning of the Na,K-ATPase by the beta subunit. *Scientific Reports* **6**, 20442, doi:10.1038/srep20442 (2016).

46 Larsen, B. R. *et al.* Contributions of the Na^+/K^+-ATPase, NKCC1, and Kir4.1 to hippocampal K^+ clearance and volume responses. *Glia* **62**, 608-622, doi:10.1002/glia.22629 (2014).

47 Sweadner, K. J. & Rael, E. The FXYD gene family of small ion transport regulators or channels: cDNA sequence, protein signature sequence, and expression. *Genomics* **68**, 41-56, doi:10.1006/geno.2000.6274 (2000).

3.7 Figures and Figure Legends

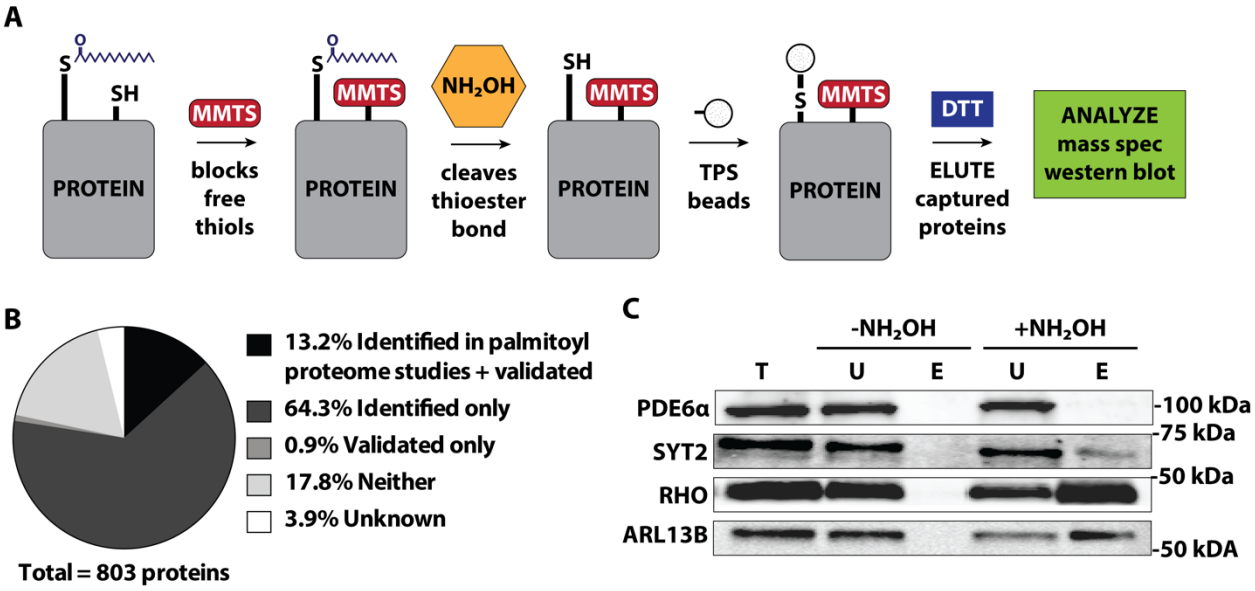

Figure 3.1. Identification of palmitoylated proteins in the murine retina. (A) Scheme demonstrating the experimental procedure for acyl resin-assisted capture, or acyl-RAC. –SH groups represent free thiol groups. MMTS = methylmethanethiosulfonate, NH_2OH = hydroxylamine, TPS = Thiopropyl Sepharose-6B resin, DTT = dithiothreitol. **(B)** Pie chart demonstrating categorization of 803 proteins which were chosen from the mass spectrometry data after following cross-referencing with the Swiss Palm database of known palmitoylated proteins. **(C)** Immunoblot analysis of acyl-RAC retinal samples validates palmitoylation of several previously identified proteins which are palmitoylated, including synaptotagmin-2 (SYT2), rhodopsin (RHO), and ADP-ribosylation factor-like protein 13B (ARL13B). Rod phosphodiesterase 6 subunit alpha (PDE6α) was used as a negative, non-palmitoylated control. T = total, U = unbound, E = elute

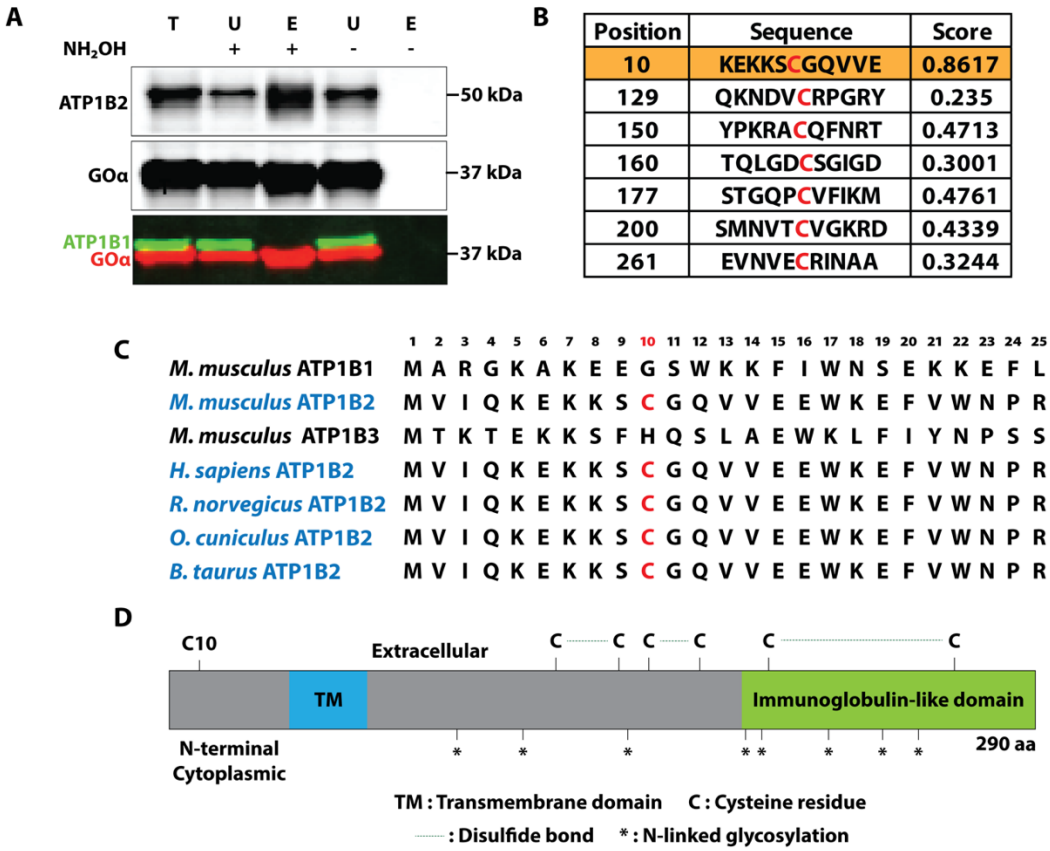

Figure 3.2. The retinal Na^+,K^+-ATPase β2-subunit is palmitoylated in the retina. (A) Immunoblot analysis of retinal lysate subjected to acyl-RAC demonstrating palmitoylation of ATP1B2, but not its homologue, the β1-subunit isoform of the Na^+,K^+-ATPase (ATP1B1). GOα is a known palmitoylated protein and was analyzed as a positive control. T = total, U = unbound, E = elute. **(B)** GPS-Palm prediction software shows a palmitoylation prediction score for each cysteine residue in ATP1B2, with Cys^{10} receiving a medium confidence score as the predicted palmitoylated residue. **(C)** Scheme demonstrating that Cys^{10} is unique to ATP1B2 among its other β-subunit isoform homologues and is conserved across several mammalian species. **(D)** Scheme demonstrating the known structural domains and post-translational modifications of mouse ATP1B2.

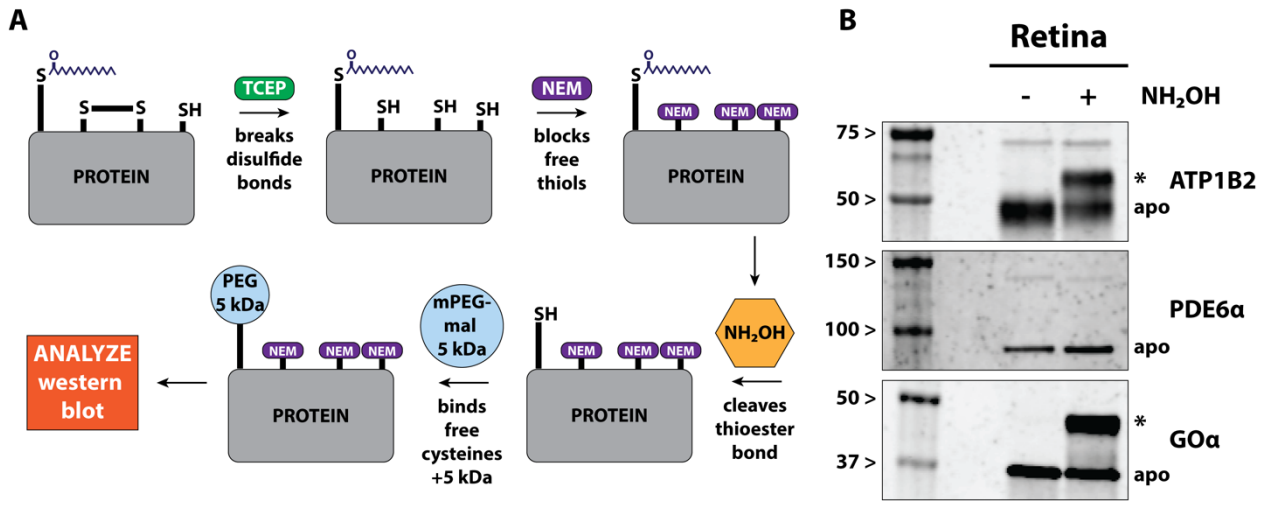

Figure 3.3. Acyl-PEG exchange confirms palmitoylation of ATP1B2 in the retina. (A) Scheme demonstrating the methodology behind acyl-PEG exchange. –SH groups represent free thiol groups. NEM = N-ethyl maleimide, NH_2OH = hydroxylamine, mPEG-mal 5 kDa = methoxy PEG maleimide. **(B)** Immunoblot analysis of retinal lysate subjected to acyl-PEG exchange demonstrating palmitoylation of ATP1B2. GOα is a known palmitoylated protein and was analyzed as a positive control. Rod phosphodiesterase 6 subunit alpha (PDE6α) was used as a negative, non-palmitoylated control. Palmitoylated proteins which are PEGylated are indicated by asterisks in the +NH_2OH fraction, while proteins labeled apo represent the non-palmitoylated fraction of the protein which is non-PEGylated.

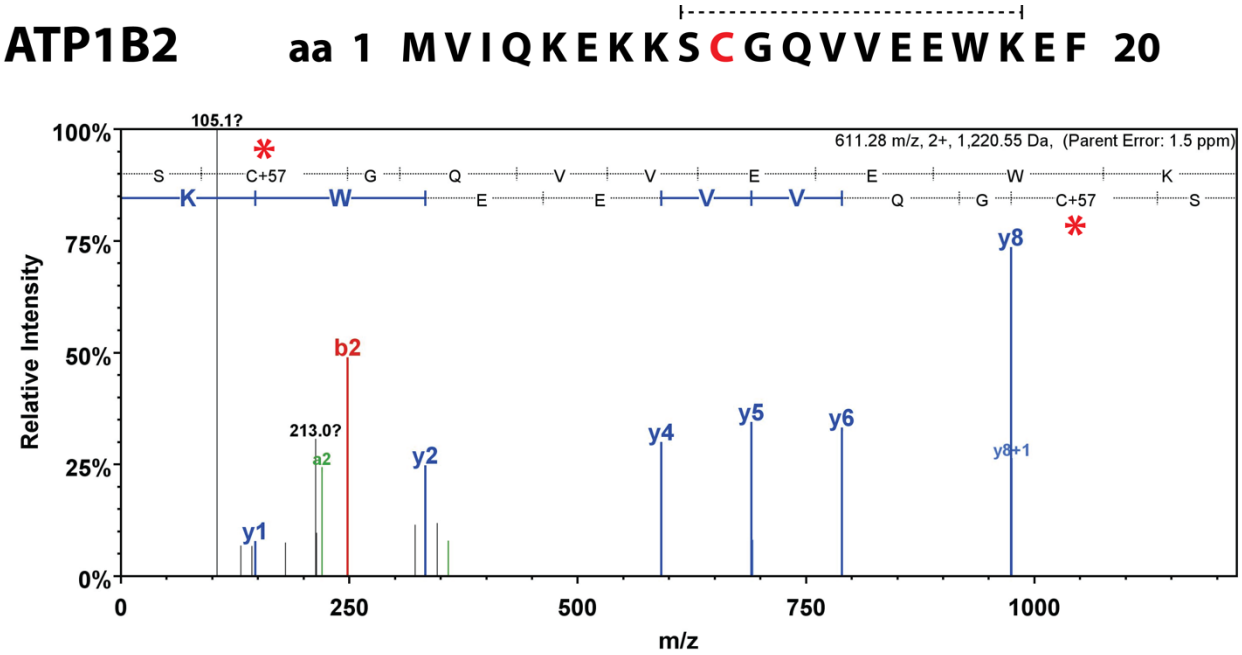

Figure 3.4. MS/MS spectra of carbamidomethyl modified cysteine in ATP1B2 peptides. S-palmitoylation sites are labelled with carbamidomethyl demonstrates that is Cys^{10} ATP1B2 is palmitoylated. Carbamidomethylation of cysteine residues indicated as C+57, asterisks in red (MS/MS spectra shown in both directions indicate carbamidomethylation of Cys^{10}).

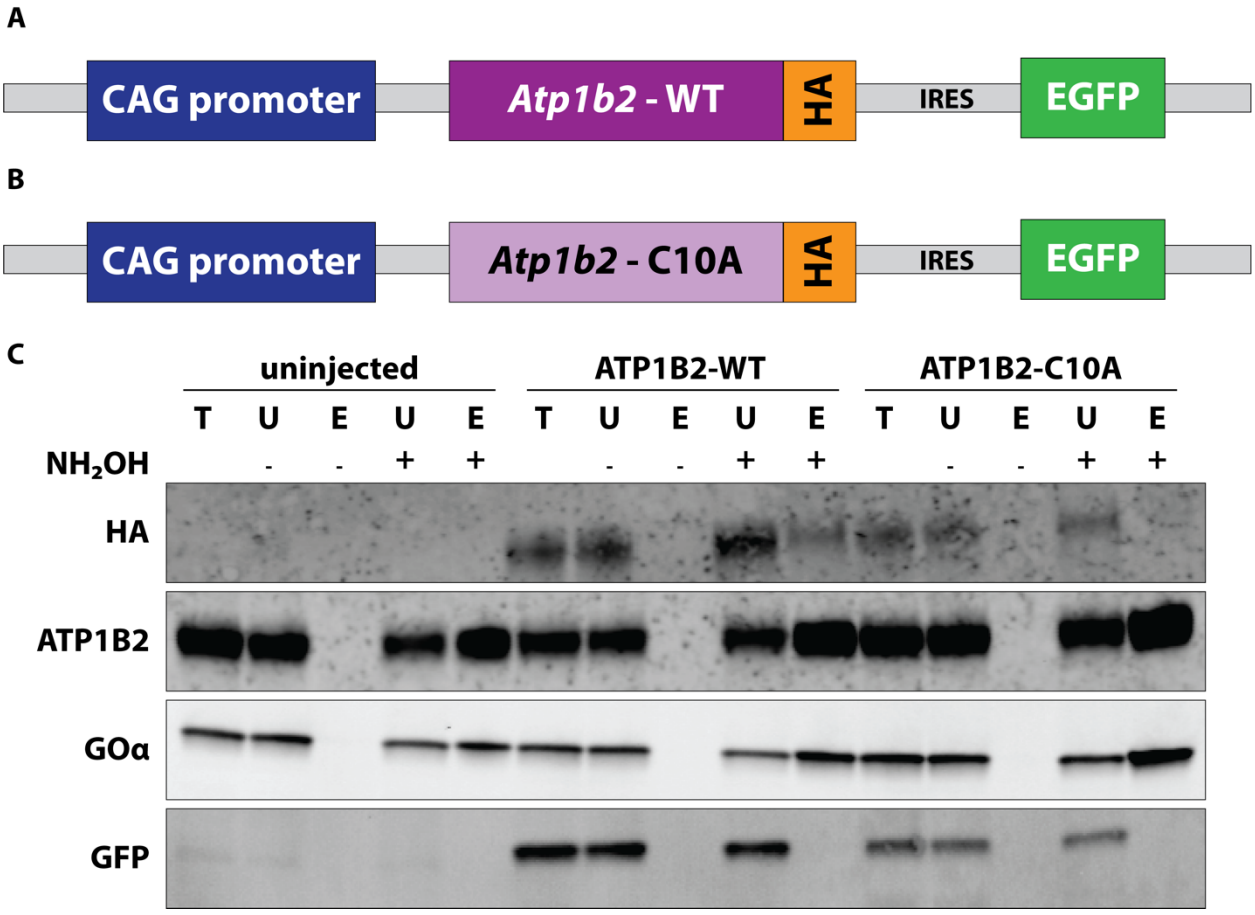

Figure 3.5. A C10A mutation in ATP1B2 results in loss of palmitoylation. (A) Scheme demonstrating the lab-generated plasmid constructs of HA-tagged wild-type and mutant-C10A ATP1B2 in a pCAG-IRES-EGFP vector. **(B)** Immunoblot analysis of retinal lysate following subretinal injection and electroporation of WT- and C10A- ATP1B2 following acyl-RAC. HA = hemagglutinin tag. GOα is a known palmitoylated protein and was analyzed as a positive control. Green fluorescent protein (GFP) was used as a negative, non-palmitoylated control. T = total, U = unbound, B = bound.

3.8 Tables

Table 3.1. List of primers used for cloning of WT and C10A ATP1B2 constructs

Primer name	Sequence
SK114 – ATP1B2 pCAG forward, SalI	5' – CTG CGA TCG GTC GAC CCG GTC GCC ACC ATG GTC ATC CAG AAA GAG – 3'
SK139 – C10A-ATP1B2 mutant pCAG forward	5' – ATG GTC ATC CAG AAA GAG AAG AAG AGC GCC GGG CAG GTG GTT GAG GAG TGG AAG GAG – 3'
SK115 – ATP1B2 pCAG reverse, HA tag, BamHI	5' – GCG CTC GGA TCC TCA AGC GTA ATC TGG AAC ATC GTA TGG GTA GGT TTT GTT GAT CCG GAG – 3'

Table 3.2. List of primary antibodies used in this study.

Antibody	Source	Dilution
Rabbit anti-ATP1B2	Proteintech, #22338-1-AP	1:2,000
Rabbit anti-GNAO1	Proteintech, #12635-1-AP	1:2,000
Rat anti-HA	Roche, #11867423001	1:2,000
Mouse anti-GFP	Proteintech, #66002-1-Ig	1:2,000
Rabbit anti-PDE6α	Thermo Fisher, #PA1-720	1:2,000
Rabbit anti-ATP1B1	Millipore Sigma, #05-382	1:2,000
Mouse anti-SYT2	Santa Cruz Biotechnology, #sc-136089	1:200
Mouse anti-RHO (4D2)	Gift from R. Molday, Univ. British Columbia	1:2,000
Rabbit anti-ARL13B	Gift from V. Ramamurthy, WVU	1:2,000

Chapter 4 – Conclusions and Future Directions

The key proteins studied in Chapter 2 and Chapter 3 of this dissertation are directly linked to either maintenance of photoreceptor structure (PRCD) or to proper photoreceptor function (ATP1B2), both of which are required for visual perception and have been extensively shown to influence one another. Photoreceptor neurons possess many unique structural features which are needed for their intrinsic function, including specialized cellular compartments such as the OS, IS, and synapse. These distinct compartments serve to create hubs for localization of specific proteins and to segregate proteins involved in different cellular processes. Any defects in these unique structural features of photoreceptors lead to flaws in function and dysregulation of photoreceptor function often leads to morphological abnormalities.

4.1 Conclusions and Future Directions – Chapter 2

PRCD is a small, 54 amino acid, photoreceptor-specific protein which is localized to photoreceptor disc membranes[1]. The only known binding partner of PRCD is rhodopsin, which initiates visual transduction in rod photoreceptors, although the significance of this interaction is not well understood[2]. Mutations in PRCD are associated with slow and progressive photoreceptor degeneration, characterized by disoriented OS disc membranes and disorganized OS, and are linked to RP[3-7]. An interesting hallmark of PRCD-associated disease is that it is extremely heterogeneous, as demonstrated by the varying phenotypes observed in different dog breeds carrying a C2Y mutation in PRCD[3]. Although we now know that PRCD plays an important role in disc morphogenesis, little is known regarding how PRCD is specifically involved in this process.

The objective of the 2nd chapter of this dissertation was to further investigate the role of PRCD in disc morphogenesis through characterization of our *Prcd*-KO mouse model, which was generated using Crispr/Cas9 gene editing. Through the combination of ultrastructural analysis and electroretinography (ERG) studies, we demonstrated that rods lacking PRCD show defects in both structure and function beginning at P30. It is important to note that while these structural and functional changes are observed at P30, degeneration of photoreceptors does not occur until after P120. Moreover, we demonstrate that loss of PRCD leads to formation of a population of rod photoreceptor disc membranes which are packaged with a lower rhodopsin density and with fewer rhodopsin nanodomains. The number of these disc membranes containing altered rhodopsin packaging increase from 30% of *Prcd*-KO discs at P30 to 50% at P120, indicating that these defects in rhodopsin packaging occur well before degeneration. Although PRCD and rhodopsin have been shown to interact with one another, these findings are the first to show any reported changes to rhodopsin prior to degeneration as a result of loss of PRCD.

Interestingly, even well documented changes to the bioavailability of rhodopsin do not seem to affect rhodopsin density or number of rhodopsin packaged into disc membranes. A mouse model under-expressing rhodopsin shows changes to disc diameter and OS length, but not changes to density or number of rhodopsin[8,9]. Interestingly, one environmental variable which does also alter the packing density of rhodopsin is light. Just as we see in our *Prcd*-KO mice at P30 and P120, disc membranes from WT mice housed in constant light for 10 days also have fewer rhodopsin molecules and a lower

rhodopsin packing density compared to WT mice housed in cyclic light[10]. Alternatively, discs from mice which are housed in constant dark for 10 days present with an increased number of rhodopsin molecules and rhodopsin packing density compared to mice housed in cyclic light, changes which only continue to increase the longer mice are housed in constant dark (20 and 30 days)[10]. Strikingly, these increases in rhodopsin number and packing density are also associated with improved rod visual function in mice housed in constant dark after 20-30 days compared to those housed in cyclic light[10].

To further elucidate the specific role of PRCD in disc morphogenesis, a future direction of the lab is to continue our AFM studies through analysis of disc membranes from *Prcd*-KO mice housed in constant light and dark. Animals with mutations in or lacking PRCD have shown to exhibit delayed renewal and phagocytosis of photoreceptor OS[4]. Furthermore, renewal rates of OSs have been shown to be slower in the dark (0.63 μm/day) and faster in the light (0.97 μm/day), compared to cyclic light (12hr light/12hr dark; 0.83 μm/day)[11]. It is possible that housing mice in constant dark could help to postpone onset of PRCD-associated disease, as renewal rates in the dark are already slower, potentially giving photoreceptors lacking PRCD more time to meet OS renewal and phagocytosis needs. Alternatively, knowing that mice housed in constant dark adapt by increasing the rhodopsin packing density and number of rhodopsin molecules which are incorporated into discs, it is also possible that housing mice in constant dark could exacerbate PRCD-associated disease if PRCD is needed for regulation of rhodopsin packaging into newly forming discs.

Multiple outcomes are also possible for *Prcd*-KO mice housed in constant light. Only a portion of irregular disc membranes containing a reduced number and packing density of rhodopsin are present in *Prcd*-KO mice at P30 (30%) and P120 (50%). As WT mice housed in constant light adapt by decreasing rhodopsin packing density and number of rhodopsin molecules, it is possible that PRCD-associated disease could be slowed due to the reduced number of rhodopsin being packaged into discs. More likely, housing mice in constant light would be very detrimental to photoreceptor health, as increased need for renewal would not be able to be met by *Prcd*-KO photoreceptors with slowed OS renewal and phagocytosis. Furthermore, there is a strong likelihood that many discs would contain even fewer molecules of rhodopsin with an even lower rhodopsin packing density if PRCD is truly required for regulation of rhodopsin incorporation into disc membranes.

To determine the consequences of long-term light or dark exposure to *Prcd*-KO photoreceptors, I propose that we compare dark-reared *Prcd*-KO animals to *Prcd*-KO animals housed in cyclic light and in constant light from birth until they reach P30 (cohort I) and P120 (cohort II). I propose that we do ultrastructural analysis to examine photoreceptor structure and electroretinography (ERG) to measure photoreceptor function. Furthermore, it would be important to measure renewal rates in these animals, which could be accomplished by immunofluorescent staining and quantification of the number of phagosomes present in the RPE [12]. Rhodopsin protein levels and mRNA levels would be assessed as described in Chapter 2 and AFM analysis would be utilized in order to determine alterations to rhodopsin packaging in disc membranes from all three groups. WT mice would also be examined as controls. These studies could help to provide further

insight into the mechanistic role of PRCD in disc morphogenesis, and more specifically, in mediating incorporation of rhodopsin molecules into disc membranes.

Another interesting phenotype which varies between different animal models with mutations in PRCD is the presence of vesicular profiles in the interphotoreceptor space[4,5,7]. Although these vesicles are a hallmark of PRCD-associated disease in miniature poodles, they are absent from English cocker spaniels[3]. The other two mouse models lacking PRCD, which are studied in a C57BL6/J background, see evidence of these vesicles accumulating in the interphotoreceptor space[4,5]. However, our *Prcd*-KO mouse model was studied in a 129/SV-E background and we do not see significant evidence of extracellular vesicles. Allon *et al* utilizes classic methods of fixation for TEM and ultrastructural analysis to see these structures, while Spencer *et al* uses a specific technique for fixation which helps to ensure staining of nascent structures, such as newly forming discs at the base of the OS[4,5]. To determine if this discrepancy in our *Prcd*-KO mouse model is due to phenotypic variations between mouse strains or a result of improper fixation of these newly formed structures, our lab plans to use a similar method of fixation to study ultrastructure and search for the presence of these vesicles in our mouse model.

Finally, another interest of the lab is to further study the predicted structural domains in PRCD to help to further elucidate its role in the photoreceptor. For such a small protein (54 amino acids), PRCD has three predicted structural domains including a transmembrane or hydrophobic domain, polybasic region, and VxPx motif[2,13].

Interestingly, each of these structural domains is closely associated with at least one mutation that is linked to RP. Our lab plans to generate plasmid constructs of each disease-associated mutation in PRCD within a pCAG-IRES-GFP vector as described previously[13]. The first mutation, which is located before the hydrophobic region of PRCD is C2Y, and has been studied extensively in canines[3,14,15]. PRCD-C2Y has been shown to be mislocalized to the IS *in vivo* and protein stability is severely reduced[2,13]. The major difference in PRCD-C2Y protein is loss of palmitoylation, a post-translational lipid modification linked to many biological processes including protein stability[13,16].

Other mutations which have not been studied in depth include the R17C and R18X mutations in the polybasic region of PRCD, as well as a P25T mutation in the VxPx motif[15,17,18]. To understand how these mutations could lead to PRCD-associated disease, we will transfect hRPE1 cells to study the protein stability, localization, membrane association, and palmitoylation status. Additionally, we will also utilize subretinal injection of these constructs to determine how these mutations affect the fate of PRCD protein stability, localization and interaction with binding partner rhodopsin. Little is known regarding the importance of these structural domains in PRCD. Polybasic regions have been shown to strengthen interactions between proteins and membranes through electrostatic interactions, while the VxPx motif has been studied thoroughly in rhodopsin as a ciliary targeting motif[19-22]. It is not known whether PRCD requires this polybasic region for proper OS disc membrane association or the VxPx motif for proper trafficking and localization to the OS. Studying these mutations would help to clarify the need for these structural domains in PRCD function and localization.

Due to the inconspicuous nature of PRCD because of its small size, it took many years for scientists to link disease-causing mutations to the small gene which codes for PRCD protein. Although several animal models with mutations in or loss of PRCD have been characterized, still very little is known about PRCD and its significant contribution to maintenance of retinal health. Studies, including ours, have demonstrated that PRCD plays an important role in OS disc morphogenesis. We know that discs do not form properly and rhodopsin incorporation into disc membranes is not consistently maintained in the absence of PRCD, yet the specific requirement for PRCD in regard to its mechanistic role in OS maintenance remains undiscovered. These proposed experiments could provide crucial information required to uncover these answers.

4.2 Conclusions and Future Directions – Chapter 3

Many studies have demonstrated the unique requirement of the β2-subunit of the retinal Na^+, K^+-ATPase (ATP1B2) in maintenance of retinal health. Not only do half of all photoreceptors degenerate in the absence of ATP1B2 by P17, but other β-subunit isoforms have demonstrated the inability to compensate for loss of ATP1B2, as demonstrated in a β1/β2 knock-in animal model where ATP1B1 is expressed in place of ATP1B2[23,24]. In fact, western blot analysis of retinal lysate from animals lacking ATP1B2 also demonstrates severe reduction of the sole α-subunit isoform in photoreceptors (ATP1A3), suggesting loss of Na^+, K^+-ATPase from photoreceptors altogether. The α-subunit of the Na^+, K^+-ATPase is known to be responsible for the enzymatic activity of the ion pump and the β-subunit has been shown to be responsible for maturation and trafficking of the holoenzyme to the plasma membrane[25]. However, very little is known

regarding the role of the β-subunit, and specifically of the β2-subunit of the Na^+, K^+-ATPase in the retina.

Apart from its role as part of the ion pump, ATP1B2 has recently been shown to serve as a membrane anchor for retinoschisin-1 (RS1), a protein which is secreted by and works to maintain synaptic connections between photoreceptors and bipolar cells[26-31]. Mutations in RS1 have been linked to X-linked retinoschisis (XLRS), a blinding disorder which mainly affects males and results in early macular degeneration. XLRS is specifically characterized by splitting (or "schisis") of layers of the retina[32-36]. While it is possible that the degeneration in the aforementioned β1/β2 knock-in could be explained by loss of membrane anchorage of RS1 due to loss of ATP1B2, degeneration occurs more quickly than retina lacking RS1 and no "schisis" is apparent, suggesting an important role for ATP1B2 which is separate from its role as an ion pump and in membrane anchorage of RS1[24,37]. Therefore, it is likely that there is another role of ATP1B2 in the retina which has not yet been identified.

In the 3rd chapter of this dissertation, our lab used a myriad of techniques to determine that ATP1B2 undergoes S-palmitoylation on its 10th amino acid (Cys^{10}). Not only is Cys^{10} heavily conserved within ATP1B2 across several mammalian species, it is unique to the β2-subunit isoform. All post-translational modifications of the b-subunit isoforms of the Na^+, K^+-ATPase have proven to be important in their maturation and unique cellular functions, including the number of N-linked glycosylations[25,38]. Therefore, it is highly likely that post-translational lipid modification of ATP1B2 by S-palmitoylation plays a role in its

intrinsic function within the retina. Interestingly, preliminary studies in our lab demonstrate that endogenous ATP1B2 is only palmitoylated in retina, brain, and skeletal muscle, all of which are very metabolically active tissues (Fig. 4.1). We plan to isolate additional tissue to analyze by acyl-PEG exchange to determine whether palmitoylation status of ATP1B2 is exclusive to these aforementioned tissues.

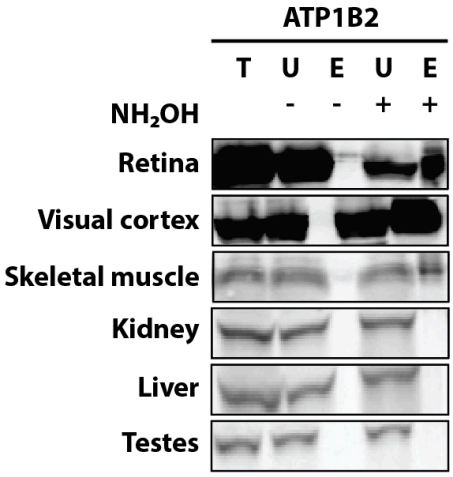

Figure 4.1. Palmitoylation status of ATP1B2 in various tissues was determined using acyl-RAC and western blot. T = total, U = unbound, E = elute, NH_2OH = hydroxylamine

Unfortunately, elucidating the role of ATP1B2 has proven challenging, as acyl-RAC analysis of hRPE1 cells transfected with our HA-tagged WT-ATP1B2 plasmid constructs (ATP1B2-HA) shows only slight palmitoylation of our ectopically expressed ATP1B2 protein. Similarly, subretinal injection of our plasmid constructs in WT retina only yields a small palmitoylated fraction of ATP1B2-HA, though a large amount of endogenous ATP1B2 clearly undergoes palmitoylation. We believe that there are several explanations for this. First, it is highly possible that the machinery in the retina required for palmitoylation of ATP1B2 is occupied by and preferentially chooses endogenously expressed ATP1B2. Another possible explanation is that transfection of our plasmid constructs by subretinal injection may not be reaching the appropriate retinal cell types

housing the machinery required to palmitoylate ATP1B2, as our constructs are not photoreceptor-specific. Therefore, in cell culture or subretinal injection, transfection of ATP1B2 into cells which do not endogenously express and palmitoylate ATP1B2 could lack the required palmitoylation machinery. Finally, it is possible that the C-terminal HA-tag could alter the structure of ATP1B2, impeding interactions between the proper DHHC motif-containing palmitoyl acyltransferase (DHHC-PAT) enzyme and HA-tagged ATP1B2.

In order to understand the role of palmitoylation of ATP1B2, our first goal is to establish and standardize an expression system where WT ATP1B2 is palmitoylated properly in cell culture. Once we do this, we can easily compare our HA-tagged WT ATP1B2 construct with our non-palmitoylated ATP1B2-C10A mutant. To determine the proper system for expression of palmitoylated ATP1B2, we first plan to transfect hRPE1 cells with a plasmid construct expressing untagged WT ATP1B2 and evaluate its palmitoylation status using acyl-RAC. This experiment will tell us if the HA tag is altering the structure of ATP1B2, preventing access to DHHC-PATs. As hRPE1 cells only express the α1- and β1- subunits of the Na^+, K^+-ATPase, we can use a commercially available antibody against ATP1B2 for western blot analysis of our acyl-RAC samples without worrying about endogenous expression of the protein. If the palmitoylation status of untagged ATP1B2 remains low, we plan to purchase commercially available cell lines which endogenously express ATP1B2, such as the human retinoblastoma cell lines WERI-Rb-1 or Y79. As these retina-derived cells express ATP1B2 and ATP1A3, it is likely that they would contain the proper DHHC-PATs required for palmitoylation of ATP1B2, so we could evaluate the palmitoylation status of our HA-tagged WT and C10A ATP1B2 constructs

using acyl-RAC. Alternatively, we could attempt to co-transfect hRPE1 cells with different DHHC-PATs in order to determine which DHHC isoforms enhance palmitoylation of ATP1B2, though 23 isoforms have been identified[39]. Once we establish a proper expression system of palmitoylated WT ATP1B2, we plan to transfect cells with our WT and mutant C10A ATP1B2 constructs. After confirming loss of palmitoylation by a C10A mutation in ATP1B2 in those cells by acyl-RAC, we plan to investigate the importance of palmitoylation, through evaluation of differences in protein-protein interactions between WT or mutant ATP1B2 and its $\alpha 3$-subunit, as well as Na^+, K^+-ATPase localization and membrane association.

As mentioned in the discussion of chapter 3, many tissues express a third subunit which has been shown to associate with the α- and β- subunits of the Na^+, K^+-ATPase, known as the γ-subunit[25]. Seven different isoforms of the γ-subunit have been identified and are expressed in a tissue-specific manner (FXYD1-7), all of which have been implicated in modulation of Na^+,K^+-ATPase activity[40,41]. In the retina, no γ-subunit of the Na^+, K^+-ATPase has yet been identified. Due to the large number of energy-dependent processes in the retina, such as phototransduction, neurotransmitter release, and intracellular protein trafficking, and hyperpolarization/depolarization, it is unexpected that the retina would not utilize an extra level of Na^+, K^+-ATPase modulation. One of our lab's hypotheses is that palmitoylation of ATP1B2 contributes an extra level of regulation to Na^+,K^+-ATPase activity in the retina[42]. The reversible nature of palmitoyl lipid modifications give rise to a dynamic role through palmitoylation and depalmitoylation of a protein. To determine whether palmitoylation of ATP1B2 influences ion pump activity, we

would compare Na^+,K^+-ATPase activity between transfected cells expressing palmitoylated HA-tagged WT and non-palmitoylated mutant ATP1B2-C10A constructs. We can measure Na^+,K^+-ATPase activity of transfected cell lysate using a commercially available colorimetric or fluorometric ATPase activity assay which allows for quantification of ATP (https://www.abcam.com/atp-assay-kit-colorimetricfluorometric-ab83355.html).

Though the specific requirement for the β2-subunit of the Na^+, K^+-ATPase in the retina remains uncertain, it is clear that retinal health is dependent on its expression. Further work must be done to determine how loss of ATP1B2 from the retina influences photoreceptor and inner retinal neuron function. Due to the high amount of ATP utilization by the Na^+, K^+-ATPase and the number of energy-demanding processes which take place in the retina, it is unusual that this metabolically active tissue lacks the γ-subunit of the Na^+, K^+-ATPase, an additional regulator of Na^+, K^+-ATPase ATP consumption. Further investigation of palmitoylation of ATP1B2 will lead to elucidation of the unique requirement of ATP1B2 in the retina, as well as its role in Na^+, K^+-ATPase pump activity.

4.3 References

1 Skiba, N. P. *et al.* Proteomic identification of unique photoreceptor disc components reveals the presence of PRCD, a protein linked to retinal degeneration. *J Proteome Res* **12**, 3010-3018, doi:10.1021/pr4003678 (2013).

2 Spencer, W. J. *et al.* Progressive Rod–Cone Degeneration (PRCD) Protein Requires N-Terminal S-Acylation and Rhodopsin Binding for Photoreceptor Outer Segment Localization and Maintaining Intracellular Stability. *Biochemistry* **55**, 5028-5037, doi:10.1021/acs.biochem.6b00489 (2016).

3 Aguirre, G. D. & Acland, G. M. Variation in retinal degeneration phenotype inherited at the prcd locus. *Experimental Eye Research* **46**, 663-687, doi:https://doi.org/10.1016/S0014-4835(88)80055-1 (1988).

4 Allon, G. *et al.* PRCD is concentrated at the base of photoreceptor outer segments and is involved in outer segment disc formation. *Hum Mol Genet* **28**, 4078-4088, doi:10.1093/hmg/ddz248 (2019).

5 Spencer, W. J. *et al.* PRCD is essential for high-fidelity photoreceptor disc formation. *Proc Natl Acad Sci U S A* **116**, 13087-13096, doi:10.1073/pnas.1906421116 (2019).

6 Aguirre, G., Alligood, J., O'Brien, P. & Buyukmihci, N. Pathogenesis of progressive rod-cone degeneration in miniature poodles. *Investigative Ophthalmology & Visual Science* **23**, 610-630 (1982).

7 Aguirre, G. D. & Rubin, L. F. Progressive retinal atrophy in the Miniature Poodle: an electrophysiologic study. *Journal of the American Veterinary Medical Association* **160**, 191-201 (1972).

8 Rakshit, T. & Park, P. S. Impact of reduced rhodopsin expression on the structure of rod outer segment disc membranes. *Biochemistry* **54**, 2885-2894, doi:10.1021/acs.biochem.5b00003 (2015).

9 Liang, Y. *et al.* Rhodopsin Signaling and Organization in Heterozygote Rhodopsin Knockout Mice. *J Biol Chem* **279**, 48189-48196 (2004).

10 Rakshit, T. *et al.* Adaptations in rod outer segment disc membranes in response to environmental lighting conditions. *Biochim Biophys Acta Mol Cell Res* **1864**, 1691-1702, doi:10.1016/j.bbamcr.2017.06.013 (2017).

11 Besharse, J. C., Hollyfield, J. G. & Rayborn, M. E. Photoreceptor outer segments: accelerated membrane renewal in rods after exposure to light. *Science* **196**, 536-538, doi:10.1126/science.300504 (1977).

12 Sethna, S. & Finnemann, S. C. Analysis of photoreceptor rod outer segment phagocytosis by RPE cells in situ. *Methods Mol Biol* **935**, 245-254, doi:10.1007/978-1-62703-080-9_17 (2013).

13 Murphy, J. & Kolandaivelu, S. Palmitoylation of Progressive Rod-Cone Degeneration (PRCD) Regulates Protein Stability and Localization. *J Biol Chem* **291**, 23036-23046, doi:10.1074/jbc.M116.742767 (2016).

14 Goldstein, O. *et al.* Linkage disequilibrium mapping in domestic dog breeds narrows the progressive rod-cone degeneration interval and identifies ancestral disease-transmitting chromosome. *Genomics* **88**, 541-550, doi:10.1016/j.ygeno.2006.05.013 (2006).

15 Zangerl, B. *et al.* Identical mutation in a novel retinal gene causes progressive rod-cone degeneration in dogs and retinitis pigmentosa in humans. *Genomics* **88**, 551-563, doi:10.1016/j.ygeno.2006.07.007 (2006).

16 Resh, M. D. Fatty acylation of proteins: The long and the short of it. *Prog Lipid Res* **63**, 120-131, doi:10.1016/j.plipres.2016.05.002 (2016).

17 Pach, J., Kohl, S., Gekeler, F. & Zobor, D. Identification of a novel mutation in the PRCD gene causing autosomal recessive retinitis pigmentosa in a Turkish family. *Mol Vis* **19**, 1350-1355 (2013).

18 Remez, L., Zobor, D., Kohl, S. & Ben-Yosef, T. The progressive rod-cone degeneration (PRCD) protein is secreted through the conventional ER/Golgi-dependent pathway. *Exp Eye Res* **125**, 217-225, doi:10.1016/j.exer.2014.06.017 (2014).

19 Gelabert-Baldrich, M. *et al.* Dynamics of KRas on endosomes: involvement of acidic phospholipids in its association. *Faseb j* **28**, 3023-3037, doi:10.1096/fj.13-241158 (2014).

20 Williams, C. L. The polybasic region of Ras and Rho family small GTPases: a regulator of protein interactions and membrane association and a site of nuclear

localization signal sequences. *Cell Signal* **15**, 1071-1080, doi:10.1016/s0898-6568(03)00098-6 (2003).

21 Matt, L., Kim, K., Chowdhury, D. & Hell, J. W. Role of Palmitoylation of Postsynaptic Proteins in Promoting Synaptic Plasticity. *Frontiers in Molecular Neuroscience* **12**, doi:10.3389/fnmol.2019.00008 (2019).

22 Mazelova, J. *et al.* Ciliary targeting motif VxPx directs assembly of a trafficking module through Arf4. *Embo j* **28**, 183-192, doi:10.1038/emboj.2008.267 (2009).

23 Magyar, J. P. *et al.* Degeneration of neural cells in the central nervous system of mice deficient in the gene for the adhesion molecule on Glia, the beta 2 subunit of murine Na,K-ATPase. *J Cell Biol* **127**, 835-845, doi:10.1083/jcb.127.3.835 (1994).

24 Weber, P., Bartsch, U., Schachner, M. & Montag, D. Na,K-ATPase subunit beta1 knock-in prevents lethality of beta2 deficiency in mice. *J Neurosci* **18**, 9192-9203, doi:10.1523/jneurosci.18-22-09192.1998 (1998).

25 Clausen, M. V., Hilbers, F. & Poulsen, H. The Structure and Function of the Na,K-ATPase Isoforms in Health and Disease. *Front Physiol* **8**, 371, doi:10.3389/fphys.2017.00371 (2017).

26 Friedrich, U. *et al.* The Na/K-ATPase is obligatory for membrane anchorage of retinoschisin, the protein involved in the pathogenesis of X-linked juvenile retinoschisis. *Hum Mol Genet* **20**, 1132-1142, doi:10.1093/hmg/ddq557 (2011).

27 Molday, L. L., Wu, W. W. & Molday, R. S. Retinoschisin (RS1), the protein encoded by the X-linked retinoschisis gene, is anchored to the surface of retinal photoreceptor and bipolar cells through its interactions with a Na/K ATPase-SARM1 complex. *J Biol Chem* **282**, 32792-32801, doi:10.1074/jbc.M706321200 (2007).

28 Plössl, K. *et al.* Identification of the retinoschisin-binding site on the retinal Na/K-ATPase. *PLOS ONE* **14**, e0216320, doi:10.1371/journal.pone.0216320 (2019).

29 Molday, L. L., Hicks, D., Sauer, C. G., Weber, B. H. F. & Molday, R. S. Expression of X-Linked Retinoschisis Protein RS1 in Photoreceptor and Bipolar Cells. *Investigative Ophthalmology & Visual Science* **42**, 816-825 (2001).

30 Plössl, K. *et al.* Retinoschisin is linked to retinal Na/K-ATPase signaling and localization. *Mol Biol Cell* **28**, 2178-2189, doi:10.1091/mbc.E17-01-0064 (2017).

31 Plössl, K., Weber, B. H. F. & Friedrich, U. The X-linked juvenile retinoschisis protein retinoschisin is a novel regulator of mitogen-activated protein kinase signalling and apoptosis in the retina. *J Cell Mol Med* **21**, 768-780, doi:10.1111/jcmm.13019 (2017).

32 Gehrig, A. E., Warneke-Wittstock, R., Sauer, C. G. & Weber, B. H. F. Isolation and characterization of the murine X-linked juvenile retinoschisis (Rs1h) gene. *Mammalian Genome* **10**, 303-307, doi:10.1007/s003359900991 (1999).

33 Sauer, C. G. *et al.* Positional cloning of the gene associated with X-linked juvenile retinoschisis. *Nature Genetics* **17**, 164-170, doi:10.1038/ng1097-164 (1997).

34 George, N. D., Yates, J. R., Bradshaw, K. & Moore, A. T. Infantile presentation of X linked retinoschisis. *British Journal of Ophthalmology* **79**, 653, doi:10.1136/bjo.79.7.653 (1995).

35 Rao, P., Dedania, V. S. & Drenser, K. A. Congenital X-Linked Retinoschisis: An Updated Clinical Review. *The Asia-Pacific Journal of Ophthalmology* **7** (2018).

36 Tantri, A. *et al.* X-linked retinoschisis: A clinical and molecular genetic review. *Survey of Ophthalmology* **49**, 214-230, doi:https://doi.org/10.1016/j.survophthal.2003.12.007 (2004).

37 Zeng, Y. *et al.* RS-1 Gene Delivery to an Adult Rs1h Knockout Mouse Model Restores ERG b-Wave with Reversal of the Electronegative Waveform of X-Linked Retinoschisis. *Investigative Ophthalmology & Visual Science* **45**, 3279-3285, doi:10.1167/iovs.04-0576 (2004).

38 Tokhtaeva, E., Munson, K., Sachs, G. & Vagin, O. N-glycan-dependent quality control of the Na,K-ATPase beta(2) subunit. *Biochemistry* **49**, 3116-3128, doi:10.1021/bi100115a (2010).

39 Plain, F. *et al.* Control of protein palmitoylation by regulating substrate recruitment to a zDHHC-protein acyltransferase. *Communications Biology* **3**, 411, doi:10.1038/s42003-020-01145-3 (2020).

40 Sweadner, K. J. & Rael, E. The FXYD gene family of small ion transport regulators or channels: cDNA sequence, protein signature sequence, and expression. *Genomics* **68**, 41-56, doi:10.1006/geno.2000.6274 (2000).

41 Geering, K. Function of FXYD proteins, regulators of Na, K-ATPase. *J Bioenerg Biomembr* **37**, 387-392, doi:10.1007/s10863-005-9476-x (2005).

42 Wong-Riley, M. T. Energy metabolism of the visual system. *Eye Brain* **2**, 99-116, doi:10.2147/eb.S9078 (2010).